NASA TECHNICAL NOTE

NASA TN D-4968

C. 1

NASA TN D-4968

INTERIM SUMMARY OF LIQUID ROCKET ACOUSTIC-MODE-INSTABILITY STUDIES AT A NOMINAL THRUST OF 20 000 POUNDS

by E. William Conrad, Harry E. Bloomer, John P. Wanhainen, and David W. Vincent

Lewis Research Center
Cleveland, Ohio

NATIONAL AERONAUTICS AND SPACE ADMINISTRATION • WASHINGTON, D. C. • DECEMBER 1968

NASA TN D-4968

INTERIM SUMMARY OF LIQUID ROCKET ACOUSTIC-MODE-INSTABILITY STUDIES AT A NOMINAL THRUST OF 20 000 POUNDS

By E. William Conrad, Harry E. Bloomer, John P. Wanhainen, and David W. Vincent

Lewis Research Center
Cleveland, Ohio

NATIONAL AERONAUTICS AND SPACE ADMINISTRATION

For sale by the Clearinghouse for Federal Scientific and Technical Information
Springfield, Virginia 22151 – CFSTI price $3.00

ABSTRACT

Acoustic-mode-stability data for both hydrogen-oxygen and earth-storable propellant combinations were collected and correlated as far as possible. Several injector variables that presumably affect the oscillatory energy generation process provided significant stability improvements. Complete stabilization of hydrogen-oxygen rockets was achieved by proper selection of injection areas, element size, and oxidizer tube extension. Several injector variables influenced the stability of earth-storable propellants; however, dynamic stability was not achieved through injector modification. Energy absorbers were effective in suppressing acoustic-mode instability with both propellant combinations. Preliminary design guides for acoustic liners are also given.

CONTENTS

INTERIM SUMMARY OF LIQUID ROCKET ACOUSTIC-MODE-INSTABILITY STUDIES AT A NOMINAL THRUST OF 20 000 POUNDS

by E. William Conrad, Harry E. Bloomer, John P. Wanhainen, and David W. Vincent

Lewis Research Center

SUMMARY

Recent acoustic-mode-stability data for both hydrogen-oxygen and earth-storable (nitrogen tetroxide (N_2O_4) and 50 percent unsymmetrical dimethylhydrazine (UDMH) - 50 percent hydrazine (N_2H_4)) propellant combinations were collected and correlated as far as possible. The data were obtained in the rocket-engine test facilities of the NASA Lewis Research Center by using engines of about 20 000 pounds (88.964 kN) thrust.

Concentric-tube injectors were used exclusively for the hydrogen-oxygen propellants and were stability rated in terms of the minimum stable operating hydrogen temperature. Several injector variables that presumably affect the oscillatory energy generation process provided significant improvements in stability. In this respect, complete stabilization of hydrogen-oxygen rockets was achieved by proper selection of injection areas, injection element size, and oxidizer tube extension. The hydrogen-temperature stable operating limits correlated with a stability-limit parameter. With this parameter, the change in stable operating limits can be predicted for several geometric and operating variables.

For earth-storable propellants, triplet injectors were used and rated by discharging bombs into the chamber through tangential ports. Although some improvement in stability was achieved through injector modification, the stability with earth-storable propellants was relatively insensitive to injector design variables.

Devices classified as energy absorbers (e.g., baffles and acoustic liners) were effective in suppressing or eliminating acoustic-mode instability with both propellant combinations. In addition to the rocket engine tests, this report included the results of nonfiring acoustic studies made to examine several aspects of acoustic liner design. Some preliminary design guides for acoustic liners are given together with a discussion of the problems associated with flow past the apertures and the properties of the gas in the resonators.

INTRODUCTION

Since early 1964, an intensive and continuous investigation of high-frequency combustion instability (screech) conducted with rocket engines of about 20 000 pounds (88.964 kN) nominal thrust has been in progress at the NASA Lewis Research Center. The twofold objectives of this work were (1) to find preventive measures that could be applied immediately whether or not complete understanding of screech was obtained, and (2) to obtain a more fundamental knowledge of the phenomena that could help in the analytical treatment of high-frequency combustion instability. This knowledge could then be used to formulate design rules adequate to provide a high degree of assurance of stable operation in the initial firing of new development rocket engines. Based on existing combustion theories (refs. 1 to 4) and previous experimental combustion studies, a substantial number of potentially important variables were selected for investigation. Where confidence was high, the variables were studied in depth, and the results are reported in references 5 to 17. The objectives of this report are (1) to compare and consider the relative contribution of these variables, (2) to examine these findings in the light of existing theory, and (3) to search for new theoretical models. In addition, certain new results are included, which are significant but were not studied in sufficient depth to warrant separate reports. The information reported herein covers the data obtained up to July 1, 1966 and the subsequent analysis thereof.

The seriousness of the screech problem is dramatized by the photographs of figure 1, showing two virtually identical propellant-cooled injectors that were operated stably for 50 seconds (fig. 1(a)) and for only 0.4 second of screech (fig. 1(b)). For new engines presently entering development testing (very small engines excepted), the chances are great that the initial configuration will be dynamically unstable and quite likely that it will be statically unstable. The trial-and-error solutions to obtain stability have been enormously expensive in terms of both manpower and money because of the lack of adequate design knowledge. For manned spacecraft in particular, it is almost imperative that a great margin of stability be obtained in the engines to ensure against large random-triggering disturbances even though their statistical occurrence may be low.

The bulk of the experimental work discussed herein was conducted with a thrust chamber diameter of 10.78 inches (27.381 cm) and a nozzle throat diameter of 7.8 inches (19.81 cm). Most engine operation was accomplished at a chamber pressure of 300 psia (2068.41 kN/m^2) yielding a thrust of 20 000 pounds (88.964 kN) at sea level with a low-area-ratio exhaust nozzle. This engine size, although selected to allow reasonable flexibility and cost, was large enough to allow confidence in the applicability of the test results. The effects of systematic changes in the test variables were assessed by screech rating. This rating was accomplished for hydrogen-oxygen propellants by reducing the

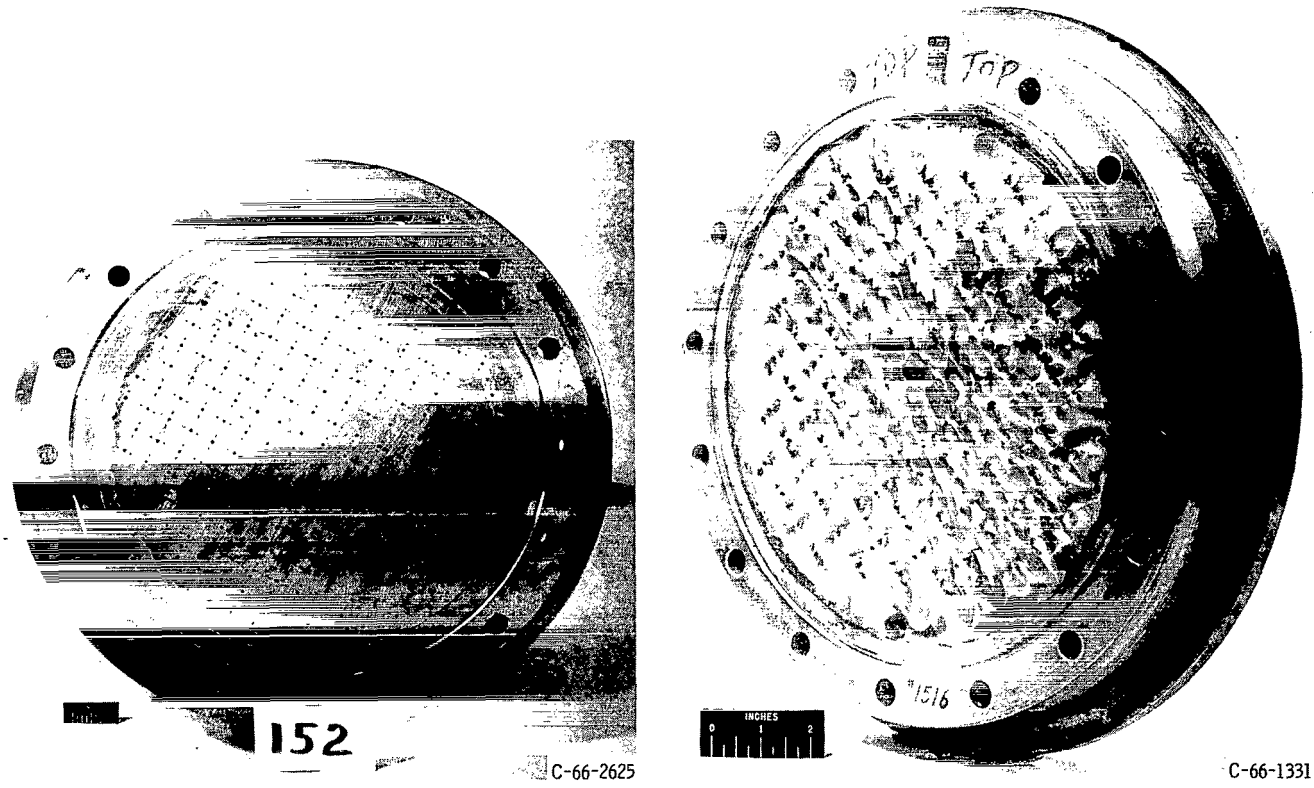

(a) Before operation in screech.

(b) After operation in screech for duration of 0.4 second.

Figure 1. - Effect of screech on injector integrity.

hydrogen temperature until transition into screech occurred. For storable propellants (nitrogen tetroxide (N_2O_4) and a mixture of 50 percent hydrazine (N_2H_4) plus 50 percent unsymmetrical dimethylhydrazine (UDMH)), a bomb-rating technique was employed.

In addition to the rocket engine tests, a rather extensive study was made by using electrically or pneumatically driven sound fields in a simulated thrust chamber. These "cold acoustic" studies were conducted to examine several aspects of acoustic liner design under conditions that could be more closely controlled than was possible in an operating rocket. Sound pressure levels up to about 190 decibels were used.

The scope of the overall program was limited to manageable proportions by using a discrete injector type for each of the two propellant combinations. For use with the hydrogen-oxygen combinations, the concentric-tube injector element was selected on the basis of previous evaluation at Lewis and subsequent excellent performance in the RL-10 and J-2 engines. For the storable-propellant combination, a triplet element was selected, again on the basis of previous in-house experience, as well as on that of industry.

SYMBOLS

A	aperture area, $in.^2$; cm^2
A_H/A_O	injection area ratio
$\mathscr{A}$	contraction ratio
C	sonic velocity, ft/sec; m/sec
C^*	characteristic exhaust velocity, ft/sec; m/sec
D	injector orifice diameter, in.; cm
E	number of injector elements
f	frequency, Hz
g	gravitational constant, (lb mass/lb force) $(in./sec^2)$; (kg/kN) (m/sec^2)
k	damping coefficient, dB/sec
L^*	characteristic length, in.; cm
l	cavity depth, in.; cm
l_{eff}	liner aperture effective length, in.; cm
O/F	oxidant-fuel ratio
P	pressure, psi; N/m^2
T	temperature, ^oR; K
t	liner thickness or aperture neck length, in.; cm
V	velocity, ft/sec; m/sec
v	resonator volume, $in.^3$; cm^3
W	propellant flow rate, lb/sec; kg/sec
$\mathscr{W}_{cr}$	stability parameter, lb mass/(sec)$(in.)^{3/4}$; kg/(sec)$(m)^{3/4}$
α	absorption coefficient
Δ	differential
η_{C^*}	characteristic-exhaust-velocity efficiency, percent
θ'	angle between neck axis and wave vector, deg
ρ	density, lb mass/ft^3; kg/m^3
σ	liner open area ratio

Subscripts:

c	chamber
F	fuel
Fa	axial fuel component
Fr	radial fuel component
flo	flow
H	hydrogen
O	oxidant
o	resonance
p	pressure
R	ratio
r	decay rate
t	total
tr	transition

APPARATUS

Engine Installations

The engines using hydrogen-oxygen propellants were tested in the Rocket Engine Test Facility that is described in reference 5. The engines were mounted vertically and fired downward, as shown in figure 2, into a large water spray chamber from which the exhaust gases discharged to the atmosphere. Propellants were supplied to the engine from pressurized tanks.

Tests with storable propellants were conducted in an altitude chamber of the Propulsion Systems Laboratory facility. Inasmuch as low-area-ratio (1.3) exhaust nozzles were used, altitude capability was not mandatory. Such a facility was used only to ensure safe handling of the toxic exhaust products.

The engine installation shown in figure 3 was horizontal, with the engine mounted on a cradle suspended by four flexure plates. Thrust was measured by a calibrated load cell. Propellants were supplied from pressurized tanks. A more complete description is given in reference 9.

Cold acoustic testing of perforated screech suppression liners was accomplished with the thrust chamber isolated on a bench having cover plates on both ends, or with the

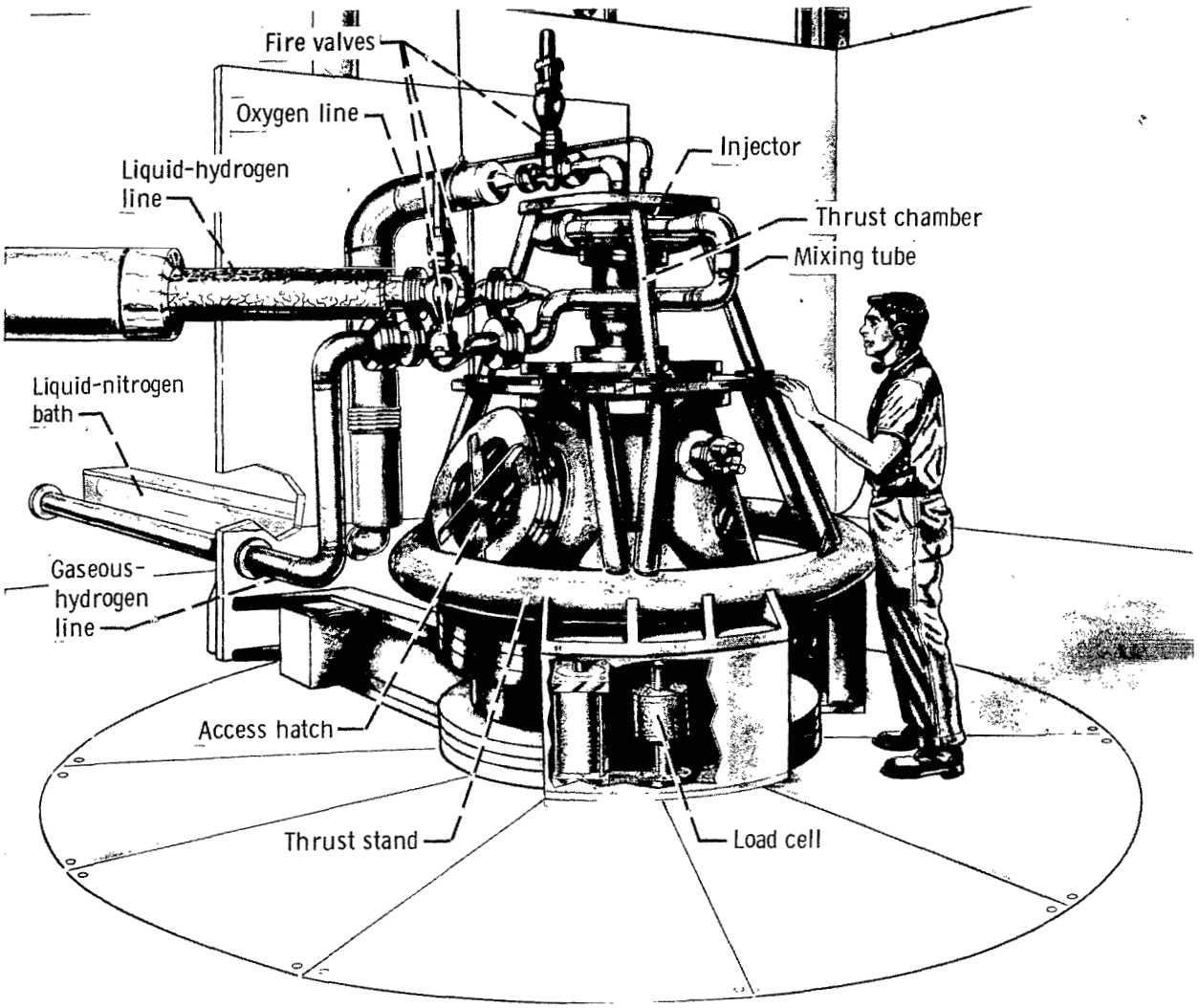

Figure 2. - Hydrogen-oxygen engine installation.

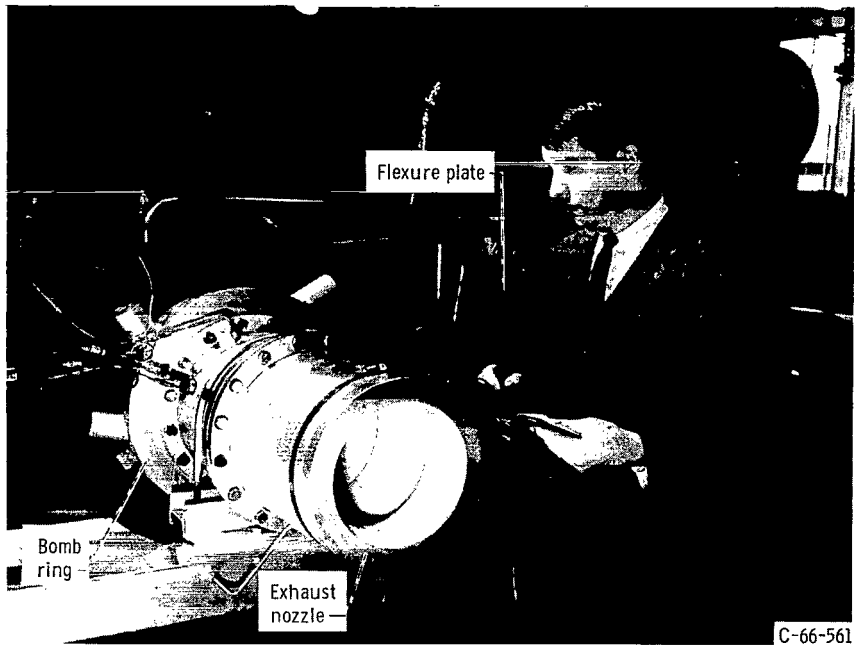

Figure 3. - Storable-propellant engine installation.

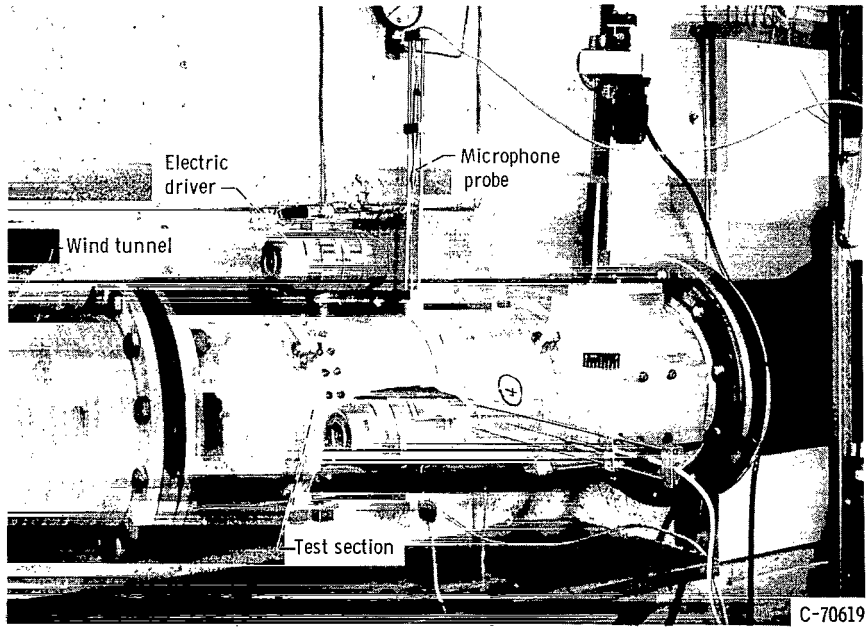

Figure 4. - Nonfiring acoustic liner test installation.

thrust chamber mounted as an integral part (test section) of a subsonic wind tunnel (fig. 4). This latter installation was used to determine the effect of flow velocity past the liner perforations. Electric or pneumatic devices were used to create acoustic resonance modes at sound pressure levels up to 170 and 190 decibels, respectively.

Engine

The nominal engine assemblies and hardware (fig. 5) were identical for both propellant combinations, with the exception of the injector type and the inclusion of the bomb ring shown in figure 3. The assembly used for the majority of the testing comprised an injector, a cylindrical heat-sink thrust chamber with a 10.78-inch (27.381-cm) inside diameter and a convergent-divergent exhaust nozzle with a contraction ratio of 1.9 and an expansion area ratio of 1.3. The inner surfaces of the mild-steel heat-sink thrust chamber and nozzle were coated with 0.030-inch- (0.0762-cm-) thick flame sprayed zirconium oxide to reduce the rate of heat transfer into the metal. This construction allowed a run duration of 3 seconds, which was adequate to obtain the required data. Variations in chamber length, chamber diameter, and nozzle contraction ratio were made and are defined when specific tests results are discussed.

Injectors

The two basic types of injectors employed are illustrated in figures 6 and 7. With the hydrogen-oxygen propellant combination (fig. 6), the oxygen entered the oxidizer cavity on the centerline and flowed through the tubes into the thrust chamber. The hydrogen entered the hydrogen cavity radially inward from a manifold (not shown) and then flowed into the thrust chamber through annular passages surrounding each oxidizer tube. Tube concentricity was maintained by small fins on each tube. Faceplate material was either oxygen-free copper for heat-sink cooling or a porous sintered wire screen material for transpiration cooling. Variations in injector design were numerous inasmuch as such variations comprised the test variables. The design details involved are discussed in the RESULTS AND DISCUSSION section.

The nominal configuration of the injectors used with storable propellants (fig. 7) was similar to the hydrogen-oxygen injector on the oxidizer side; that is, the oxidizer entered the thrust chamber axially through the long tubes brazed into the assembly. The fuel, used to provide cooling for the faceplate, entered the thrust chamber through ori-

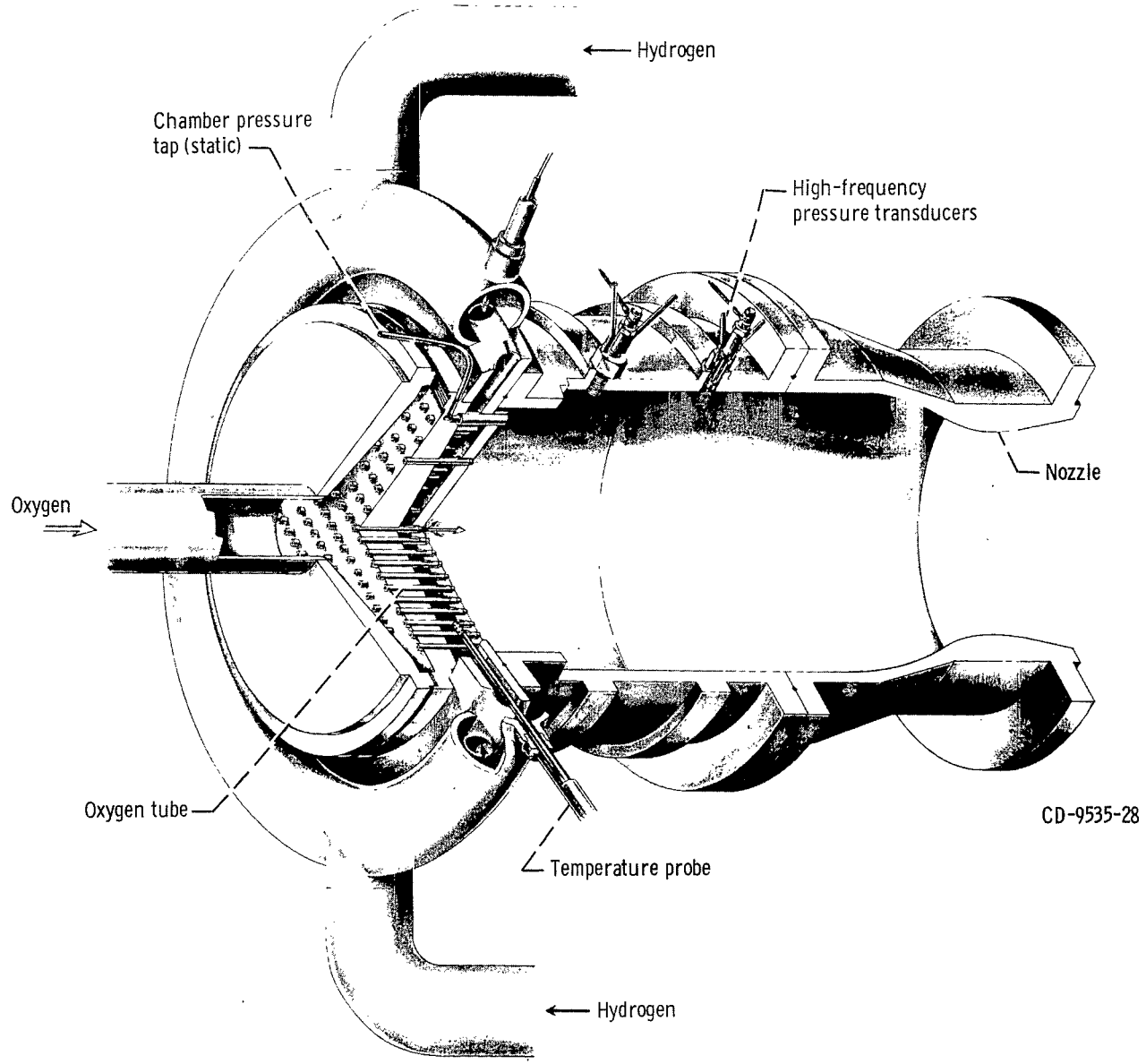

Figure 5. - Cutaway view of hydrogen-oxygen engine assembly.

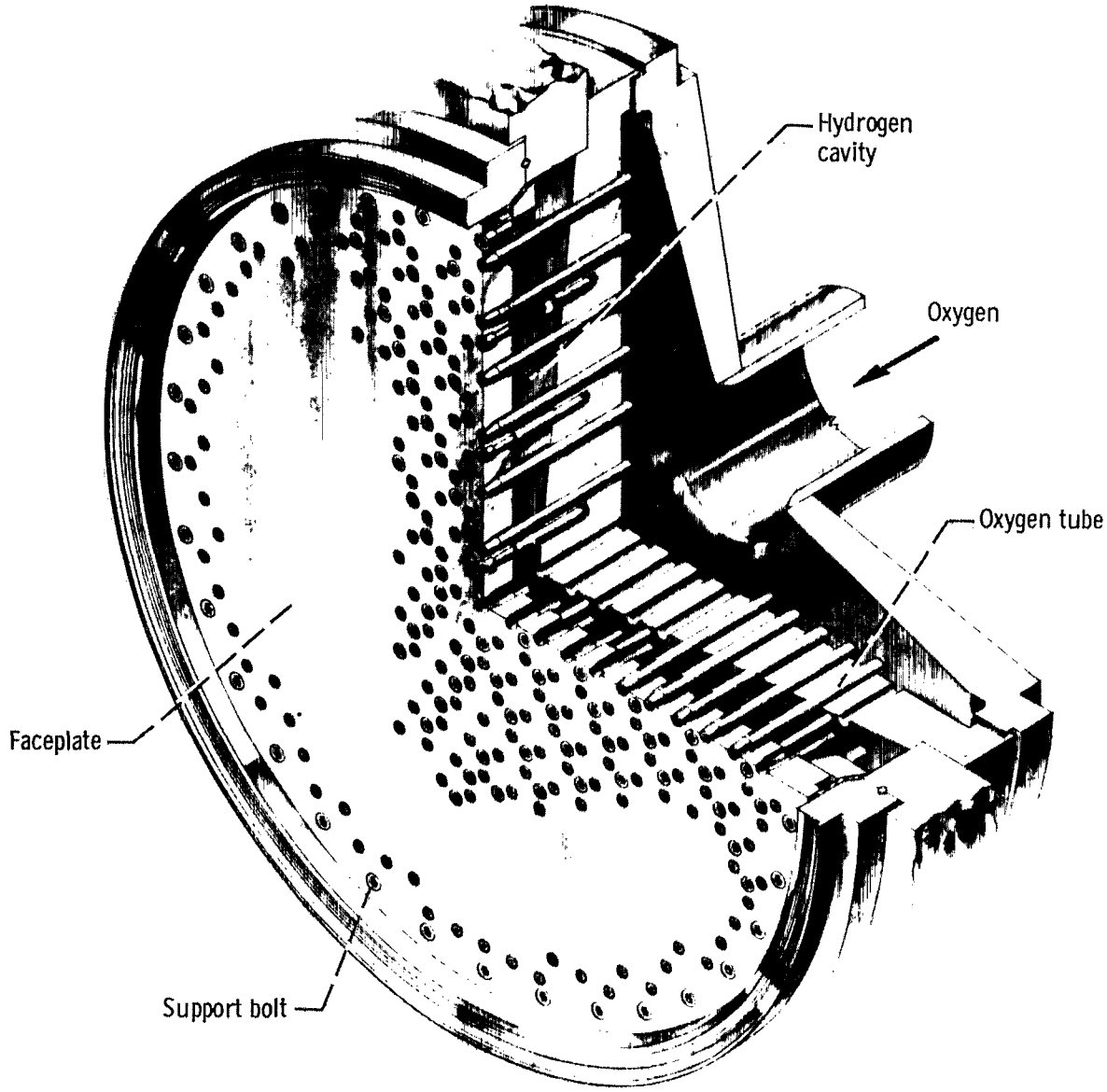

Figure 6. - Cutaway view of concentric-tube injector used with hydrogen-oxygen propellants.

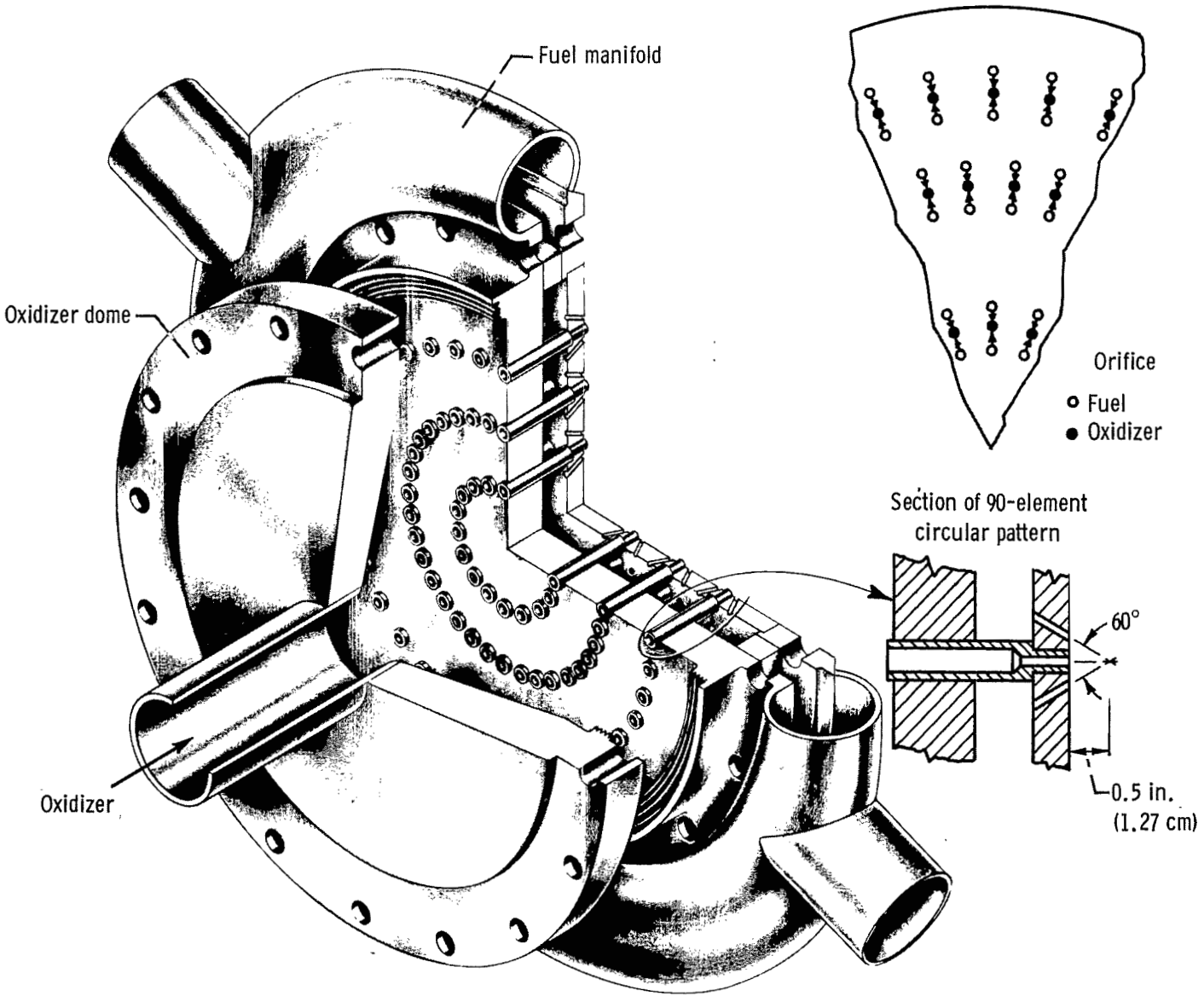

CD-8203-28

Figure 7. - Cutaway view of coplaner triplet injector used with storable propellants.

fices on either side of the oxidizer streams. These orificies were canted to impinge the two fuel streams upon the oxidizer stream. Impingement distance and angle, injection velocity, and distribution pattern were test variables and are described along with the results in the RESULTS AND DISCUSSION section. In addition, some tests were conducted with the propellants reversed to provide two oxidizer streams on one fuel stream.

SCREECH-RATING DEVICES

For hydrogen-oxygen engines, the stability rating is given in terms of the minimum stable hydrogen-injection temperature. Varying the hydrogen temperature was accomplished by mixing warm gaseous hydrogen with the liquid hydrogen in a mixing tube near the injector (fig. 2). This system could provide a rate of temperature reduction of as much as 25° R per second (13.9 K/sec) in a typical run. Details of the mixing device are given in reference 5.

For storable propellants, virtually all screech rating was done with bombs discharged into the chamber through tangential ports in the chamber wall. The bomb assembly is shown in figure 8. The bomb was initiated by a 20 000-volt pulse through an explosive bridge wire that triggered a 1.63-grain (105.6-mg) pentaerythritol tetranitrate (PETN) primer charge. Various grain-size tablets of 98 percent cyclotrimethylenetrinitramine (RDX) were stacked as required to vary the bomb strength. Usually four

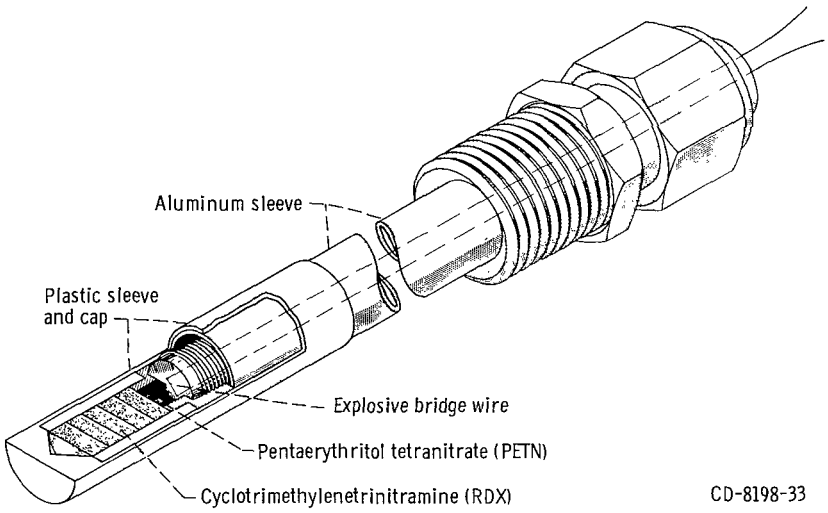

Figure 8. - Explosive bomb assembly.

bombs of various strengths were fired at 200-millisecond intervals during the steady-state portion of each engine run.

INSTRUMENTATION

For hydrogen-oxygen engines, the instrumentation used and the location of transducers are shown in figure 9. Signals from the transducers were transmitted to an automatic digital data-recording system. At three locations on the thrust chamber, water-cooled flush-mounted transducers were used to determine the characteristics of the pressure field and to identify screech modes. The response of the transducers as installed was flat to within 10 percent to 6000 hertz with a nominal resonant frequency of about 20 000 hertz.

Liquid-hydrogen flow rate was measured by using a venturi, and gaseous-hydrogen flow rate was measured by using an orifice plate. Oxygen propellant flow rate was obtained with a vane-type flowmeter that was calibrated with water by using a static weighing system. The correction that accounted for dimensional change in the instrument with temperature was supplied by the flowmeter manufacturer. Liquid flow temperatures were measured by platinum resistance sensors.

The instrumentation used with storable propellants was essentially the same as that used for the cryogenic propellants, except that propellant temperatures were obtained with iron-constantan thermocouples, and both propellant flows were obtained with vane-type flowmeters calibrated with the appropriate propellant.

For the cold acoustic testing, input monitoring and control included the use of a frequency oscillator, a phase shifter, amplifiers, and a frequency counter. Tunnel flow conditions were measured with a traversing pitot-static tube and a manometer or micromanometer. Sound field measurements were made with a 1-millimeter-diameter traversing probe tube attached to a quarter-wave condenser microphone. Steady-state data of root-mean-square pressure against position were recorded on an X, Y-plotter. Pressure decay data at a given location were obtained from a film record of an oscilloscope trace.

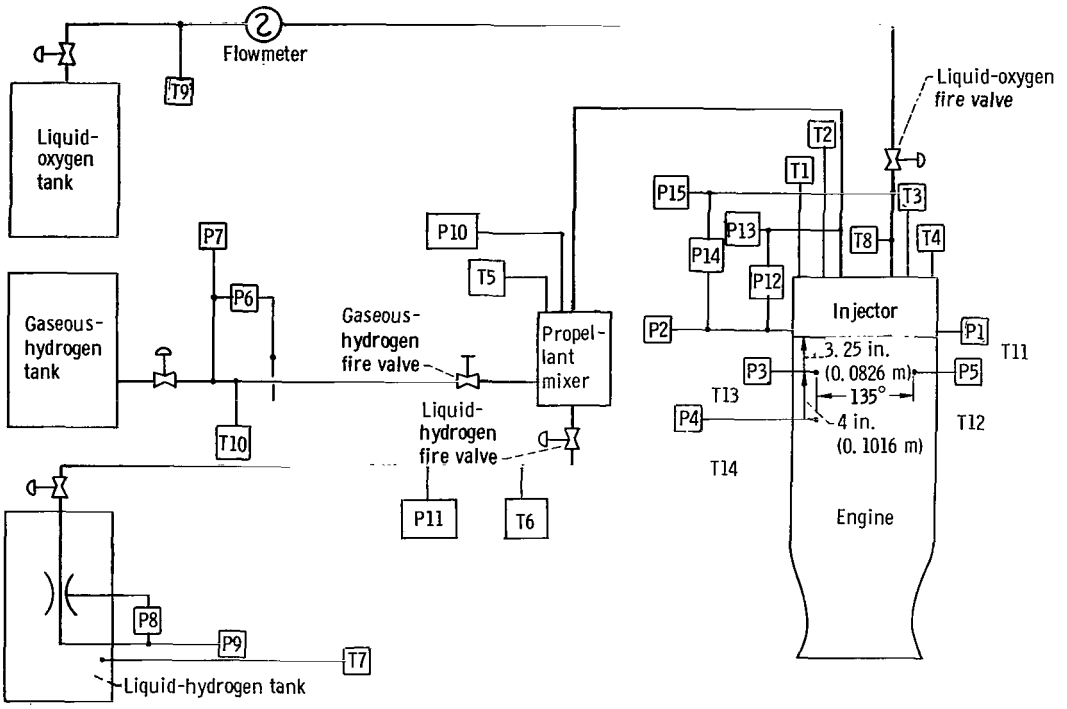

P1	Static chamber pressure (injector face), four-arm strain-gage transducer 1
P2	Static chamber pressure (injector face), four-arm strain-gage transducer 2
P3	Dynamic chamber pressure, water-cooled quartz pressure transducer 3
P4	Dynamic chamber pressure, water-cooled quartz pressure transducer 4
P5	Dynamic chamber pressure, water-cooled quartz pressure transducer 5
P6	Gaseous-hydrogen orifice differential pressure, four-arm strain-gage transducer
P7	Gaseous-hydrogen orifice pressure, four-arm strain-gage transducer
P8	Liquid-hydrogen venturi differential pressure, four-arm strain-gage type
P9	Liquid-hydrogen venturi pressure, four-arm strain-gage transducer
P10	Hydrogen-mixer pressure, four-arm strain-gage transducer
P11	Liquid-hydrogen line pressure, four-arm strain gage transducer
P12	Hydrogen-injection differential pressure, four-arm strain-gage transducer
P13	Hydrogen-injection pressure, four-arm strain-gage transducer
P14	Oxygen-injection differential pressure, four-arm strain-gage transducer
P15	Oxygen-injection pressure, four-arm strain-gage transducer
T1	Hydrogen-injector temperature, carbon resistor sensor probe 1
T2	Hydrogen-injector temperature, carbon resistor sensor probe 2
T3	Hydrogen-injector temperature, carbon resistor sensor probe 3
T4	Hydrogen-injector temperature, carbon resistor sensor probe 4
T5	Hydrogen-mixer temperature, carbon resistor sensor probe
T6	Liquid-hydrogen line temperature, carbon resistor sensor probe
T7	Liquid-hydrogen venturi temperature, platinum type
T8	Oxygen-injection temperature, copper-constantan thermocouple
T9	Oxygen flowmeter temperature, platinum type
T10	Gaseous-hydrogen orifice temperature, iron-constantan thermocouple
T11, T12, T13, T14	Cavity gas temperature, Chromel-Alumel thermocouple

Figure 9. - Test instrumentation and transducer locations.

PROCEDURE

For hydrogen-oxygen engines, an initial hydrogen temperature was selected by presetting the hydrogen valves upstream of the mixer. After rated chamber pressure was reached, the gas valve was ramped toward a closed position and the liquid valve toward an open position to reduce the temperature of the injected hydrogen to a value below the anticipated screech limit. All valve scheduling was accomplished by the use of an automatic sequence timer. The screech limit was obtained over a range of oxidant-fuel ratios from high-speed recorder data. The hydrogen temperature in the injector cavity was read at the instant screech occurred, as indicated by the oscillograph trace of a flush-mounted pressure transducer. A limited number of bombing runs (described in the section RESULTS AND DISCUSSION) were made in an attempt to establish a correlation between the rating methods.

With storable propellants, four RDX bombs of different grain sizes were mounted in the four tangential bomb ports. Program timers were used to sequence the operation of the fuel and oxidizer control valves for a 3-second (nominal) firing duration and to sequence the firing of the four RDX bombs during the full chamber pressure portion of the run. Throughout the run, the chamber pressure and the oxidant-fuel ratio were maintained constant by the use of an electronic controller in conjunction with the propellant valves. An analysis of high-speed oscillograph records of chamber pressure was used to determine the critical bomb size or the pulse size required to induce sustained screech.

In the nonfiring acoustic bench tests, a particular mode was excited with drivers mounted 90^{o} apart. The frequency input was varied within a few hertz of the predicted frequency for that mode until the sound pressure at the antinodal point reached a maximum value. A probe traverse of the internal sound field was made to ensure mode identity. Decay coefficients were obtained with the probe at the maximum sound pressure position by stopping the drivers and recording the decay with an oscilloscope. For the decay tests, a narrow-band filter was used to eliminate stray resonance in the system.

RESULTS AND DISCUSSION

Although at the present no generally accepted and complete model exists for the screech phenomenon, it seems obvious that, for screech to commence, the generation of organized acoustic energy must exceed the rate of energy dissipation. Accordingly, two approaches can be taken in working toward a solution; namely, (1) applying effort to those factors likely to reduce the generation of organized wave systems, and (2) applying effort to those concepts and devices that show promise of increasing the rate of energy

dissipation. The text to follow is organized along these broad lines; however, the inclusion of some suppression concepts, such as baffles, under one or the other approach may be arbitrary inasmuch as the reason for their contribution to stability has not yet been conclusively shown.

Before the effects of the test variables are discussed, it is appropriate to establish a quantitative relation between the commonly used bomb-rating technique and the hydrogen temperature margin (above screech transition temperature) for the cryogenic portion of the investigation discussed herein. Such a relation is needed, for example, to confirm that an engine with a cooling-jacket-outlet hydrogen temperature 40° R (22.2 K) above the screech transition temperature for that engine can tolerate large random pressure spikes. It is important to note that, when a bomb of a given charge size is detonated in an operating rocket engine, the pressure spikes produced are commonly much larger than those produced in an identical test using the same chamber pressurized with inert gas (ref. 9). This increase has been referred to as chemical augmentation. A comparison of the peak-to-peak pressure disturbance with bomb size (grains of RDX explosive) for various hydrogen temperature margins is presented in figure 10. Because the hydrogen temperature control (steady state) was not precise, the data points are grouped in shaded bands of approximately constant temperature margins. Examination of the results shows that the sensitivity of the combustion process to a pressure disturbance (chemical augmentation) decreased as the temperature margin increased. For example, at 115° R (63.9 K) above the screech transition temperature, the pressure dis-

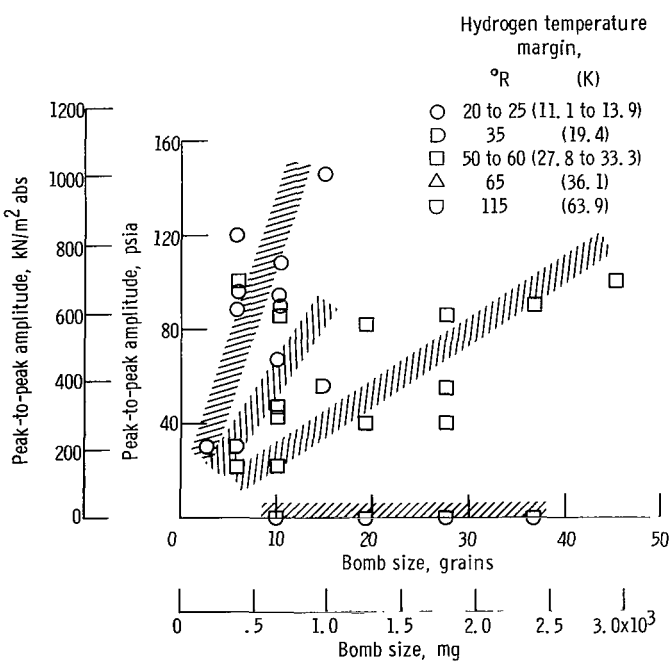

Figure 10. - Comparison of pressure disturbance with bomb size for various hydrogen temperature margins.

turbance expected from the detonation of a 36.2-grain (2345.7-mg) bomb was completely absorbed or damped with no resulting amplitude variation in chamber pressure discernable from the high-response pressure transducers. Isolated instances of bombs producing no measurable pressure spikes have been reported in the industry, but prior to these tests, no correlation to test parameters had been noted. At the other extreme, 20° to 25° R (11.1 to 13.9 K) above the transition temperature, peak-to-peak pressure disturbances with amplitudes as high as 150 psia (1034.21 kN/m^2 abs) and several instances of sustained instability were noted with bombs of only 4.5 grains (291.6 mg). It can be concluded from these results that the hydrogen temperature margin is a good measure of the dynamic stability of an engine.

Energy Generation: Hydrogen-Oxygen Propellants

The effects of several geometric and operating variables on the stable operating limits of a gaseous-hydrogen - liquid-oxygen rocket engine were determined in a relatively systematic manner. These results include the effects of (1) injection areas, (2) contraction ratio, chamber pressure, and weight flow per element, (3) the size of injection elements, (4) oxygen tube recess, (5) oxygen tube exentsion, (6) oxygen-injection temperature or density, (7) fluorine additive to the oxygen, and (8) film cooling.

From these results, which represent a considerable amount of data over a wide range of geometric variables and operating conditions, it was possible to obtain a correlation that explains the effect of most variables studied and provides some insight into the mechanism influencing the stability of hydrogen-oxygen engines. The best representation of the stability limit over the range of variables investigated was provided by the equation (from ref. 6)

$$\left(\frac{2g\,\Delta P_H}{\rho_H}\right)^{1/2} \rho_O (D_O)^{1.25} \left(\frac{1}{O/F}\right)^{1/2} = \mathscr{W}_{cr} \tag{1}$$

This equation describing the stability limit is considerably different from the correlation presented in reference 5, where the limit was represented by a constant value of the hydrogen- to oxygen-injection-velocity ratio. This form of the correlating equation was suggested by the response-factor model of reference 17, and its use herein is supported by the fact that it provides an improved correlation of the recessed-element data of reference 5. More details concerning the development of equation (1) are given in reference 6.

Effect of propellant injection areas. - Because propellant injection velocities were believed to play a significant role in combustion stability (ref. 2) and because design information was lacking, a matrix of 13 injector configurations was evaluated early in the overall program with hydrogen-oxygen propellants to determine the effects of injection velocities. Both hydrogen- and oxygen-injection areas were varied systematically by successively enlarging either the hydrogen flow annuli or the oxygen orifices in each of several injectors. Test details and results are given much more completely in reference 5. However, it should be noted here that the results presented in figure 11 represent transition temperatures (hydrogen) into screech for the following conditions:

Thrust chamber diameter, in.; cm	10.78; 27.381
Contraction ratio	1.9
Chamber pressure, psia; kN/m^2 abs	300; 2068.41
Thrust per element, lb; kN	48; 0.2135
Thrust (at sea level and expansion ratio of 1.3), lb; kN	20 000; 88.964

Hydrogen temperatures for transition into screech were determined for each configuration over a range of oxidant-fuel ratios from about 4 to 7. The results were cross plotted at an oxidant-fuel ratio of 5.0 and are represented by the data points in figure 11. The screech mode was predominantly first tangential (3400 Hz) with a secondary peak (4100 Hz) corresponding to a combined first-tangential - first-longitudinal mode.

The data show that the variation of the hydrogen transition temperature is nearly a linear function of the hydrogen-oxygen area ratio. As the injection area ratio was decreased, the stability improved until the transition temperature was below the minimum value obtainable with the facility (55° to 60° R or 30.6 to 33.3 K) at area ratios below about 0.5. For the conditions of these tests, then, decreasing the hydrogen-oxygen area ratio represents a solution to the screech problem, and the trend established may be of great benefit to engine designers. Although the range of engine variables over which full suppression will be achieved remains to be determined, it is important to note (fig. 11(b)) that, for these relatively fine elements the improved stability was achieved with no decrease in performance. Values of characteristic-exhaust-velocity efficiency above 0.97 percent prevailed, even to hydrogen temperatures as low as 60° R (33.3 K).

The engine designer must, of course, work within the constraints on the injector pressure drop that relate to "chugging" instability at the low values and pumping capability at the high values. As discussed in reference 5, the method of taper reaming or counterboring the ends of the oxidizer tubes may be used to retain in both a low area ratio for screech suppression and a high injector pressure drop to avoid chugging. Data encompassing these variations followed a trend similar to that shown in figure 11.

The transition data for the experiments reported in reference 5, including the variations in oxidizer tube exits just discussed, are plotted in the form of equation (1) against

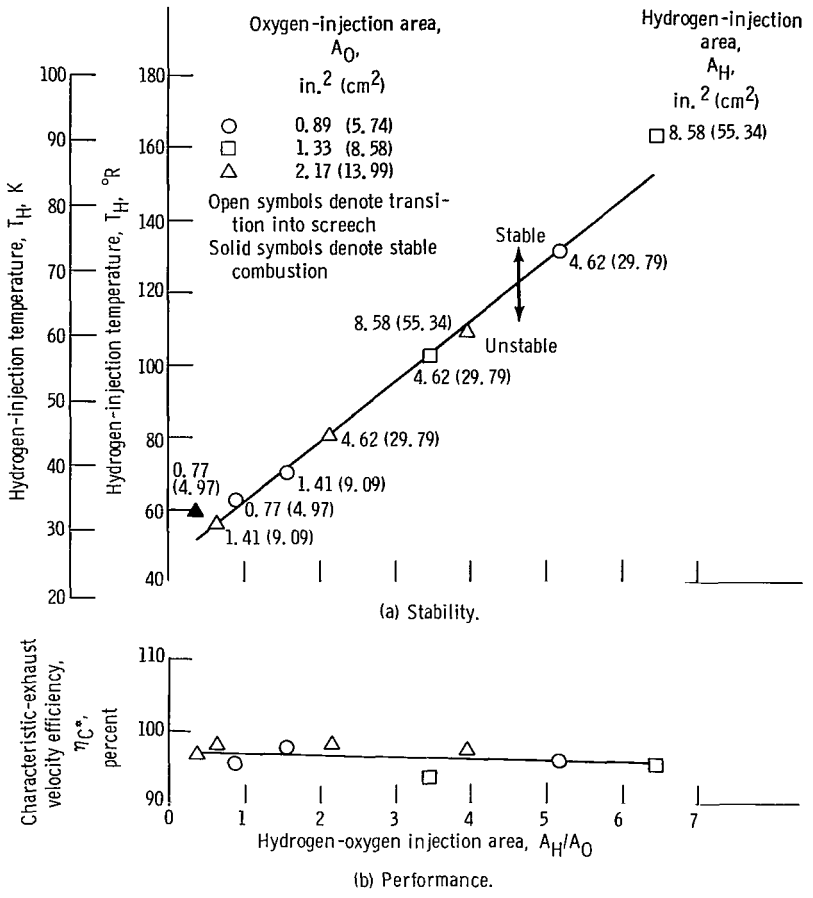

Figure 11. - Correlation of screech limits with injection area ratio. Oxidant-fuel ratio, 5.0.

the oxidant-fuel ratio in figure 12. This figure shows that all the injector variables studied are reasonably correlated by equation (1), the average value of this constant being 4.4 with a standard deviation of ±17 percent for the data.

The effect of injection area on stability can be seen more clearly from an equation written in terms of the hydrogen transition temperature. A completely general expression cannot be given because of the complex behavior of the density of cold hydrogen with pressure and temperature; however, in the range of 65° to 130° R (36.1 to 72.2 K), the interdependence is approximated by

$$P \propto \rho\left(T_H\right)^2$$

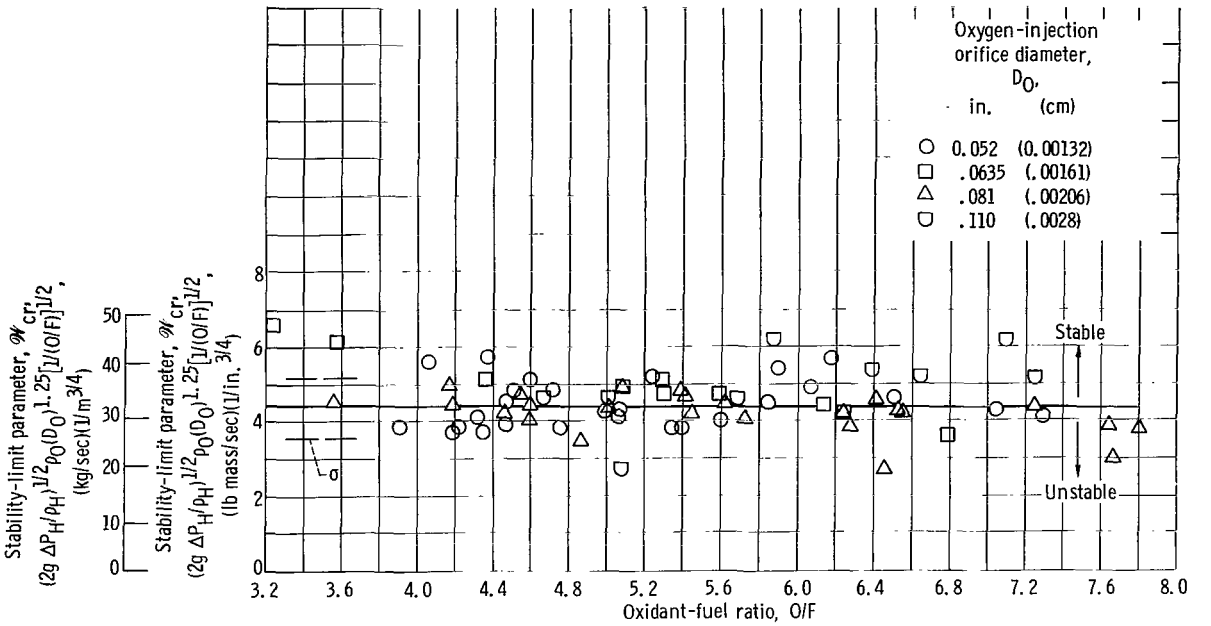

Figure 12. - Correlation of stability limits of various 421-element concentric-tube injector configurations. (Data from ref. 5.)

In this temperature region, equation (1) can be approximated by

$$T_{H,\,tr} \propto \left(\frac{P_c}{2g\ \Delta P_H}\right)^{1/2} \frac{1}{\rho_O\ D_O^{\ 1.25}} \left(\frac{O}{F}\right)^{1/2} \tag{2}$$

Considering the parameters of equation (2) related only to the hydrogen system and neglecting the minor contribution of the oxidant-fuel-ratio term enable one to see that the hydrogen-injector pressure drop is the real determinant of the screech limit at any given chamber pressure operating condition. The hydrogen transition temperature is inversely proportional to the square root of the injector pressure drop; thus, an increase in hydrogen pressure drop, which was accomplished in reference 5 by decreasing the hydrogen flow area, will lower the hydrogen transition temperature and increase the stable operating range. Also, from equation (2), the parameters that relate to the oxygen system and influence stability are the oxygen density and the oxygen jet diameter. From the data of reference 5, the variation in hydrogen transition temperature was determined to be inversely proportional to the oxygen jet diameter to the 1.25 power. The affect of oxygen orifice diameter is believed to be associated with the oxygen droplet size. The drop size produced will vary with the orifice diameter, and since the oxygen response to a pressure perturbation depends on drop size (ref. 18), the orifice diameter might be expected to exert a strong influence on stability.

Effects of contraction ratio, chamber pressure, and weight flow per element. - The atomization and vaporization of the oxygen droplets are a function of the difference in velocities of the surrounding gas and the oxygen; thus, during the latter phase of the evaporation process, the surrounding gas velocity must be influenced by the available flow area of the thrust chamber and, hence, by chamber contraction ratio. The effects of the contraction ratio on screech have been shown to be both significant and inconsistent (refs. 19 and 20). The inconsistency may be associated with the fact that it is not physically possible to isolate directly the contraction ratio as a discrete variable in an experimental study. Accordingly, a matrix of the three variables, contraction ratio, chamber pressure, and weight flow per element, was used in which different pairs were varied so that the effect of each parameter alone could be isolated. Thus, the three variables are discussed together herein and in reference 6, where more detail is given. The nominal test conditions for this matrix are presented in table I. All data were obtained for a 421-element concentric-tube injector having a diameter of 10.78 inches (27.381 cm) and an injection area ratio of 5.17.

Test series A runs were made by simple line throttling wherein the chamber pressure was varied from 125 to 380 psia (861.84 to 2619.98 kN/m^2 abs) while contraction ratio and exhaust nozzle throat area were constant. With this mode of operation, the propellant weight flow per element also varied in the same manner as the chamber pressure (as shown in table I where the values of thrust per element are based on a nozzle

TABLE I. - NOMINAL TEST CONDITIONS

Series	Chamber pressure, P_c		Thrust per element		Weight flow per element, W_t/E		Contraction ratio
			lb	kN			
	psia	kN/m^2 abs			lb/sec	kg/sec	
A	125	861.84	20	0.088	0.0635	0.0291	1.9
	190	1309.99	30	.133	.0962	.0436	↓
	300	2068.41	48	.214	.1518	.069	
	380	2619.98	60	.267	.192	.0872	↓
B	300	2068.41	20	0.088	0.0635	0.0291	4.5
	↓	↓	30	.133	.0962	.0436	3.0
			48	.214	.1518	.069	1.9
			60	.267	.192	.0872	1.5
C	475	3275.00	48	0.214	0.1518	0.069	3.0
	300	2068.41	48	.214	.1518	.069	1.9
	235	1620.00	48	.214	.1518	.069	1.5

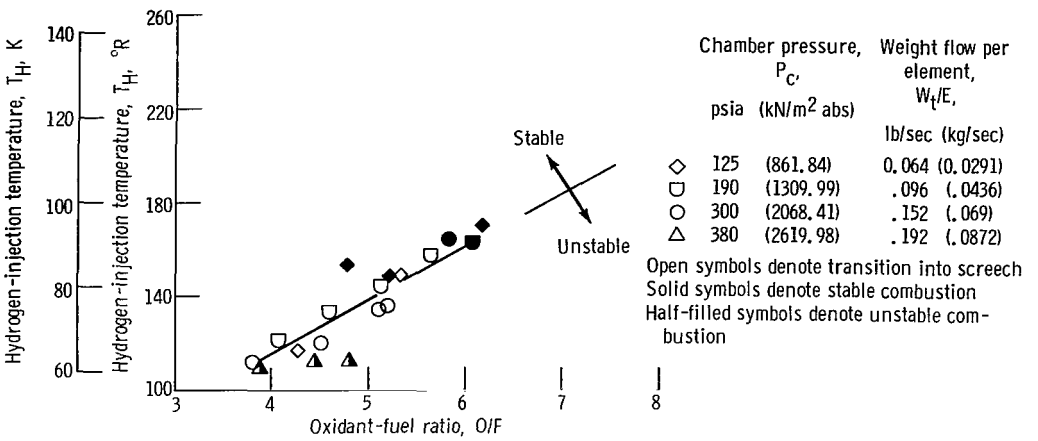

Figure 13. - Effect of chamber pressure on variation of screech-transition temperature. Contraction ratio, 1.9.

expansion ratio of 1.3). The screech characteristics are given in figure 13 which shows that, within the accuracy of the data scatter, chamber pressure (or concommitant flow per element) had no effect on the screech temperature limit.

In the series B tests, chamber pressure was held constant at a nominal value of 300 psia (2068.41 kN/m^2 abs) while the nozzle throat area was varied to change the contraction ratio from 1.5 to 4.5. The propellant weight flow per element again varied as required by the change in the nozzle throat area (ignoring secondary effects of changing combustion efficiency). When the contraction ratio was varied in this manner, a marked change in screech limits occurred as shown in figure 14. Decreasing the contraction ratio (by increasing the nozzle area at constant chamber pressure) from 4.5 to 1.5 improved stability by reducing the transition temperature from 243° to 117° R (135 to 65 K) at an oxidant-fuel ratio of 5.0.

The series C tests (table I) were run in the same manner as those of series B except that the chamber pressure was deliberately varied so that the propellant weight flow per element remained essentially constant as the nozzle area (hence, the contraction ratio) changed. (It should be noted that a contraction ratio of 4.5 could not be evaluated because of facility tank pressure limitations.) The results are given in figure 15. Again as in series B, the stable operating limit was improved as the contraction ratio was decreased from 3.0 to 1.5.

The transition data presented in figures 13 to 15 in the form of the stability parameter of equation (1) are plotted against the oxidant-fuel ratio in figure 16. Similar to the results of figure 12, the stability limit occurred at a value of the constant of 4.4. The standard deviations for these data were less than 9 percent.

With the aid of equation (2), the effects of chamber pressure, weight flow per element and contraction ratio on stability (hydrogen transition temperature) can be explained. In

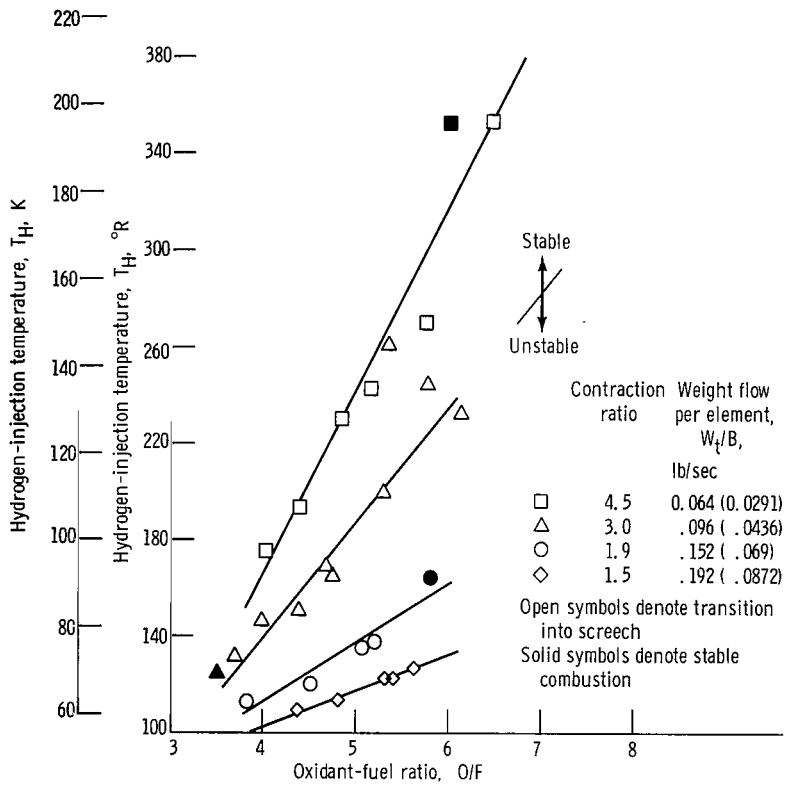

Figure 14. - Effect of nozzle contraction ratio on variation of screech-transition temperature. Chamber pressure, 300 psia (2068.41 kN/m^2 abs).

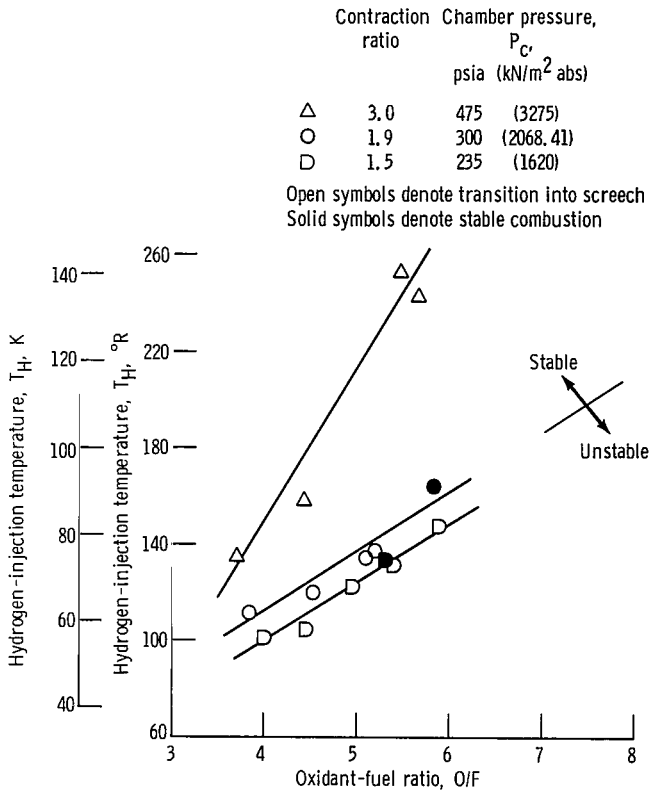

Figure 15. - Effect of chamber pressure and contraction ratio on variation of screech-transition temperature. Weight flow per element, 0.152 pound per second (0.069 kg/sec).

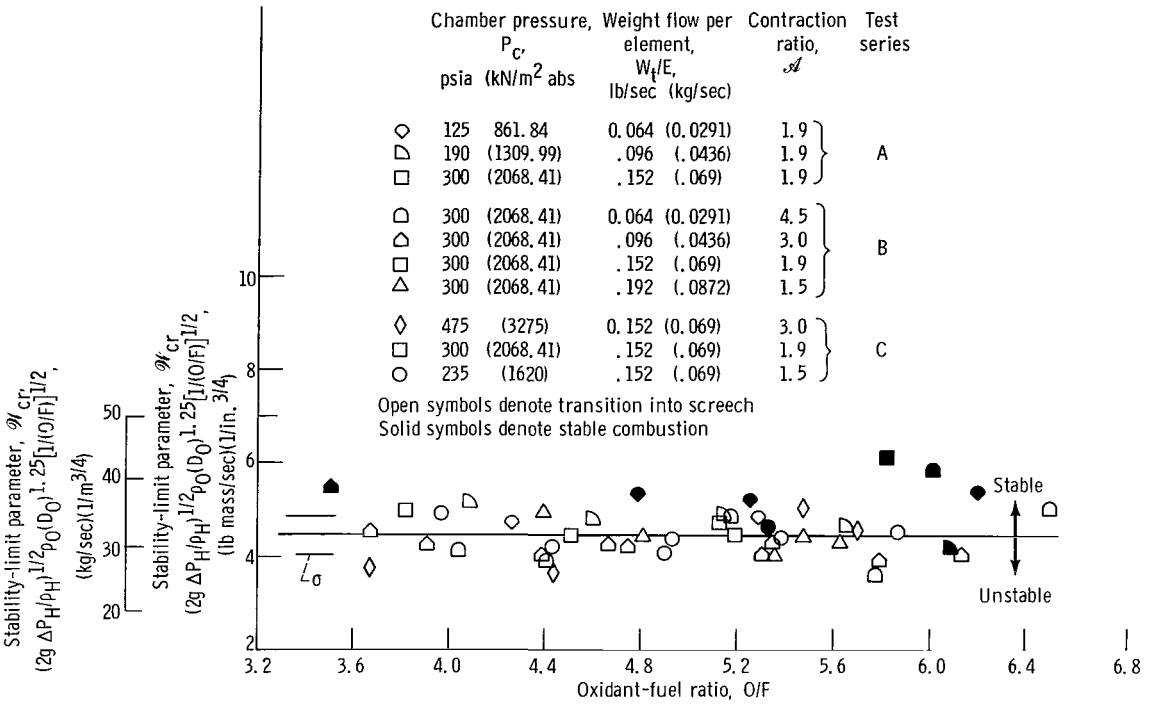

Figure 16. - Correlation of stability limits of 421-element injector of various operating conditions.

test series A (fig. 13), the three weight-flow - chamber-pressure operating conditions resulted in the same transition temperature because chamber pressure and injector pressure drop (both vary proportionally to weight flow) varied together so that the ratio remained constant. Therefore, no change in hydrogen transition temperature occurred. The contraction ratio does not appear as an independent parameter in equation (2); however, the variation of stability with this parameter results from its effect on the total propellant flow and thus on the chamber pressure or injector pressure drop. Also, since both chamber pressure and injector pressure drop vary nearly proportionally to propellant flow, it can be seen from equation (2) that the variation in transition temperature with changes in the contraction ratio will be the same regardless of which parameter is varied (as was determined in series B and C).

The combustion performance of the injector at the minimum stable hydrogen-injection temperature for each test conducted (table I) is shown in figure 17. Varying the total propellant flow to affect a change in chamber pressure (test series A) had no significant effect on combustion performance (fig. 17(a)). The characteristic-exhaust-velocity efficiency remained nearly constant at about 100 percent over the entire range of chamber pressure (weight flow per element) investigated. Examination of the results of figure 17(b) (test series B) shows that the combined effect of decreasing the total weight flow per element and increasing the contraction ratio (the free-stream Mach

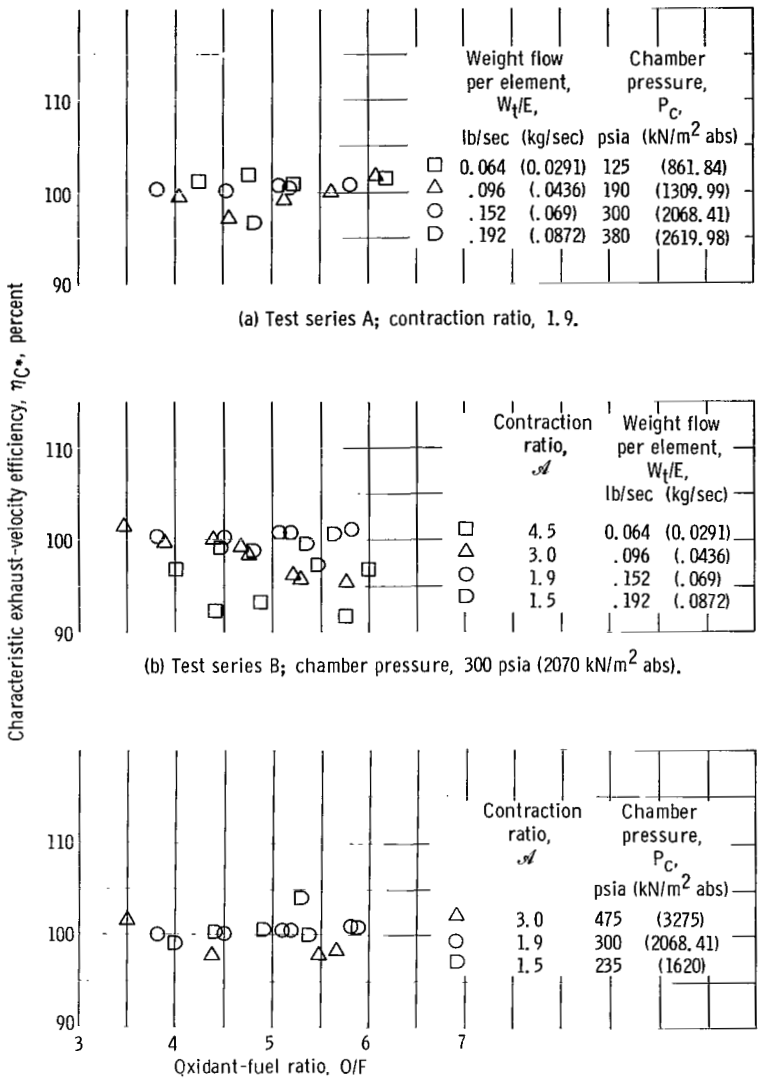

(a) Test series A; contraction ratio, 1.9.

(b) Test series B; chamber pressure, 300 psia (2070 kN/m^2 abs).

(c) Test series C; total weight flow per element, 0.152 pound per second (0.069 kg/sec).

Figure 17. - Combustion performance of 421-element concentric-tube injector at screech-transition temperature.

number) was detrimental to performance. The characteristic-exhaust-velocity efficiency of the combustor with a nozzle contraction ratio of 4.5 was about 94 percent, which represents a decrease of about 5 percent compared with the performance of the combustors with contraction ratios of 1.5 or 1.9. The loss in performance may possibly result from the change in the oxygen droplet vaporization length. Both the larger drop size associated with low injection velocities and the lower droplet-combustion-gas-velocity differential have adverse effects on vaporization length. In the data of test series C (fig. 17(c)), which also included a variation in nozzle contraction ratio, it was

difficult to ascertain any significant effect of contraction ratio on performance. A decrease in performance of about 1 to 2 percent was observed in three of the four tests with the contraction ratio of 3.0; however, this variation is about equal to the estimated accuracy of the data.

Effect of size of injection elements. - From the results just discussed in which the effect of the oxygen system on stability was established, injectors having a small number of elements and, thus, large oxygen-injection orifice diameters appear to be more stable than those having many small elements. This characteristic is of interest not only with respect to stability, but also with respect to economic considerations. The results summarized herein were obtained from references 8 and 16.

The tests of the referenced series were conducted in a 20 000-pound (88.964-kN) engine using concentric-tube injectors, the variation of the number of elements being from 8 to 992 or an equivalent variation of weight flow per element from 8 to 0.06 pound per second (0.362 to 0.0272 kg/sec). The injector stability was rated by using the minimum hydrogen-injector inlet temperature at which stable operation was obtained. These data are summarized in figure 18, where the transition temperature is plotted against the weight flow per element for an oxidant-fuel ratio of 5. The results indicate a strong stabilizing influence of weight flow per element on element size.

Injectors with 100 elements or fewer (equivalent weight flow per element greater than 0.6 lb/sec or 0.272 kg/sec) operated stably at the minimum hydrogen temperature of about 60° R (33.3 K), which was available with the facility. Further evaluation of the

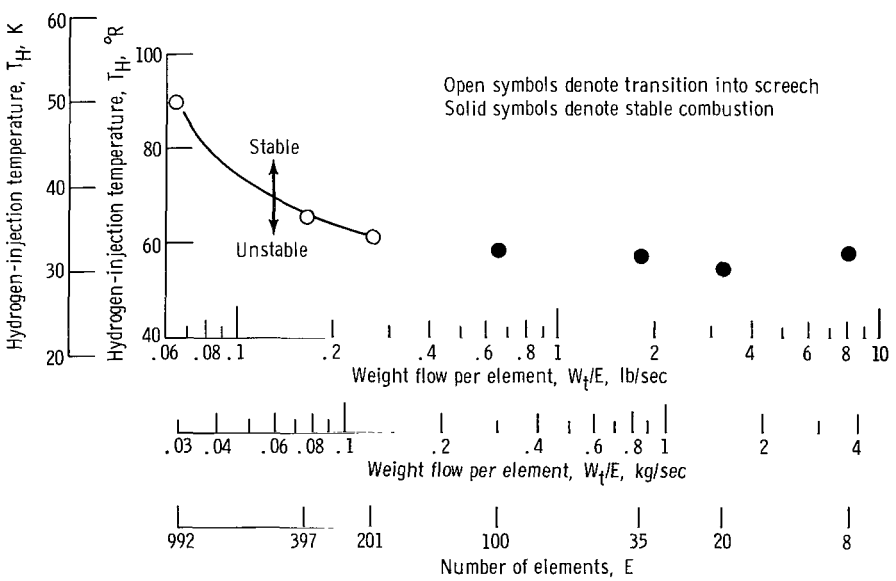

Figure 18. - Effect of weight flow per element on hydrogen-temperature stable operating limits.

stability of injectors with a high weight flow per element was made with the bomb-rating technique. The 35- and 20-element injectors were bombed with four successive charges of RDX, each of 45.23 grains (2930.8 mg) at the coldest hydrogen temperature (60° R or 33.3 K) obtainable. The resulting large pressure perturbations were successfully damped by both injector configurations.

The transition data are plotted in figure 19 in the form of the stability-limit parameter $\mathscr{W}_{cr}$ (eq. (1)). Instability was encountered for the 992-, 397-, and 201-element injector configurations at a value of $\mathscr{W}_{cr}$ of about 1.6. All other configurations (fewer number of injector elements) could not be operated at this low value. It should be noted that the present results correlated at a different value of $\mathscr{W}_{cr}$ than that of the results in figures 12 and 16. This variation is believed to be caused by changes made in the element radial distribution of the injectors used in the experiments. The results of figure 19 were obtained with 100-percent face-coverage injectors, and those of figures 12

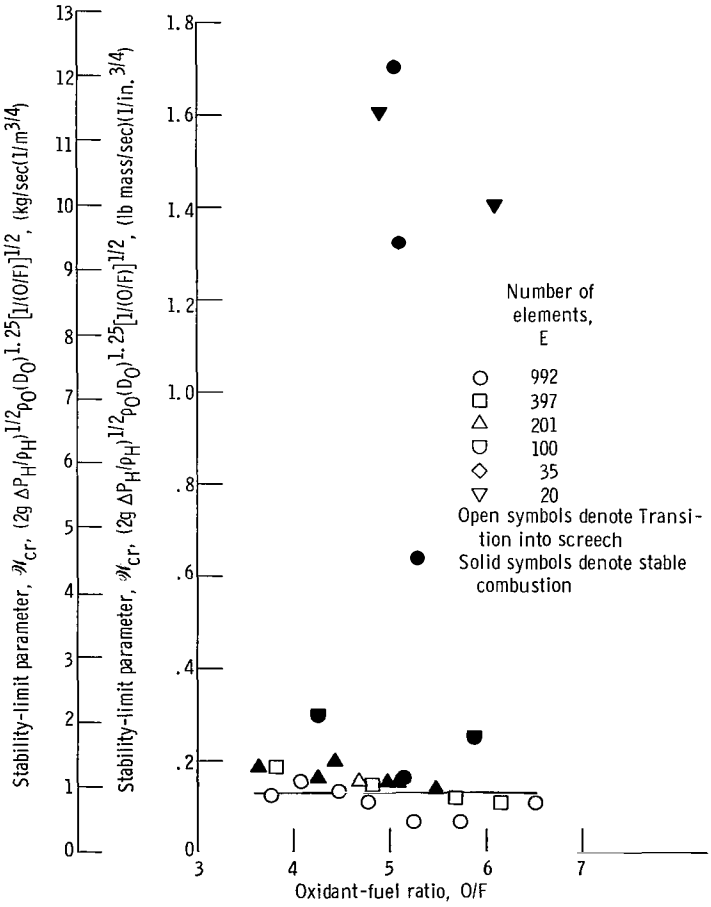

Figure 19. - Correlation of stability limits of various concentric-tube injectors.

and 16 were obtained with 85-percent face-coverage injectors. Data presented in reference 21 indicate that increasing the area void of injection elements at the periphery of the injector up to about 25 percent of the face area has a strong destabilizing effect. On the basis of these data, it is clear that the use of large elements represents a complete solution to the screech problem for hydrogen-oxygen engines in the range of sizes and chamber pressures covered; however, the utility of the technique depends also on the effects of increased element size on combustion efficiency. The combustion performance of the various injectors is shown at a hydrogen-injection temperature of 150° R (83.3 K) in figure 20 and is plotted as a function of the hydrogen-injector inlet temperature in figure 21. With reference to figure 18, complete acoustic-mode stability was achieved by increasing the weight flow per element from 0.065 to 0.65 pound per second (0.0295 to 0.295 kg/sec) with a loss in performance of only 4 percent (fig. 20). Serious performance losses were suffered at values of the weight flow per element above 0.65 pound per second (0.295 kg/sec); however, the injectors used for the study were not an end product of development and, thus, improvements in efficiency of injectors with a high weight flow per element could be made. For example, a tricentric-type element that operated at a weight flow rate of 8 pounds per second (0.362 kg/sec) per element (fig. 20) had an efficiency of 99 percent of theoretical equilibrium characteristic exhaust velocity at a hydrogen temperature of 150° R (83.3 K). Thus, it appears that a major portion of the loss associated with injectors with a large weight flow per element can be recovered by proper design. The use of relatively large elements then offers a powerful tool in the design of stably burning rocket engines.

Effect of oxygen tube recess. - During the development program for the J-2 engine, recessing the oxidizer tubes below the surface of the face plate (with concentric-tube

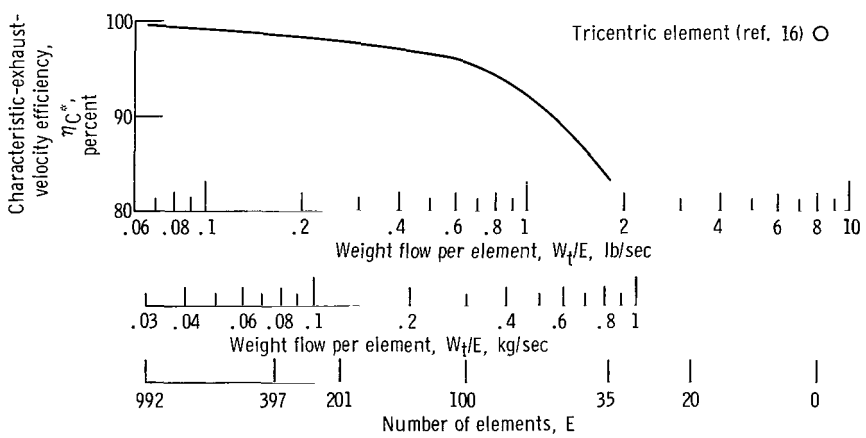

Figure 20. - Effect of weight flow per element on performance of hydrogen-injector inlet temperature of 150° R (83.3 K).

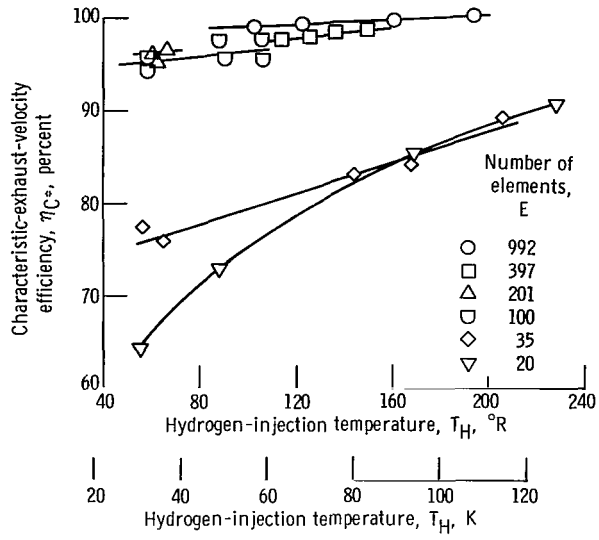

Figure 21. - Effect of hydrogen on combustion efficiency as indicated by characteristic-exhaust-velocity efficiency. Combustion chamber length, 12 inches (30.5 cm).

elements) was helpful in suppressing screech. For the investigation discussed herein, it was desirable to corroborate this finding with a rather precise rating tool (ramped hydrogen temperature) and with hardware of a different scale. Accordingly, one of the injector configurations discussed in the previous section was modified to recess the 421 oxidizer tubes about 0.1 inch (0.254 cm). The tapered hydrogen annulus around each oxidizer tube for the recessed configuration was altered to provide the same hydrogen flow area (at the oxidizer tube exit) as that of the nonrecessed configuration, thus maintaining the same velocity ratio. Results (from ref. 5) are given in figure 22(a) where the transition temperature is plotted as a function of the oxidant-fuel ratio. The data show that the 0.1-inch (0.254-cm) recess improved the stability margin by about 50° R (27.8 K) over the entire range of oxidant-fuel ratio. In addition, performance was increased by about 3 percent (fig. 22(b)).

The reason for the marked effect of oxidizer tube recess on the stability limits is that the hydraulic flow characteristics of the hydrogen system changed. Recessing the oxidizer tube below the surface of the injector faceplate caused an increase in the hydrogen-injector pressure drop, although the flow area was held constant. With reference to equation (2) (p. 20), increasing the pressure drop lowers the hydrogen transition temperature. Presented in figure 23 are values of the stability-limit parameter corresponding to the hydrogen transition temperatures for both the recessed and nonrecessed test series shown in figure 22. In figure 23, the stability limit occurred at a nearly constant value of 4.4.

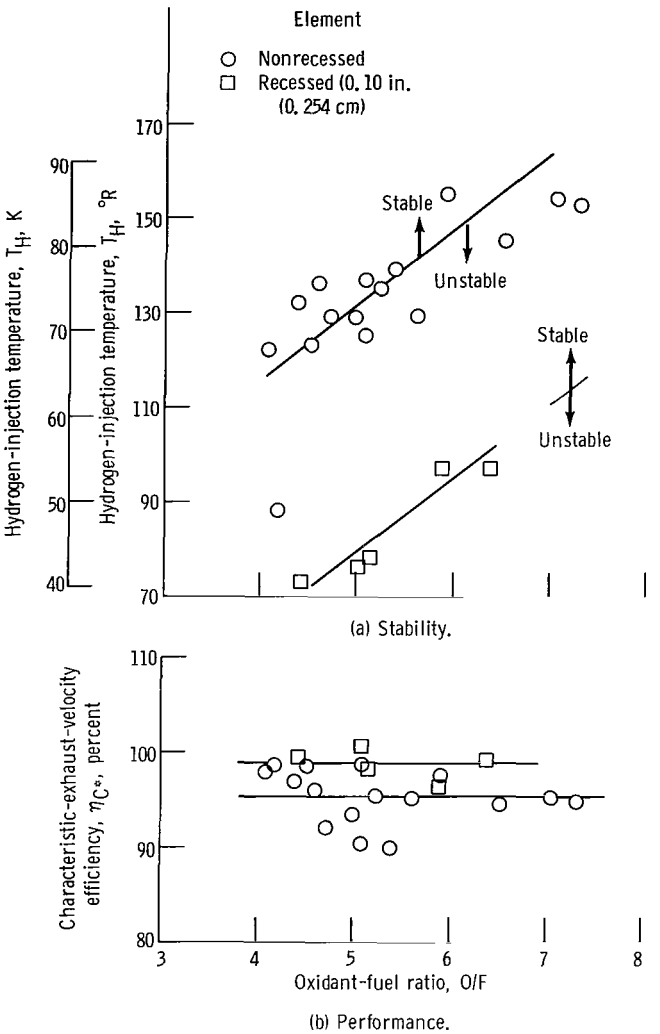

Figure 22. - Effect of oxidizer-tube recess on performance and stability of 421-element concentric-tube injector. Oxygen area, 0.89 square inch (5.74 cm^2); hydrogen area, 4.62 square inches (28.79 cm^2).

Effect of oxygen tube extension. - Very early in the program, before the effects of tube recess were known, it was postulated that, if hydrogen-oxygen engines are more stable when using warm hydrogen (as all experience had shown), a potential solution to the screech problem would be to warm the hydrogen before it contacted and reacted with the oxygen. A method for accomplishing such heating from hot gas recirculation near the injector was to extend the oxidizer tubes beyond the injector faceplate into the combustion zone. Accordingly, a 100-element injector was constructed with oxygen tubes extending 1.25 inches (3.17 cm). The tube material was a high-temperature nickel-base alloy (0.15 percent carbon, 13.0 to 16.0 percent chromium, 15.0 to 19.0 percent molybdenum,

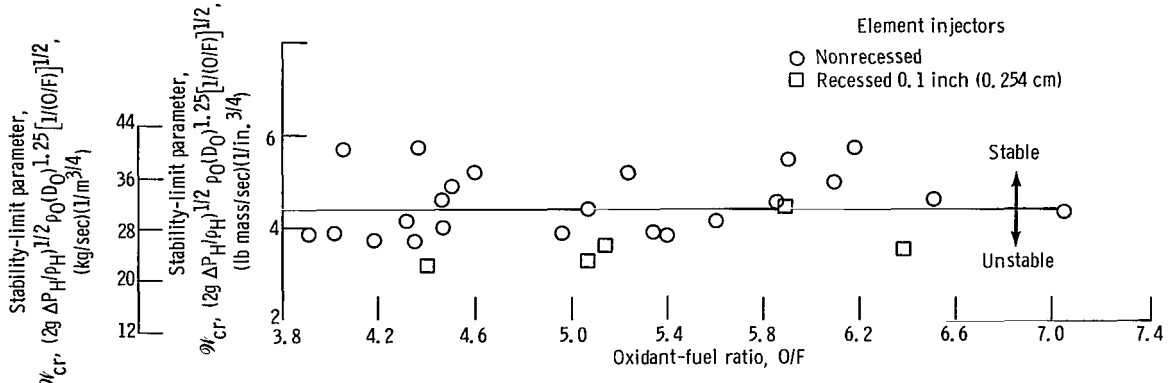

Figure 23. - Correlation of stability limits of recessed- and nonrecessed-element injectors.

3.5 to 5.5 percent tungsten, 4.0 to 7.0 percent iron). Both hydrogen- and oxygen-injection areas were kept identical to those of the unextended or flush configuration. Screech limits as a function of the oxidant-fuel ratio are shown in figure 24(a) (from ref. 7). For the flush configuration, screech occurred as the hydrogen temperature (in the injector) was ramped down to between 70° and 90° R (38.9 and 50 K). In contrast, the extended-tube configuration was stable down to the minimum hydrogen temperature available (61° R or 33.9 K) over the range of oxidant-fuel ratio covered.

The performance (as shown in fig. 24(b)) of the basic injector at transition temperature was quite low, only 91 percent at an oxidant-fuel ratio of 5.0. Extension of the injector tubes, nevertheless, further reduced efficiency to a level of about 87 percent at 80° R (44.4 K) and an oxidant-fuel ratio of 5.0. When the hydrogen temperature was further reduced to 60° R (33.3 K), efficiencies below 80 percent resulted. Thus, the tube extension of 1.25 inches (3.17 cm) resulted in significant performance losses in the configuration tested. Additional work at other lengths would be needed to determine whether or not complete stability could be retained without these performance losses.

It is noteworthy that no significant distress was apparent on the nickel-base tube extensions, which indicated their adequate durability for practical application. Thus, although extended tubes offer a complete solution for screech under the conditions tested, the performance reduction appears serious and may preclude the use of this method.

Effect of liquid-oxygen temperature. - On several occasions during the course of the screech investigation, anticipated results from an orderly series of injector variable tests were not obtained. Also, these "nonconforming" results frequently occurred when a new injector body was introduced, even though the injector faceplate design was carefully controlled. One possibility suspected was that the results were being affected by changes in the oxygen-injection temperature resulting from the differences in heat exchange with the hydrogen in the injector cavity. Since there was no known theory at the time to predict the effect quantitatively, a brief series of runs was made wherein the ox-

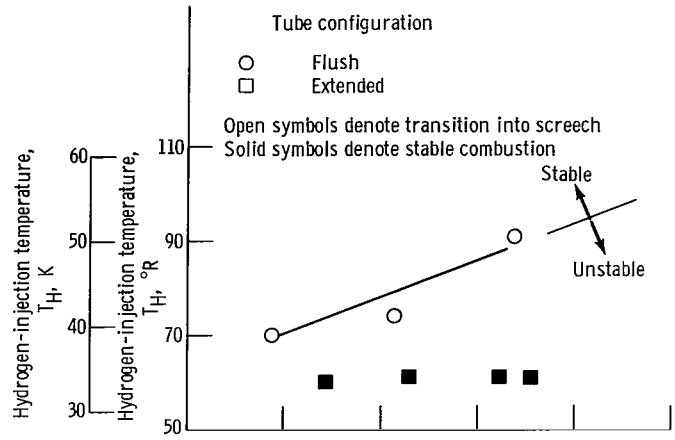

(a) Stability.

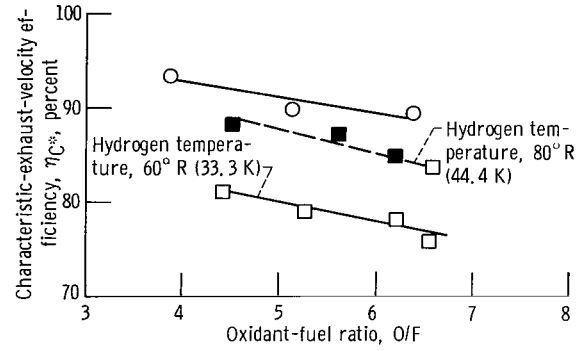

(b) Performance.

Figure 24. - Effect of oxidizer tube extension on stability and performance of 100-element injector.

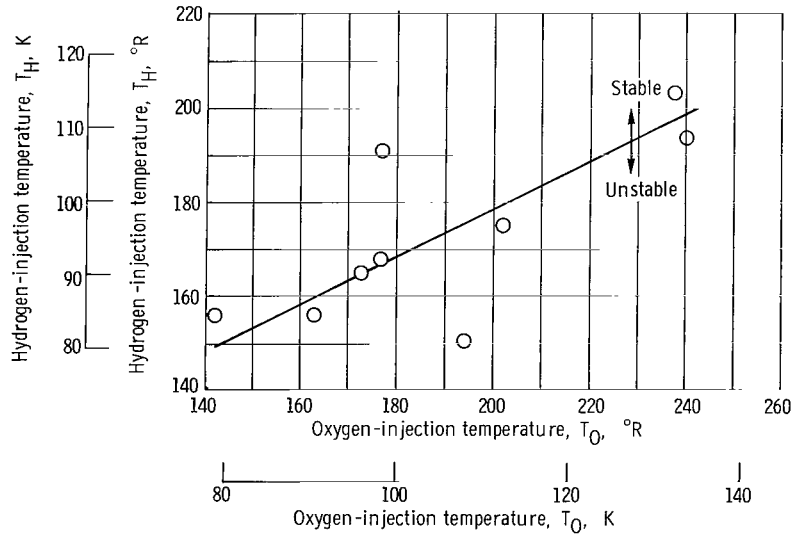

Figure 25. - Variation of hydrogen-temperature stable operating limits with oxygen-injection temperature. Oxidant-fuel ratio, 4.75 to 5.5.

ygen temperature entering the injector was varied from 140° to 240° R (77.8 to 133.3 K). The significant effect of the oxygen temperature (or density) on the stability of a hydrogen-oxygen combustor is clearly indicated in figure 25. The hydrogen screech transition temperature increased by about 50° R (27.8 K) as the oxygen temperature was increased over the range investigated.

Although it is difficult to relate this result to a theoretical model, the strong effect of oxygen temperature on stability is predictable, as can be seen in figure 26. The hydrogen screech transition temperature varies inversely proportional to the oxygen density, as expressed in equation (2). It must be noted that these data correlated at a higher value of the constant than did the results of figures 12 and 16, although the same injector was used in both investigations. The change in the value of the constant from 4.4 to 5.9 was attributed to the possible deterioration of the injector.

The significance of this finding with regard to the effect of oxygen temperature on stability is interesting from several aspects. First, it may explain some of the data scatter and even apparent discrepancies in data obtained without oxygen temperature measurements (and without precise control) in the injector cavity. Second, and more important, it implies that the injector designer should seek to tailor the oxygen-injection temperature to advantage, for example, by adding insulation between the propellants if necessary when the hydrogen from the cooling jacket is hotter than the liquid oxygen.

The third aspect relates to the theoretical implications. Why should oxygen-injection temperature have a strong effect on screech limits? One possible explanation relates to the fact that a droplet of cold (140° R or 77.8 K) oxygen must absorb about 30 percent more heat before it is fully vaporized than a droplet identical in mass injected at 208° R (115.6 K). The cold droplet would thus be expected to release its energy far-

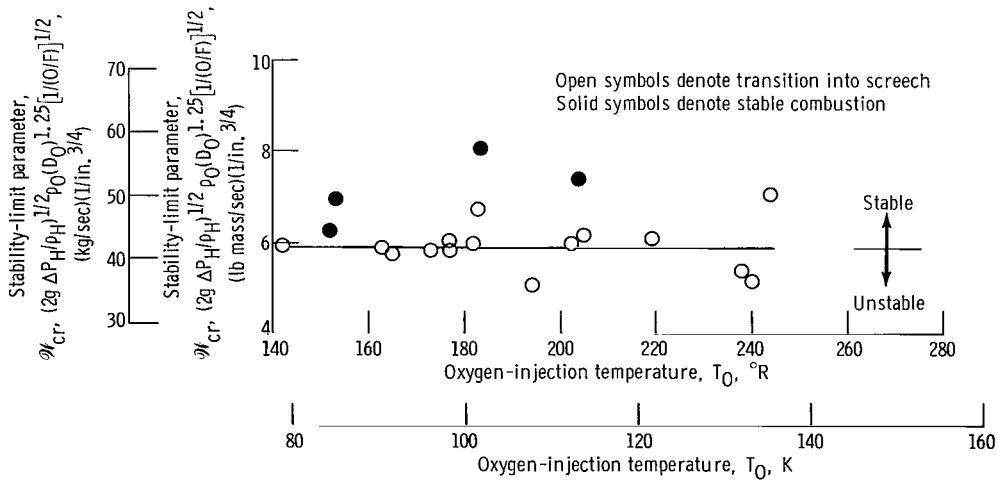

Figure 26. - Correlation of stability limits of 421-element injector at various oxygen temperatures.

ther from the injector face - a situation regarded as having a stabilizing effect. Or more likely, the cold droplet would distribute its chemical energy release over a longer axial path - a situation resulting in a more gentle heat-release gradient and thereby a possible improvement in stability (ref. 1).

Effect of fluorine additive to oxygen. - In the original formulation of the overall screech program, the matrix of variables to be examined included evaluation of the effects of propellant additives. Most of this area of work was omitted, however, when discussions revealed that personnel at the Air Force Rocket Propulsion Laboratory planned to do significant work on additives, a portion of which is reported in reference 22. However, because extensive operation with fluorine-hydrogen propellants at Lewis had never revealed screech problems and because work in the industry revealed only one known instance of screech (Bell Aerosystems), a brief series of tests was conducted (ref. 7) with fluorine (30 percent by weight) in oxygen (FLOX).

The conventional hardware and screech-rating techniques were used with the 30-percent FLOX to obtain the results shown in figure 27. For comparison, data for 100-percent oxygen are also shown. It may be concluded that, for the conditions tested, no significant effect on the screech limit occurred; however, performance improved

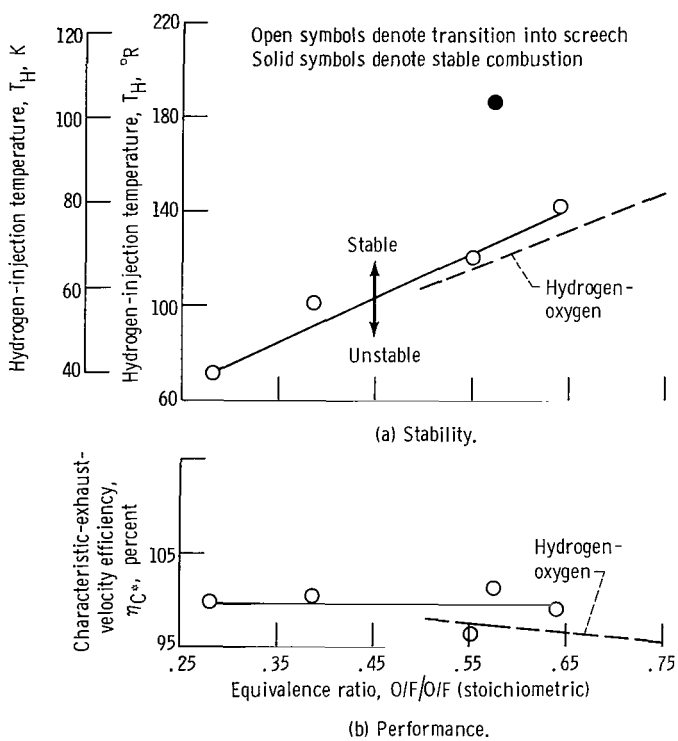

Figure 27. - Effect of fluorine additive on stability and performance of 421-element injector. Fluorine concentration, 30 percent by weight.

slightly (1 to 3 percent). From the theoretical point of view, the analysis reported in reference 22 also indicates no significant difference between fluorine and oxygen in the dynamic response of the droplet vaporization process to a traveling acoustic oscillation.

Effects of chamber wall film cooling. - In the process of designing engines for extreme environments, the designer may find it necessary to employ film cooling or resort to other less proven techniques such as thermal barrier coatings to avoid excessive chamber wall temperatures near the injector. Analysis of the M-1 engine, for example, indicated the need for 3-percent film cooling using hydrogen along the thrust chamber wall from the injector. The question then posed is what will be the effects of film cooling on stability and performance? These effects were determined by making two series of tests (ref. 7) in which a row of holes was drilled in the injector adjacent to the thrust chamber walls to divert either 10 or 20 percent of the total hydrogen for film cooling. The results obtained with this modification are compared in figure 28 with those from an identical injector tested without film-cooling holes. The screech transition temperature was not markedly affected, although at high oxidant-fuel ratios (overall) 10-percent film cooling appeared to increase the transition temperature, whereas 20-percent film cooling had no significant effect. No obvious explanation for this trend can be given.

The effects on performance were decreased(as expected) in the characteristic velocity efficiency of about 3 percent with 10-percent film cooling and 5.5 percent for

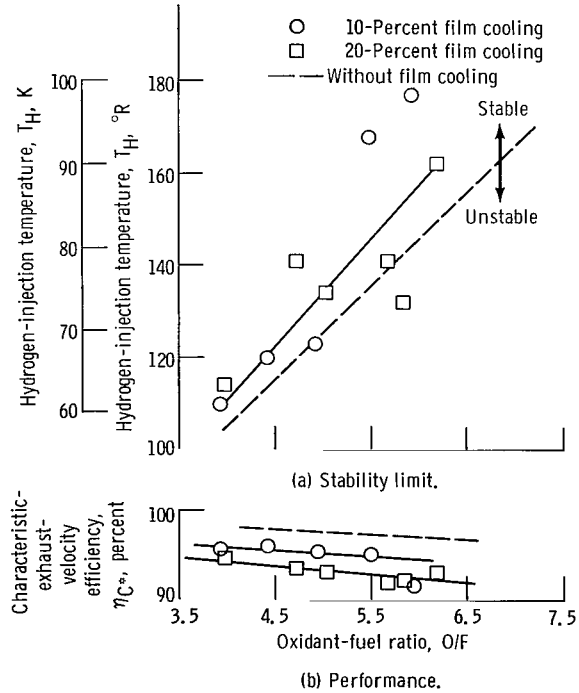

Figure 28. - Effect of film cooling on stability and performance of 421-element injector.

20-percent film cooling at an overall oxidant-fuel ratio of 5.0. These reductions were slightly greater at higher overall oxidant-fuel ratios. Thus, in the usual operating range of oxidant-fuel ratios between 5.0 and 6.0, there may be some stability loss in addition to a significant performance loss associated with the provision of film cooling. Additional information is still needed to establish the generality of these results before firm recommendations can be made.

Energy Generation: Earth-Storable Propellants

The screech investigation with earth-storable propellants (N_2O_4 plus 50 percent UDMH and 50 percent N_2H_4) was conducted with the same nominal hardware size (10.78-in. or 27.381-cm diam) as that used for the hydrogen-oxygen portion of the investigation (figs. 3 and 29). A cutaway drawing of a typical triplet injector that was used exclusively with earth-storable propellants in this program is shown in figure 7. Stability rating was done by using graduated bomb loadings (of the type shown in fig. 8) mounted tangentially in the bomb ring shown in figure 29.

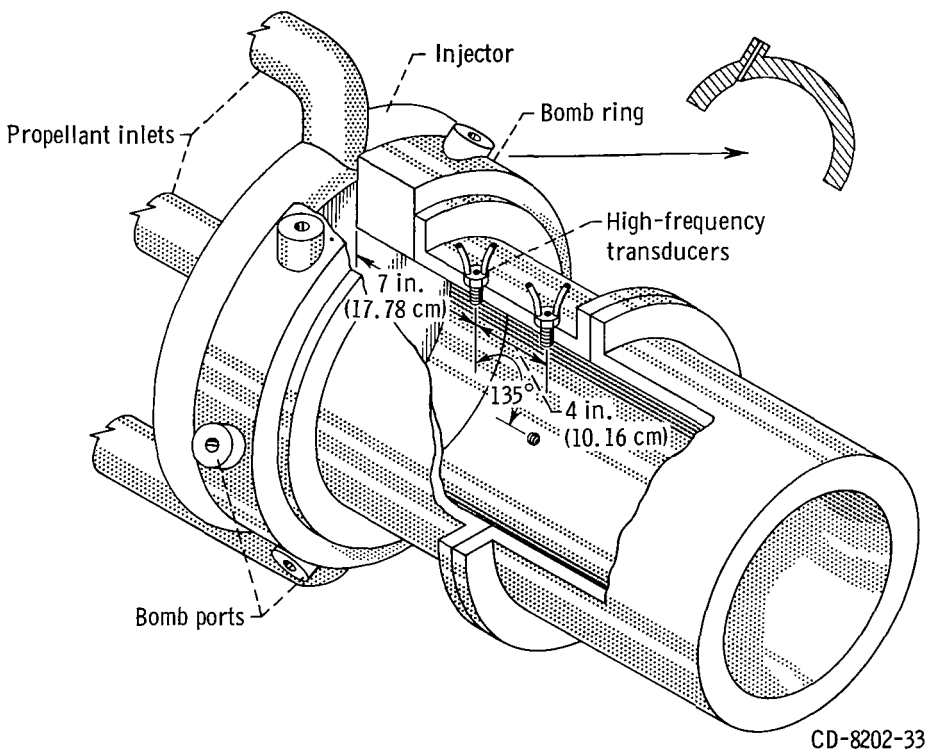

Figure 29. - Rocket combustor with bomb ring.

Attempts to use the amplitude of the initial or the maximum pressure spikes (which were usually not one and the same) produced by the bombs proved to be unsatisfactory as a stability-rating scale. A chemical augmentation by the combustion process, similar to the augmentation of pressure waves discussed in reference 23, masked the actual pressure disturbances created by the bombs and large data scatter resulted. This effect is illustrated graphically in figure 30 by a comparison made of the maximum pressure spikes of the firing and nonfiring (helium-pressurized chamber) tests. The cold-bomb data for chamber pressures of 100 and 300 psia (689.47 and 2068.41 kN/m^2 abs) resulted in two 5- to 15-psia- (34.47- to 103.42-kN/m^2 abs-) wide bands, which ranged from a mean value of 10 to 80 psia (68.95 to 551.57 kN/m^2 abs) as grain size varied from 1.6 to 41.0 grains (103.7 to 2656.7 mg). The hot-firing bomb data plotted for several runs

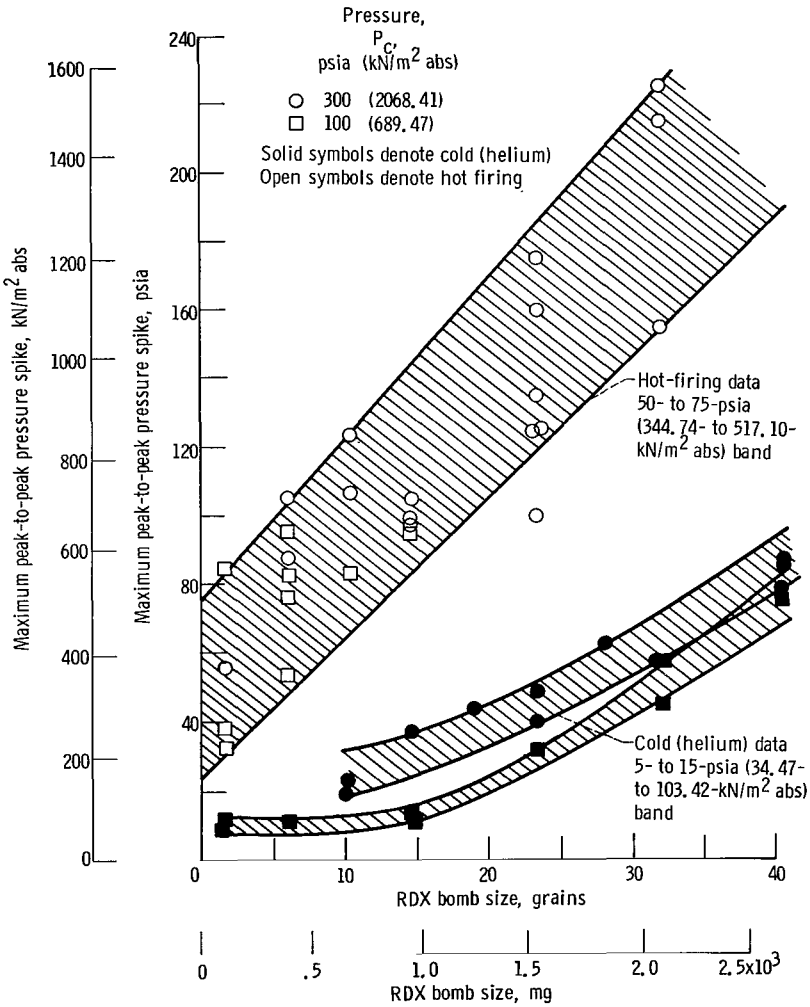

Figure 30. - RDX bomb with storable propellants.

yielded one band of 50 to 75 psia (344.74 to 517.10 kN/m^2 abs) for both chamber pressures with mean values of 58 psia for 1.6 grains (399.89 kN/m^2 abs for 103.7 mg) and 190 psia for 32.2 grains (1309.99 kN/m^2 abs for 2086.5 mg). Chemical augmentation was probably involved in the first cycle of an instability that either damped or grew. These aspects of this rating technique, as well as many other aspects, are discussed in reference 24.

In this study, for a given injector configuration, chamber pressure, and oxidant-fuel ratio, instability was repeatedly initiated by a particular bomb size. Relative stability will, therefore, be described in terms of the minimum (critical) bomb size (in grains or milligrams) required to induce screech in the combustor. The results of these tests include the effects of injection velocity, impingement angle, impingement distance, thrust per element, injector pattern, and interchanging the propellant injection arrangement.

Effects of propellant injection velocity. - At the time of these experiments, the results of the hydrogen-oxygen portion of the screech investigation indicated that injection velocities have a strong influence on combustion instability. In fact, as shown in reference 5, the stability limits of the experiments were correlated by use of the hydrogen-to oxygen-injection-velocity ratio. For the storable-propellant study, therefore, wide ranges of injection velocities and velocity ratios were investigated. Chamber pressures of 100 and 300 psia (689.47 and 2068.41 kN/m^2 abs) and oxidant-fuel ratios of 1.4 and 2.2 (fig. 31) were covered in the study. The range of injection velocity ratios, which was limited by the facility propellant systems, was approximately 0.5 to 2.5. It should be noted that the ratio of oxidizer velocity to fuel velocity (V_O/V_F) is the inverse of the ratio used in the liquid-oxygen - gaseous hydrogen studies of reference 5. This inverse ratio was used since the fuel was considered to be the controlling propellant (ref. 25).

The characteristic-exhaust-velocity efficiency η_{C^*} for stable operation and the critical bomb size required to initiate instability for the injector configurations tested are presented in figure 32 as a function of the injection velocity ratio. Shown in the figure are cross-plotted data for chamber pressures of 100 and 300 psia (689.47 and 2068.41 kN/m^2 abs) at propellant mixture ratios of 1.6 and 2.0.

Correlations using absolute and differential injection velocities were attempted, but the best correlation appeared to be with velocity ratio. At a chamber pressure of 100 psia (689.47 kN/m^2 abs) and velocity ratios less than 1.3, the combustor was marginally stable. Only the bomb initiator (1.6 grains or 103.7 mb) was required to promote instability when the configuration was not already spontaneously unstable from ignition. The trend of the data at a larger velocity ratio was toward increased stability. A charge of 6.0 grains (388.7 mg) was required to induce instability at a velocity ratio of 1.7.

At a chamber pressure of 300 psia (2068.41 kN/m^2 abs), the effect of injection velocity ratio on stability was more pronounced. A narrow band of maximum stability was found between velocity ratios of 1.0 and 1.4 within which bombs between 23.4 to 32.2

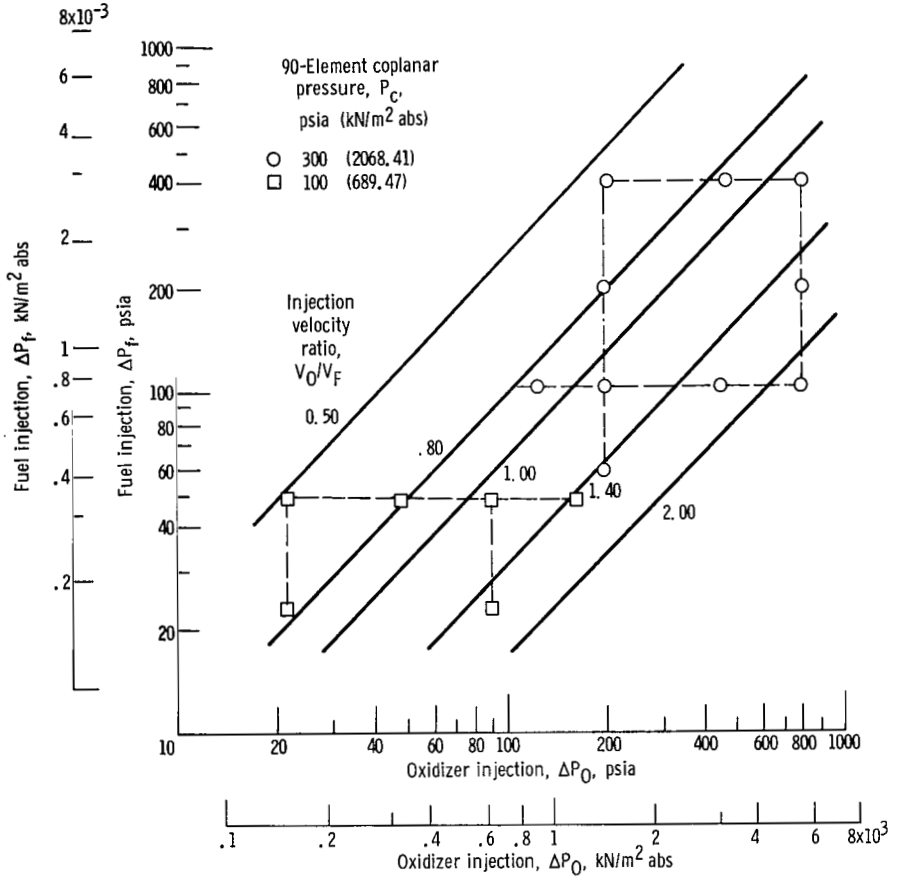

Figure 31. - Range of oxidizer-velocity to fuel-velocity ratios tested with 90-element coplanar triplet injector.

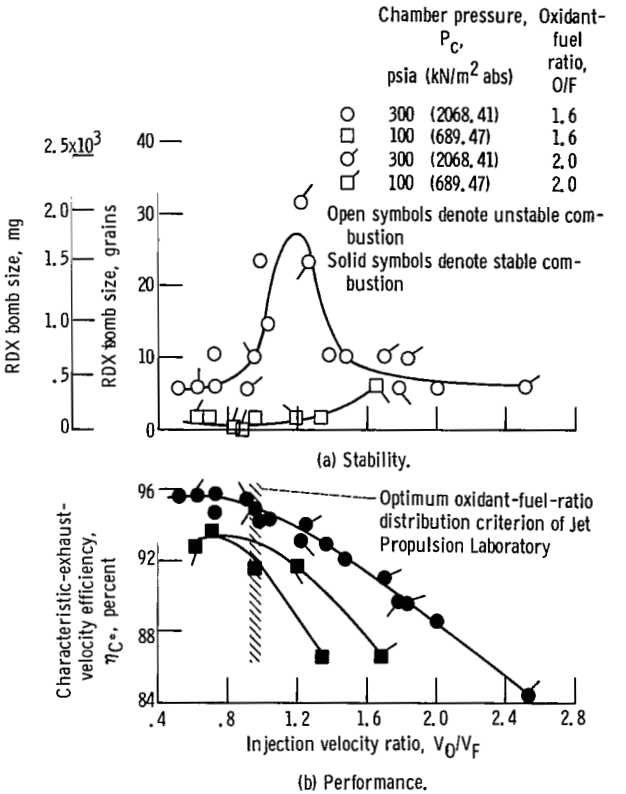

Figure 32. - Effect of injection velocity ratio on stability and performance of 90-element injector. Fuel-oxidant-fuel triplet configuration; impingement, 60° at 0.5 inch (1.27 cm).

grains (1516.3 to 2086.5 mg) were required to drive the combustor unstable. Bombs of 6.0 to 10.4 grains (388.7 to 673.9 mg) were sufficient for oxidant-fuel ratios less than 1.0 or greater than 1.4. An interesting observation was that peak stability occurred at a slightly higher velocity ratio than that for peak efficiency, and the combustor was less stable at both higher and lower levels of performance. At a chamber pressure of 100 psia (689.47 kN/m^2 abs), the performance optimized at approximately 93.5 percent, whereas the peak performance value for a chamber pressure of 300 psia (2068.41 kN/m^2 abs) was about 95.5 percent. Performance reached a maximum level for both chamber pressures between injection velocity ratios of 0.5 and 0.7, which was about 25 percent less than the ratio predicted by the Jet Propulsion Laboratory's "uniform mixture ratio distribution" criterion (ref. 26). The optimum velocity ratio for the configurations tested, based on the aforementioned criterion, was approximately 0.95. The discrepancy between the predicted and experimental values was possibly the result of the "blow-apart" phenomenon postulated for liquid-phase reacting propellants (ref. 27). However, for the limited amount of data shown in figure 32, it was observed that peak performance occurred when the fuel and oxidant stream momentums were nearly equal. For an oxidant-fuel ratio of 2.0 and a velocity ratio of 0.5 and for an oxidant-fuel ratio of 1.6 and a velocity ratio of 0.625, the propellant momentum ratio is 1. This observation suggests that efficiencies may maximize when the stream momentums are equal.

This stability behavior is in marked contrast to that exhibited by the hydrogen-oxygen combination where stability improved continuously as the velocity ratio V_H/V_O increased. In view of the different element types and hypergolicity of the storables, this contrast is not surprising. In addition to the blow-apart phenomenon, it has been shown that the storable-propellant reaction also occurs in two discrete steps (ref. 28). A much better understanding of the physical-chemical processes involved will be required before any explanation for the observed behavior can be given.

Effects of impingement angle. - The effects of the impingement angle on performance and stability were investigated by varying the angle from the 60° used in the velocity ratio study to 38° and 120°. The impingement distance of 0.5 inch (1.27 cm) from the faceplate and the injection pattern were kept constant. The ranges of chamber pressure and oxidant-fuel ratio were again 100 and 300 psia (689.47 to 2068.41 kN/m^2 abs) and 1.4 to 2.2, respectively. The effect of impingement angle variation is shown in figure 33 as a function of the injection velocity ratio V_O/V_F for cross-plotted data at a chamber pressure of 300 psia (2068.41 kN/m^2 abs) and an oxidant-fuel ratio of 2.0. As before, efficiency correlated with injection velocity ratio. It is evident that efficiency was independent of impingement angle (fig. 33(a)). Stability data, however, did not corroborate the trend found for the 60° impingement angle (fig. 33(b)); therefore, in an attempt to obtain a stability correlation, the axial and radial components of the fuel-injection velocity V_{Fa} and V_{Fr} were considered in the velocity ratio. These data are presented in fig-

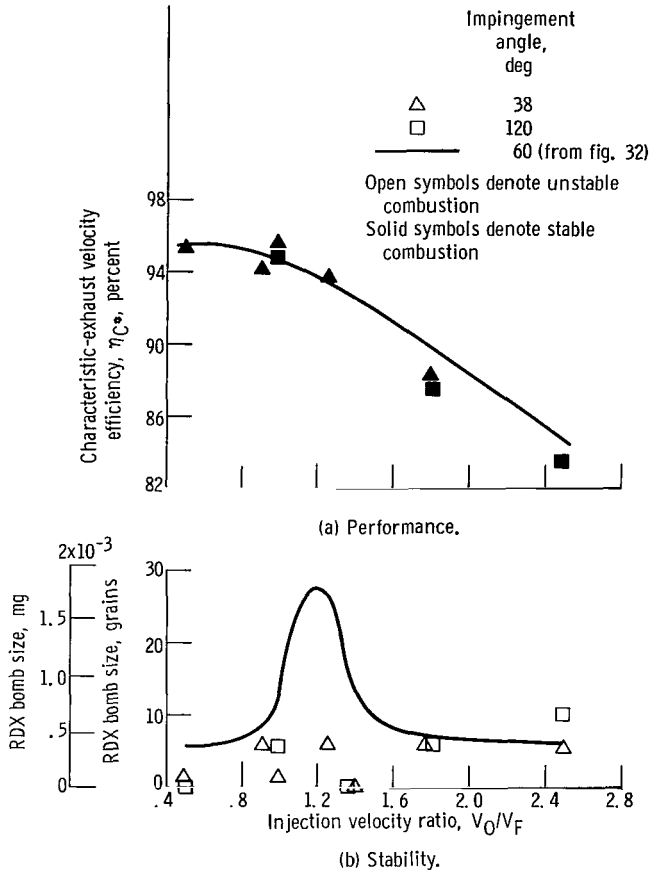

Figure 33. - Effect of impingement angle on stability and performance of 90-element injector. Fuel-oxidant-fuel triplet configuration; impingement, 0.5 inch (1.27 cm); pressure, 300 psia (2068.41 kN/m^2 abs); oxidant-fuel ratio, 2.0.

ure 34 along with the data from figure 32 at an oxidant-fuel ratio of 2.0. The better correlation was obtained with the radial component of the fuel velocity V_O/V_{Fr}, but neither correlation is strong because no configuration employing the 38° and 120° impingement angles fell in the band of maximum stability. Thus, in the range covered, there appears to be no conclusive effect of impingement angle on screech characteristics.

Effects of impingement distance. - The effects of impingement distance on performance and stability were investigated by extending the impingement distance from the 0.5 inch (1.27 cm) used in the velocity ratio study to 1.0 and 1.5 inches (2.54 and 3.81 cm), while the injection pattern and velocity ratio were held constant. The tests were conducted with both 30° and 60° included impingement angles for the 1-inch (2.54-cm) distance and only at an impingement angle of 60° for the 1.5-inch (3.81-cm) distance. The chamber pressure was 300 psia (2068.41 kN/m^2 abs) and the oxidant-fuel ratio 2.0.

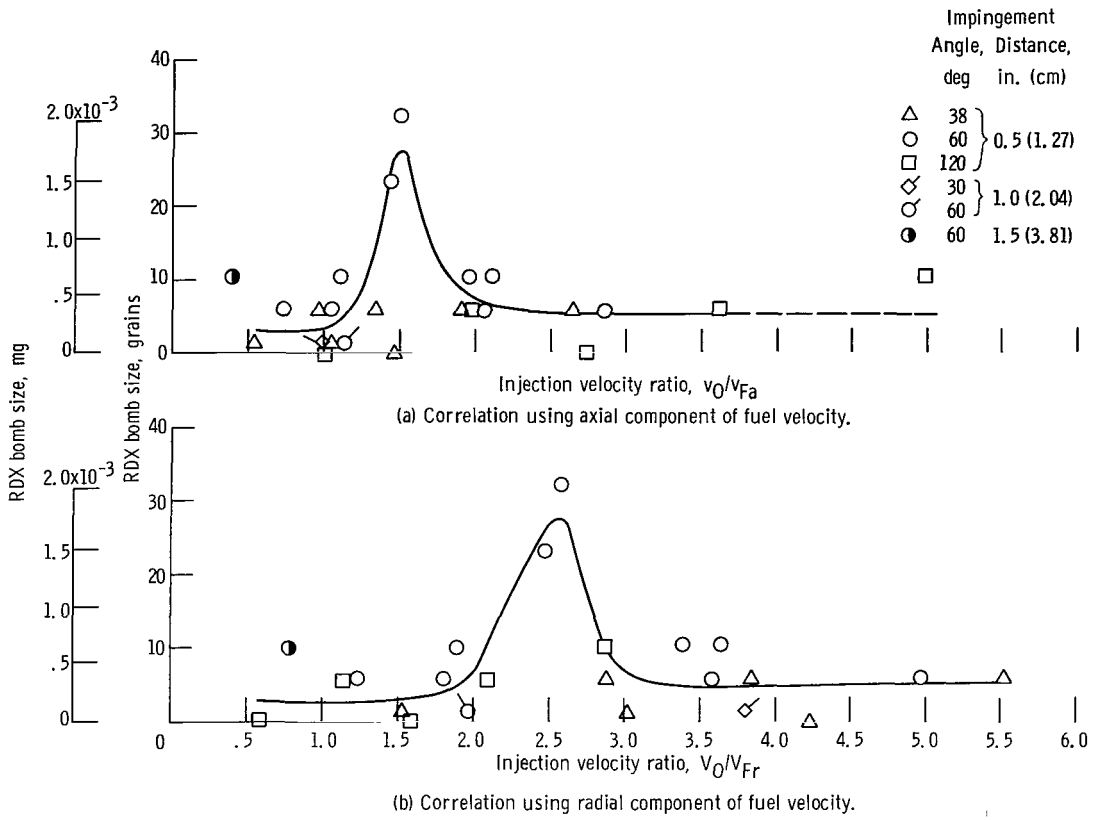

(b) Correlation using radial component of fuel velocity.

Figure 34. - Correlation of impingement angle and distance with stability of 90-element injector. Fuel-oxidant-fuel triplet configuration; pressure, 300 psia (2068.41 kN/m^2 abs); oxidant-fuel ratio, 2.0.

Again, with reference to figure 34, there appears to be only a minor effect for the configurations tested; the 1.0-inch (2.54-cm) distance appears to be less stable than the 1.5-inch (3.81-cm) distance. Performance data, which are not presented in the figure, indicated no significant effect of impingement distance. This lack of significance is perhaps surprising in view of the greater opportunity at long distances for streams to miss-impinge. However, the fact that performance was not reduced implies that the propellant mixture uniformity was not altered appreciably and, therefore, the effects on stability were also minimal.

Effects of weight flow per element. - The weight-flow-per-element investigation utilized the 60^o impingement angle and a nominal 0.5-inch (1.27-cm) impingement distance. Injectors with 50, 101, 201, and 401 elements arranged in a circular pattern (fig. 35(a)) and injectors with 52, 104, and 208 elements arranged in an alternating-grid pattern (fig. 35(b)) were tested at chamber pressures of 100 and 300 psia (689.47 and 2068.41 kN/m^2 abs) and at various injection velocity ratios. Cross-plotted data at an oxidant-fuel ratio of 2.0 are presented in figures 36(a) and (b) for chamber pressures of 100 and 300 psia (689.47 and 2068.41 kN/m^2 abs), respectively. For circular patterns,

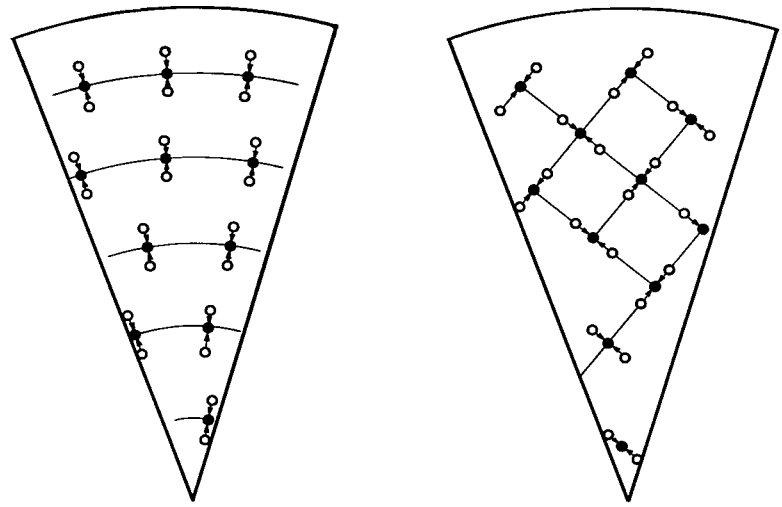

(a) 101-Element circular pattern. (b) 104-Element alternating-grid pattern.

Figure 35. - Sections of injector faces showing element patterns.

at a nominal velocity ratio of 1.8 and chamber pressures of 100 and 300 psia (689.47 and 2068.41 kN/m^2 abs), the screech limit data resulted in convex maximum curves; that is, stability and performance increased to a maximum and then decreased as the fuel mass flow per element W_F/E increased. In contrast, at a velocity ratio of 2.8 and a chamber pressure of 300 psia (2068.41 kN/m^2 abs), stability continued to increase as W_F/E increased, with a possible maximum resulting at a larger value of W_F/E than was tested. An interrelation between V_O/V_{Fr} and W_F/E is apparent in these data, and to obtain maximum stability and performance may necessitate the selection of the proper combinations of V_O/V_{Fr} and W_F/E. It was noted in the investigation that the mode of the generated instability shifted from the first radial or second tangential to the first tangential as the number of elements was decreased. This mode change is in general agreement with the sensitive time lag model in that the order of the mode decreased as the element size (drop size and thus sensitive time lag) was increased. Performance trends were similar at both velocity ratios.

Stability and performance of the alternating-grid injection patterns did not change markedly with a variation in W_F/E.

Maximum stability for the thrust-per-element study with circular patterns was not as great as that encountered in the velocity ratio portion of the investigation (discussed in the preceding paragraphs), which also used a circular pattern injector, $W_F/E = 0.33$. At least two possible explanations for this apparent anomaly are (1) that the thrust-per-element configurations were not tested in the maximum stability band since the interrelation between V_O/V_{Fr} and W_F/E was unknown and (2) that the difference in circular injection patterns used in the two investigations had an effect. The propellant distribution

variations pointed out in reference 9 are not as drastic as those reported in references 29 and 30, but the differences could still have accounted for the change in stability characteristics.

Effect of injector pattern arrangement. - As shown in figure 36, the circular pattern arrangement (where neighboring triplet fans are parallel) displayed different stability and performance trends than the alternating-grid patterns (where neighboring triplet fans are perpendicular to each other). The alternating-grid injection pattern resulted in a decrease in maximum stability and a 1- to 2-percent increase in performance (to about 98 percent of theoretical) compared with that of the circular pattern. With the grid pattern, it is possible that the blow-apart phenomenon could produce a second mixing zone; that is, fuel blown away from the oxidant jet of one element could mix with the oxidant of

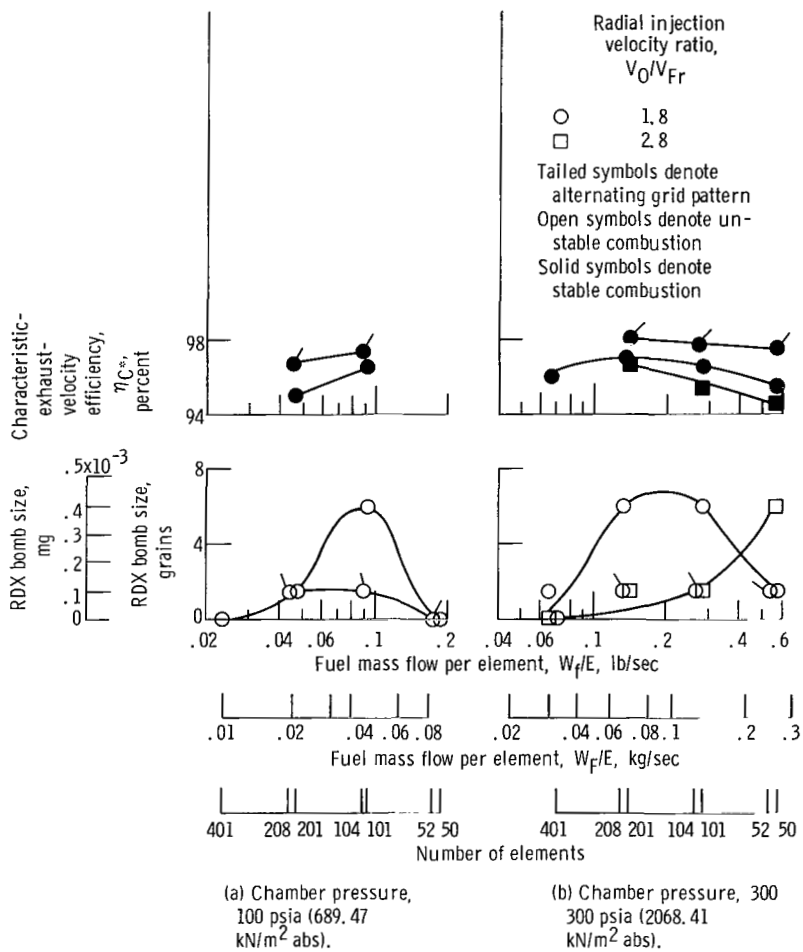

Figure 36. - Effect of fuel mass flow per element (unstable performance data not plotted) on stability and performance. Fuel-oxidant-fuel triplet configuration; impingement, 60° at 0.5 inch (1.27 cm); oxidant-fuel ratio, 2.0.

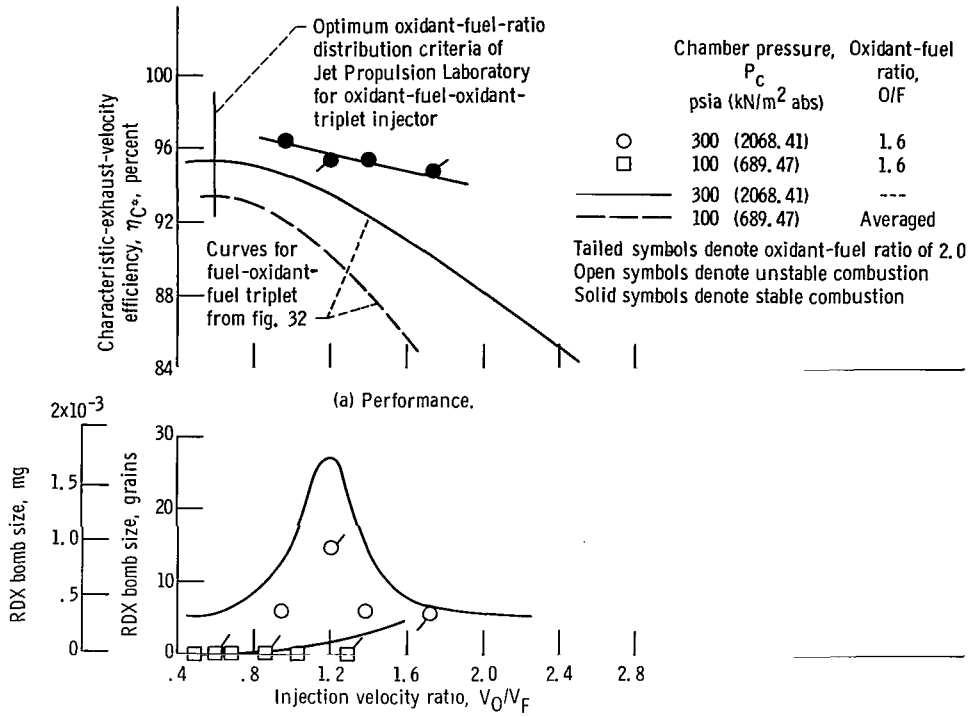

Figure 37. - Effect of interchanging propellant-injection arrangement on stability and performance of 90-element oxidant-fuel-oxidant triplet injector. Impingement, 60° at distance of 0.5 inch (1.27 cm).

a perpendicular element (fig. 35(b)). This phenomenon may be a reason for the improved performance and subsequent reduced stability.

Effect of interchanging propellant injection arrangement. - The injectors used in the velocity ratio study were primarily tested as fuel-oxidant-fuel triplets. However, some of the injectors were also tested as oxidant-fuel-oxidant triplets. Testing of the oxidant-fuel-oxidant triplets ceased early in the test program because these configurations proved to be erosive to bomb rings, chambers, and nozzles. In figure 37, the limited amount of data are superimposed on the stability limit curves of figure 32. The performance was higher and the stability was lower than for the comparable data representing the fuel-oxidant-fuel elements. No performance maximum was attained, but the curve increased toward the Jet Propulsion Laboratory (JPL) uniform oxidant-fuel-ratio distribution criterion (velocity ratio of 0.59) for the oxidant-fuel-oxidant triplet. Also, a momentum ratio of 1.0 would be obtained at velocity ratios of 0.5 and 0.625 (at oxidant-fuel ratios of 2.0 and 1.6, respectively), which are on either side of the JPL line.

Summary of Energy Generation Studies

Several injector variables that presumably affect the oscillatory energy generation process provided significant improvements in stability. In this regard, complete stabilization of hydrogen-oxygen rockets was achieved by proper selection of injection areas, size of injection element, and oxidizer tube extension. In addition to providing information useful in formulating screech-preventive measures, the results of the investigation afforded some insight into the combustion instability phenomenon, especially with respect to hydrogen-oxygen rocket engines. The contribution of hydrogen to stability is through the injector pressure drop, as shown both experimentally and theoretically. When the pressure drop becomes low enough, the hydrogen couples with and drives the chamber-pressure oscillations. Changes in hydrogen-injection areas or hydraulic flow characteristics affect the stability of the system only through changes in the injector pressure drop. Similarly, variations in weight flow per element and contraction ratio affect the stability according to their effect on the hydrogen pressure drop. In some cases, these parameters were varied enough to provide stability to the minimum hydrogen temperature attainable in the facility. In other cases, the range of the variable was large enough to show an improvement in stability but not enough to stabilize the combustor completely. It was also determined that the stability of a hydrogen-oxygen rocket is not a function of the oxygen velocity but rather the diameter of the oxygen orifice and the oxygen temperature. The oxygen droplet size varies with the orifice diameter, and since the oxygen response depends strongly on drop size, a strong influence on stability might be expected. The effect of oxygen temperature is less obvious; however, it may be associated with the physical properties of the fluid.

With earth-storable propellants, dynamic stability could not be achieved by altering any single one or a combination of injector variables. However, as with hydrogen-oxygen propellants, several parameters (e. g., injection velocities, weight flow per element, injector pattern arrangement, and propellant injection arrangement) influenced the stability characteristics.

Energy Dissipation Studies

The results discussed thus far represent the effort expended on factors likely to affect the generation of acoustic energy. As mentioned at the beginning of the RESULTS AND DISCUSSION section, another approach to minimize or eliminate screech is to increase the energy dissipation or losses of the combustion systems. The use of acoustic absorbing liners is one way to increase energy absorption, and it has the merit of probably being effective irrespective of the propellant combination. Because of the universality

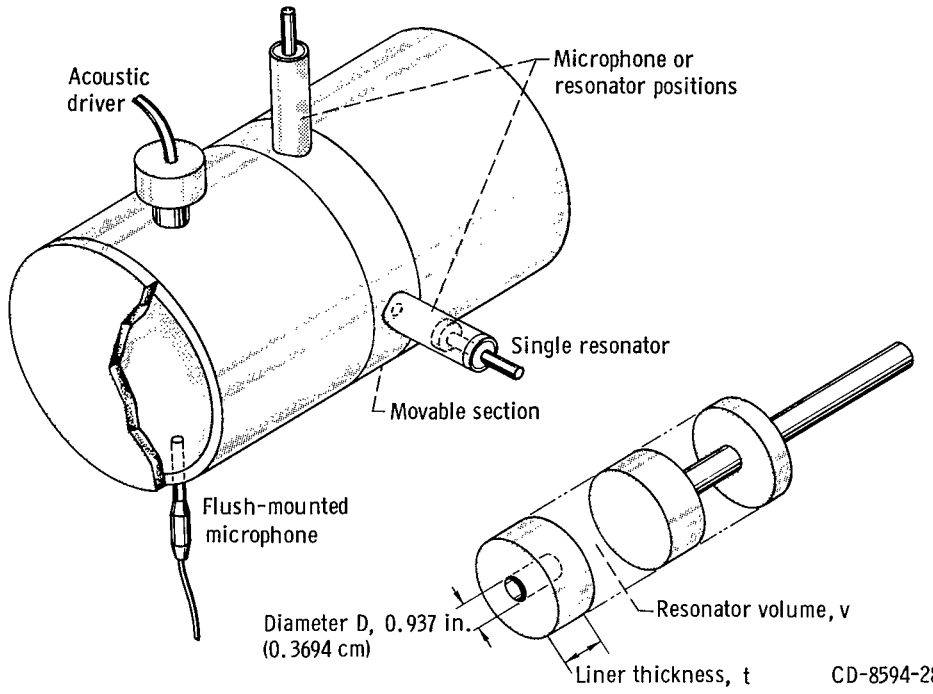

(a) Mounted on test chamber.

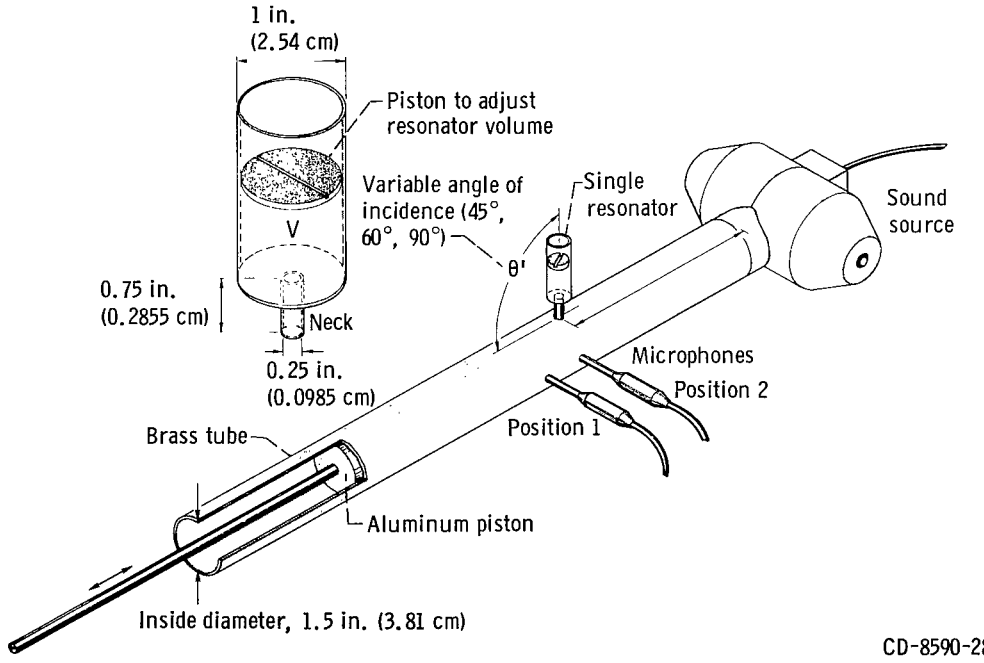

(b) Mounted on resonance tube.

Figure 38. - Single resonator.

of this approach, considerable effort has been expended on acoustic liners at the Lewis Research Center. From tests of the first liner configuration (ref. 11), it was readily apparent that liner performance was not completely predictable by theory. Therefore, to better establish a basis for later comparison of experimental results (hot) with theory, cold acoustic (bench-type) tests were conducted to confirm and extend the theory of acoustic liners. Significant results of the study (ref. 10) are presented in the following section.

Nonfiring acoustic studies. - The initial effort of the referenced study was to determine whether or not the acoustic theory and empirical studies of Morse (ref. 31), Ingaard (ref. 32), Blackman (ref. 33), and Mechel, et al. (ref. 34) could be applied to resonators of the type envisioned for rocket chamber installation.

Some of the empirical work was repeated with a single resonator, as shown in figure 38. The effects on resonator tuning and absorption of changes in resonator volume and wave amplitude were in agreement with those of previous work and are not discussed herein.

Determination of the effective neck length l_{eff} was also investigated with a single resonator and the results are presented in figure 39. The differences between the effective and the actual neck lengths are plotted against the actual neck length for the tuned condition. The results of figure 39 show relatively good agreement between theory and experiment and thus lead to a constant difference of 0.2 inch (0.508 cm) between the actual and effective neck lengths for the range of lengths tested. The equation used to calculate the theoretical l_{eff} is

$$l_{eff} = t + 0.85\, d\left[(1 - 0.7\,\sigma)^{1/2}\right]$$

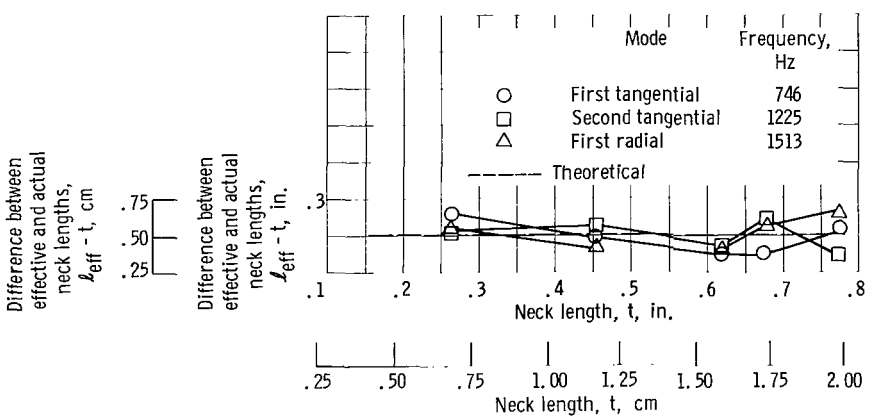

Figure 39. - Effect of neck length on effective-length correction factor for single Helmholtz resonators.

where t is the length of the aperture, d is the diameter of the aperture, and σ is the area ratio (aperture area divided by cross-sectional area of resonator cavity). The experimental l_{eff} was determined from the resonator dimensions, the input frequency, and the equation

$$l_{eff} = \frac{A}{v}\left(\frac{C}{2\pi f_o}\right)^2$$

where A is the aperture area, v is the volume of the resonator, C is the sonic velocity of the gas in the resonator, and f_o is the resonant frequency of the resonator.

The angle of incidence between the wave vector and the axis of the resonator neck was varied during the single-resonator tests. The only theory that existed (ref. 30) considered a spherical wave front traveling toward the direction of a resonator that was tilted at various angles. For an incidence angle of 90^o, the absorption was predicted to be zero. In the case of a rocket chamber, no knowledge existed as to the effect of the angle of the resonator neck in the presence of an acoustic mode. The results of varying the angle between the wave vector and the axis of the resonator neck (shown in fig. 40) indicate no change in absorption with incidence angle in the range covered from 45^o to 90^o.

Other empirical work reported in reference 10 was done with the apparatus shown in figure 41. The acoustic liners could be tested with the test section ends closed, or they could be tested as part of a wind tunnel to simulate the combustion gases flowing past the resonators. The damping effects of the following acoustic-liner design parameters were evaluated: (1) number of resonators, (2) liner cavity partitions, (3) alternating rows of different aperture diameters, and (4) mean flow past apertures. Parameters related to tuning, such as the open area ratio, liner thickness, and backing distance, were also investigated. Their effects were according to theory, as were those of the single resonators, and therefore are not discussed herein. One phenomenon that was encountered immediately in the liner investigation was the shift of the chamber resonant frequency away from the liner resonant frequency. These results are presented in fig-

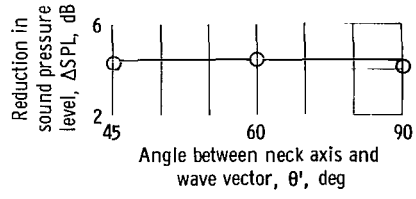

Figure 40. - Amplitude drop with resonator at incidence angles of 45°, 60°, and 90° (ref. to 10^{-4} μ bar).

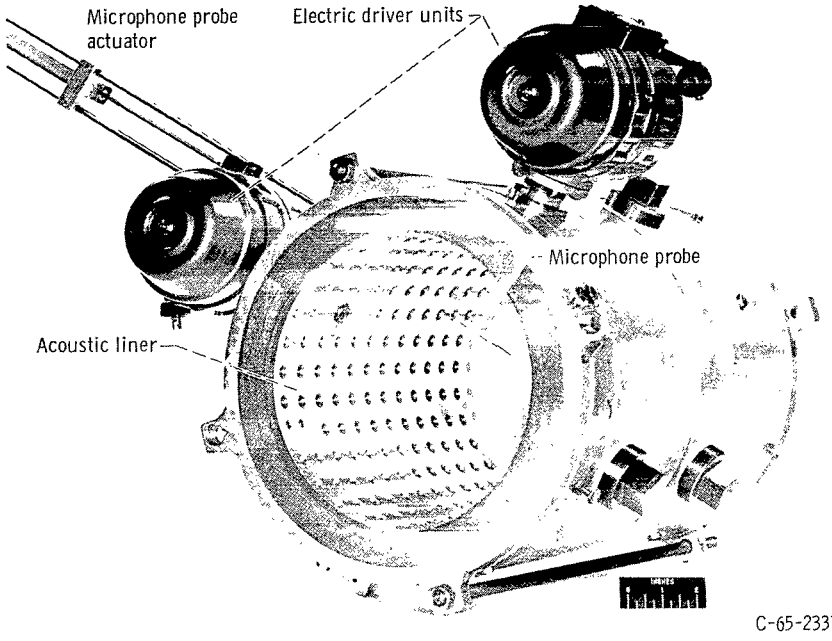

Figure 41. - Test section with acoustic liner.

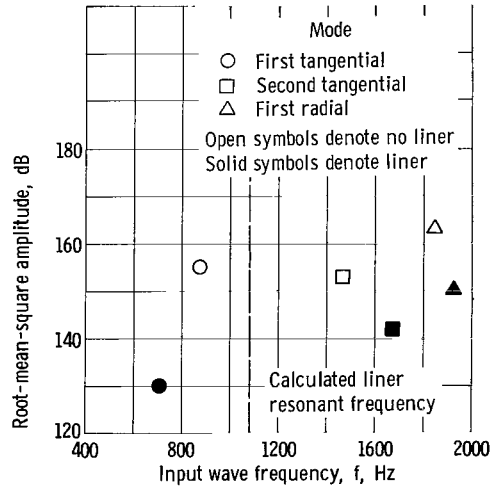

Figure 42. - Frequency shift and amplitude decrease for liner in closed-end test section. Liner thickness, 0.60 inch (1.52 cm); perforation, 5/16 inch (0.794 cm); open area, 10 percent; complete partitions; liner resonant frequency, 1051 hertz.

ure 42, where amplitude is plotted as a function of frequency. The frequency of the resonant mode of the test chamber without a liner differs from that with a liner, and it shifts away from the calculated liner resonant frequency. This result, explained by Phillips (ref. 10), is attributed to the change in the chamber wall impedance from infinite to finite when the liner is installed.

The effect of the number of resonators on damping is shown in figure 43. Axial unmasking produced an almost linear increase in damping with the number of resonators uncovered (fig. 43(a)). This increase is caused by the uniform axial distribution of the tangential modes in the test chamber, which would not be true for a rocket combustor with a localized region of high-pressure oscillations (where some axial positions would be more important than others). The circumferential unmasking (fig. 43(b)) was initiated in the region of a pressure antinode, and the change in damping with the number of resonators (slope of the line) was initially steep. Resonators 10 to 20 are in the region of the pressure node and, therefore, no large increase in damping occurred until resonators 25 to 30 were unmasked, and the slope of the line again increased. These results verify that resonators are effective only when positioned at or near the pressure antinodes.

The data of figure 44 show the effect of partitioning the liner cavity volume. The purpose of the partitions was to prevent a tangential wave from inducing a similar wave behind the liner, which might affect its performance. The data presented confirm that apparent induced tangential motion of the gases behind the liner affects tangential-mode damping. When longitudinal partitions were installed, damping increased markedly for the tangential mode. Radial-mode damping was unaffected by partitions, as expected. Since the radial wave is normal to the wall, no induced flow (into one aperture and out

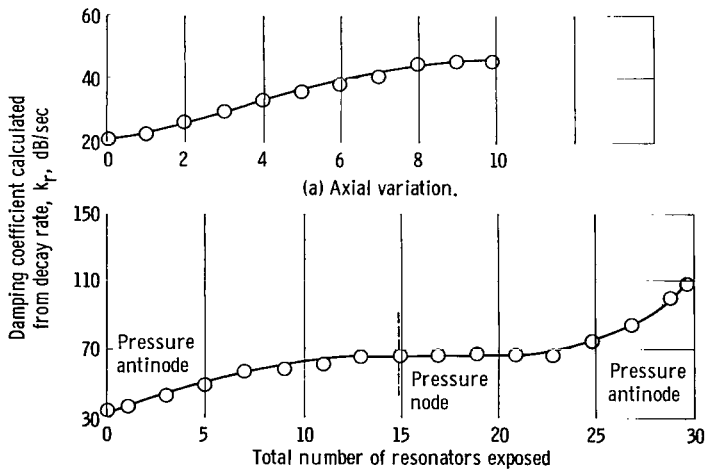

(a) Axial variation.

(b) Circumferential variation.

Figure 43. - Effect of variation in maximum number of resonators on damping in closed-end test section.

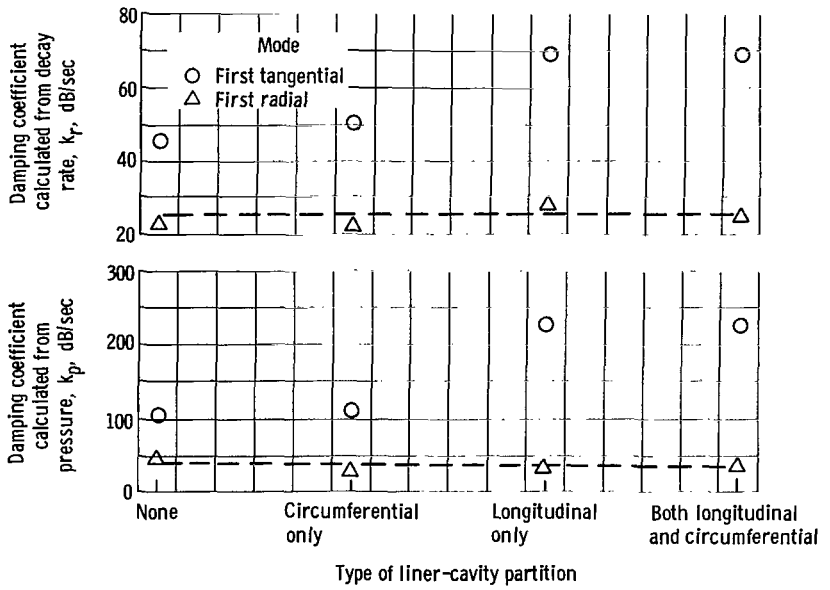

Figure 44. - Comparison of damping coefficients based on both pressure and decay rate for first tangential and first radial modes of oscillation with various conditions of backing cavity isolation. Electrical drivers; liner thickness, 0.45 inch (1.143 cm); hole diameter, 5/16 inch (0.794 cm); flow velocity, 0; hole spacing, 1 inch (2.54 cm); backing distance, 0.55 inch (1.397 cm).

others) was foreseen. This test was the first to demonstrate the effect of liner partitions on damping.

Since the variation of both the open area ratio and hole diameter produced results that were confirmed by theory, it was suggested that broader band absorption might be accomplished by alternating rows of holes of two different diameters on a single liner. The results of figure 45 show that a liner formed by two arrays of 5/16-inch (0.794-cm) and 3/8-inch (0.953-cm) holes behave as an average of two different liners, each with only one hole diameter. This finding has since been confirmed by work reported in reference 35.

The results of experiments to find the effect of mean flow past the liner apertures are presented in figure 46. The results for the first radial mode (fig. 46(a)) show good agreement with theory and with each other, which indicates the validity of the expressions from reference 34 for predicting the effect of mean flow. Shown in figure 46(b) are the results for the first tangential mode. (Note that, when based on Mach number equivalence, these velocities of up to 160 ft/sec (48.77 m/sec) (fig. 46) correspond to much higher velocities in a rocket combustor.) The inadequacy of the design equations to explain the peak in experimental absorption at 80 feet per second (24.38 m/sec) probably results from a hole-spacing flow interaction. The interaction effect would probably not occur in a conventional rocket chamber with combustion gas velocities of 1500 to 3000 feet per second (457.20 to 914.40 m/sec) because the pseudofrequency will fall an

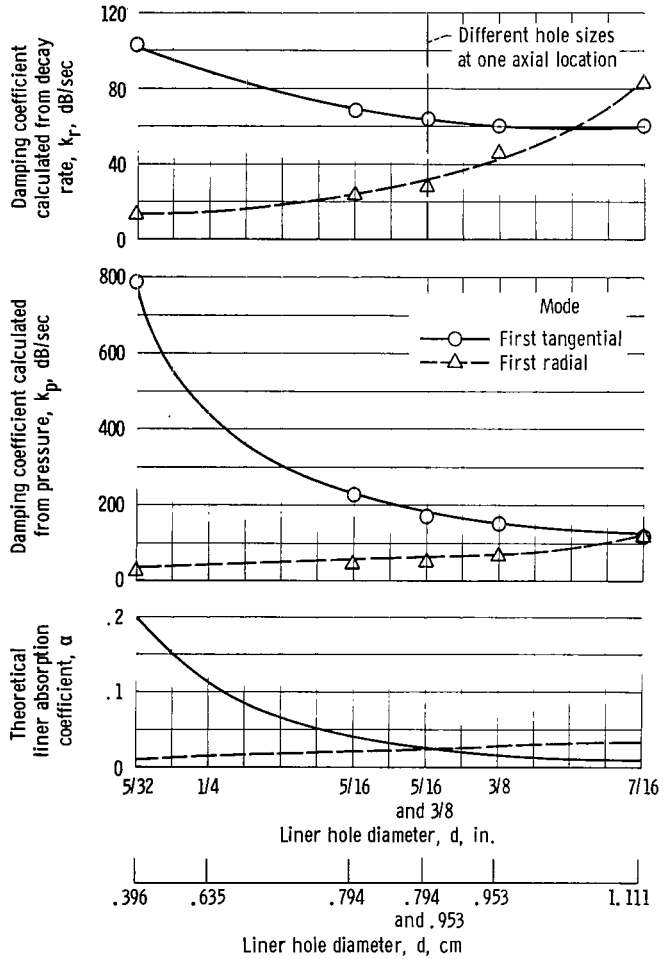

Figure 45. - Comparison of damping coefficients based on both pressure and decay rate and theoretical absorption coefficient as functions of hole diameter for first tangential and first radial modes of oscillation. Effect of two hole sizes (5/16- and 3/8-in. (0.794- and 0.953-cm) diam, spaced 1 in., 2.54 cm, apart) on one liner is shown. Liner thickness, 0.45 inch (1.143 cm); back distance, 0.55 inch (1.397 cm); hole spacing, 1 inch (2.54 cm); mean flow velocity past liner, 0; circumferential and longitudinal partitions.

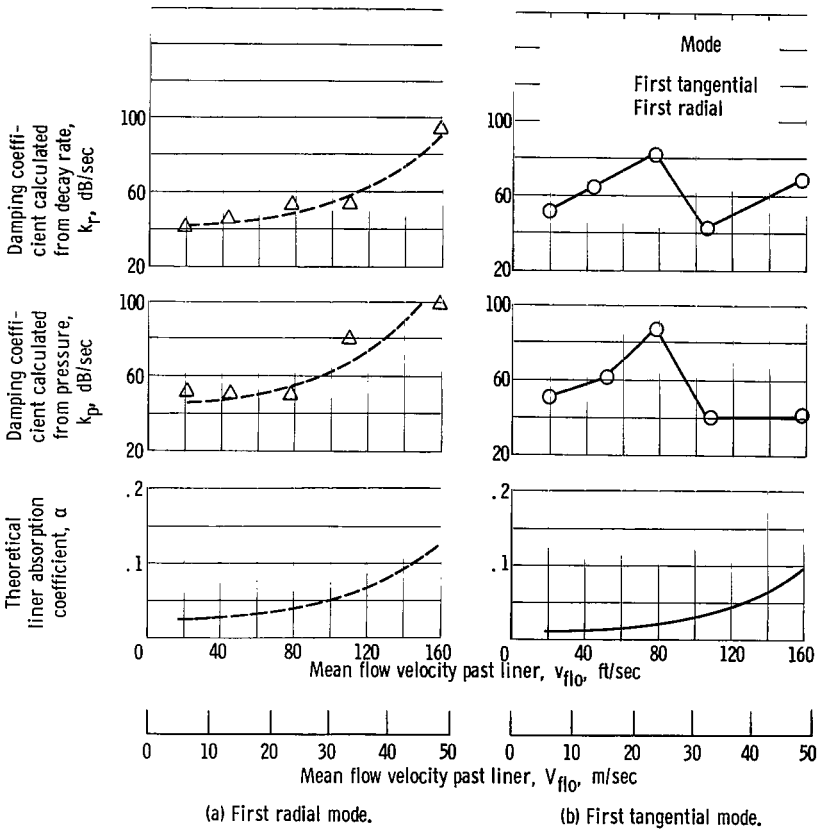

(a) First radial mode. (b) First tangential mode.

Figure 46. - Comparison of damping coefficients based on both pressure and decay rate and theoretical absorption coefficient as functions of mean flow velocity past liner for first tangential and first radial modes of oscillation. Liner thickness, 0.45 inch (1.143 cm); back distance, 0.55 inch (1.397 cm); perforation, 5/16 inch (0.794 cm); hole spacing, 1 inch (2.54 cm); partitions, circumferential and longitudinal.

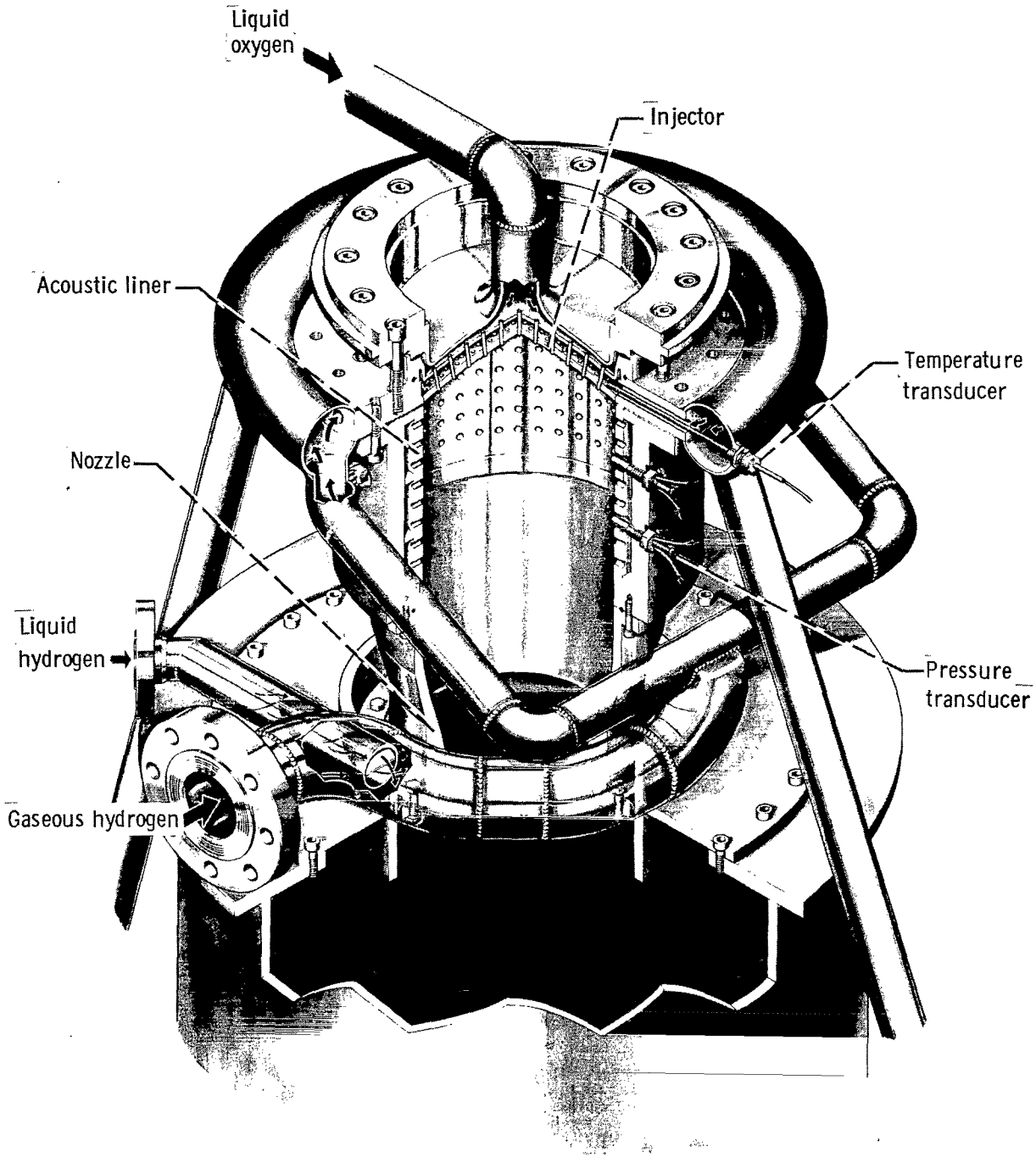

Figure 47. - Engine assembly for liner evaluation with hydrogen-oxygen propellants.

order of magnitude above most common screech modes. Thus, the present set of design equations appears adequate to account for the effect of flow.

Liner application in hydrogen-oxygen-propellant rocket engines. - The engine assembly used to investigate screech-suppression characteristics of acoustic liners with hydrogen-oxygen propellants is shown in figure 47. Nominal 10.78-inch- (27.381-cm-) diameter hardware that produced 20 000 pounds (88.964 kN) thrust at a chamber pressure of 300 psia (2068.41 kN/m^2 abs) was used. Acoustic liner configurations of several open area ratios, liner thicknesses, and aperture shapes (fig. 48) were used, and results are given in detail in reference 11. The effects of liner configuration on stability are expressed in terms of the effects on hydrogen transition temperature.

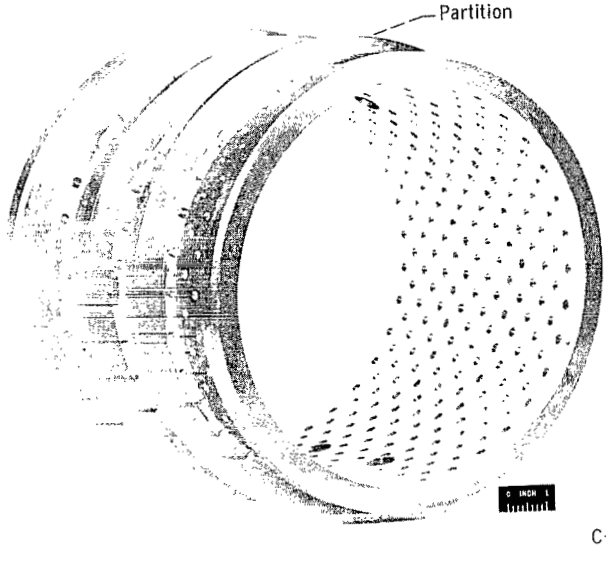

(a) Circular apertures.

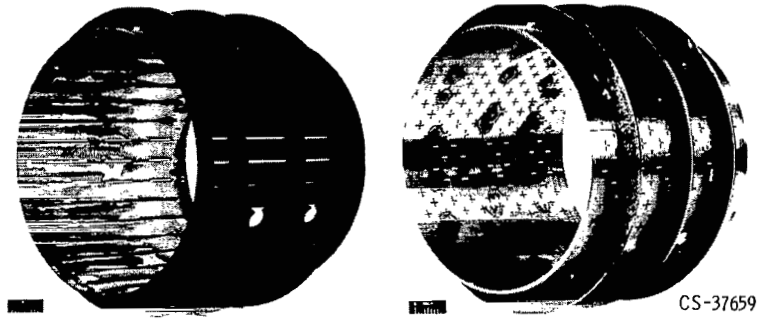

(b) Slot-shaped apertures.

(c) Cross-shaped apertures.

Figure 48. - Types of perforations evaluated.

Several instances have been reported where unstable engines have been made stable by the use of acoustic liners; however, in some cases the engines were operating quite close to their screech limit before the liner was installed. In the tests discussed herein, the injector was purposely selected to have a relatively high hydrogen temperature screech limit to provide a severe test of the liner contribution and thus allow separation of the effects of several liner variables. Results obtained without a liner (dashed curve in fig. 49) show the screech limit to be at a hydrogen temperature of about 110° R (61.1 K) at an oxidant-fuel ratio of 5.0. The predominant screech mode was first tangential (3250 Hz) with a peak-to-peak amplitude of 140 psi (965.26 kN/m^2). Data obtained at four open area ratios for several liners having circular 1/4-inch (0.635-cm) holes are given. The use of a liner having 20 percent open area improved the screech limit from about 110° to about 90° R (61.1 to 50.0 K). Both 5- and 15-percent open-area liners showed marginal stability near 60° R (33.3 K), which was the minimum hydrogen temperature possible with the facility. The configuration having 10 percent open area could not be driven unstable at the lowest hydrogen temperature available. Although hydrogen temperatures below 55° to 60° R (30.6 to 32.2 K) in the injector were not attainable, it is obvious that properly designed screech liners provided a powerful tool in improving stability and may represent on further evaluation a complete solution to the problem.

Although it was apparent that an optimum open area ratio existed at about 10 percent, a more meaningful relation with theory was sought as a basis for data correlation, which

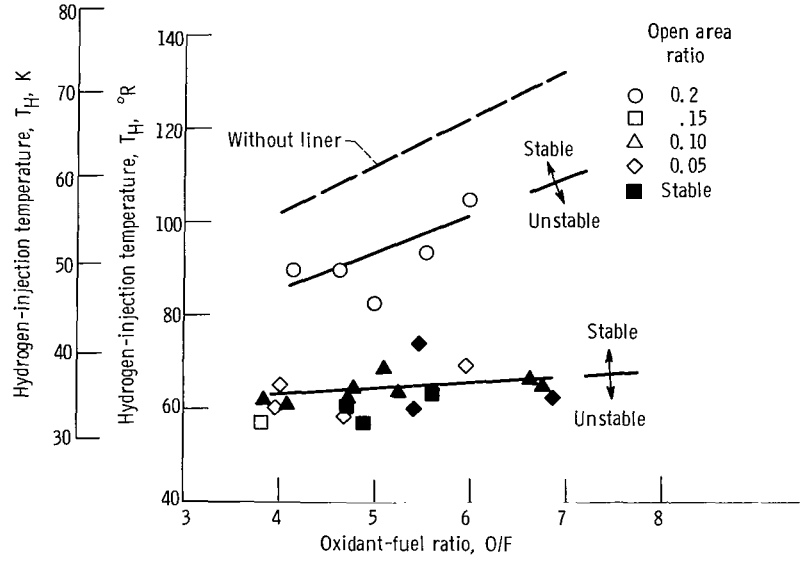

Figure 49. - Typical stability data obtained with several liner configuration. Liner wall thickness, 3/16 inch (0.476 cm); aperature diameter, 1/4 inch (0.635 cm).

resulted in the plots of figure 50. The absorption coefficient α was computed by use of a computer program (ref. 11), based on Helmholtz resonator theory and experimentally determined temperatures behind the liner (which varied from 600° to 1000° R or 333.3 to 555.6 K, depending on the open area ratio). When zero velocity past the liner apertures was assumed in the calculation, no significant relation was apparent (fig. 50(a)). Along with the uncertainty in gas properties behind the liner, the uncertainty in the velocity of flow past the liner represents a major difficulty in employing the current design procedure. In the absence of direct information on flow-past velocity, an appropriate value was inferred. This was accomplished by the substitution of several assumed values for velocity in the calculation. A reasonable correlation was obtained by using a flow-past velocity of 280 feet per second (85.34 m/sec) (fig. 50(b)). This admittedly indirect correlation nevertheless indicates that a value of α greater than 0.25 is required to eliminate screech with the unstable injector configuration selected. More important, however, is the fact that the correlation achieved provides a strong indication

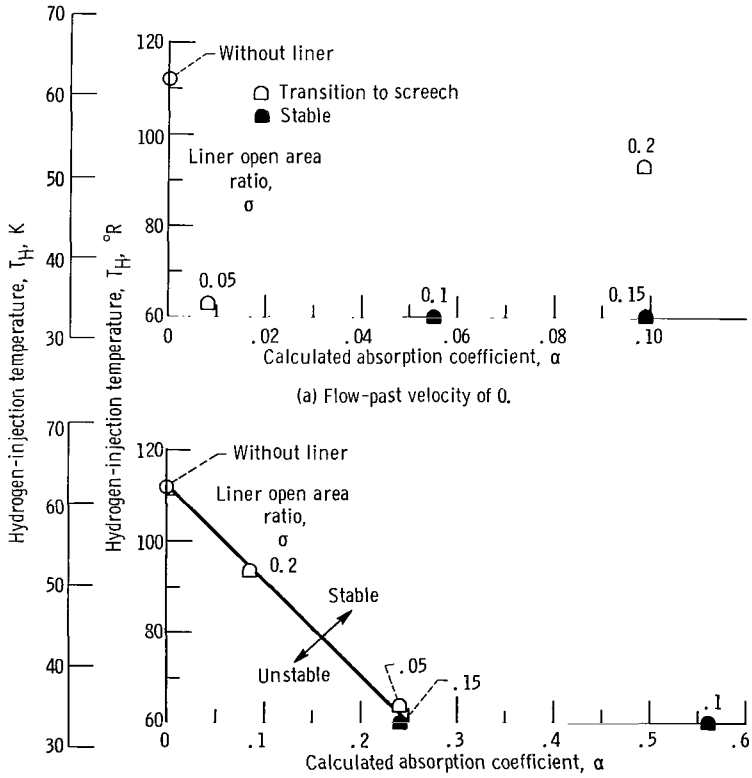

(b) Flow past velocity of 280 feet per second (85.34 m/sec).

Figure 50. - Correlation of screech limits with calculated absorption coefficient behind liner. Thickness, 3/16 inch (0.476 cm); hole diameter, 1/4 inch (0.635 cm); sound pressure level, 190 decibels; frequency, 3250 hertz.

that the analytical method can be applied in the case of actual rocket firings (as well as in cold acoustic testing).

Although not discussed fully herein (see ref. 11), several other aspects concerning acoustic liners deserve mention. The referenced investigation revealed that the gas temperature behind the liner (important in the calculations of α) varied from an average of 600° R (333.3 K) at 5 percent open area to 1000° R (555.6 K) at 20 percent. This temperature, as well as other gas properties, must be known to allow rational and accurate design calculations, but it will not be available to the designer without testing or without a comprehensive matrix of empirical data that does not exist at present. This situation suggests the need for studying the controlled bleed of inert gas behind the liner to achieve known gas properties which would facilitate design procedure. Such flow, however, must be low enough that the effects of flow through the apertures will not be serious.

The data obtained with two 3/4-inch- (1.91-cm-) thick liners did not fit the correlation of figure 50 for 3/16-inch- (0.476-cm-) thick liners, thus indicating a need for further work. Also significant is the finding, discussed in reference 11, that full-length liners may not be required for screech suppression inasmuch as a 17-percent-length liner positioned adjacent to the injector provided stability to 60° R (33.3 K). Furthermore, slits or cross-shaped holes were as effective as round holes for liner apertures. The slits, in particular, are of significance because this shape is much more amenable to most concepts for liner cooling in flight-weight hardware. In this respect, one problem of circular holes was disclosed in the failure of the first cooled flight-weight liner evaluated. This liner, shown in figure 51, was made of porous stainless steel for transpiration cooling on the hot side. Failure after only a few seconds of engine operation was associated with the anchoring of the flame on the upstream edges of the holes and the subsequent overheating directly in line downstrean. A slit-type liner would avoid this difficulty with flame anchoring.

One limitation of simple perforated-plate acoustic liners, especially at low frequencies, is that they absorb selectively in the region of resonance only. Several techniques, however, can be employed to alter the absorption frequency bandwidth of a liner. One such technique is to fill the liner cavity with a fibrous material (ref. 36). Fibrous material increases the specific acoustic resistance which extends the frequency range of absorption and simultaneously increases the absorption coefficient, provided that the specific acoustic resistance θ is less than 1.

The effect of filling the resonator volume (ref. 11) with fibrous material was evaluated by using an open area ratio of 0.2 and a 3/16-inch- (0.476-cm-) wall-thickness liner, the configuration that provided the least improvement in hydrogen temperature operating limits. The screech transition temperature for this configuration (unfilled)

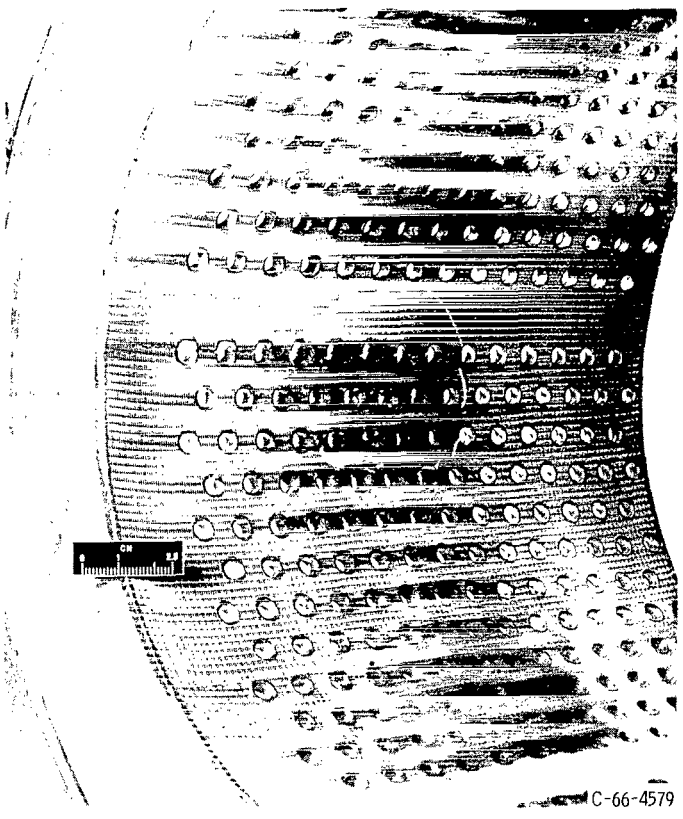

Figure 51. - Damage sustained by cooled liner.

was 93° R (51.7 K) at an oxidant-fuel ratio of 5.0 (fig. 52). The material used to fill the liner cavity was grade 2 medium steel wool packed to a density of 0.014 pound per cubic inch (387.55 kg/m^3). Examination of the results presented in figure 52 shows that a marked improvement in stability was achieved with the steel-wool-filled liner. The filled configuration provided stable operation at a hydrogen-injection temperature of about 58° R (32.2 K), the minimum available in the facility.

No attempt was made to calculate a theoretical absorption coefficient for the filled liner because adequate data on the porosity and structure factor of the fibrous material were not available. However, inasmuch as complete stabilization was achieved, the absorption coefficient of the liner must have increased to a value greater than 0.25 (minimum value of the coefficient for stable operation at 60° R or 33.3 K obtained from the correlation in fig. 50(b)). The maximum absorption coefficient for this configuration (unfilled) was about 0.09. It must be noted, however, that the use of steel wool as a liner-cavity fill material would not be suitable without some cooling method for long-duration operation, as burning occurred in the upstream portion (fig. 53) during tests having a total duration of about 11 seconds.

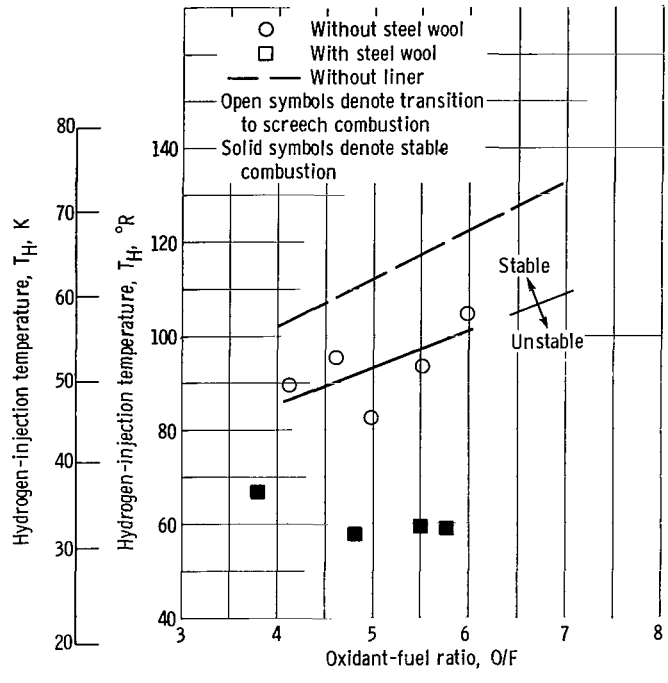

Figure 52. - Effect of packing resonator volume of wall liner with steel wool. Open area ratio, 0.2; wall thickness, 3/16 inch (0.476 cm).

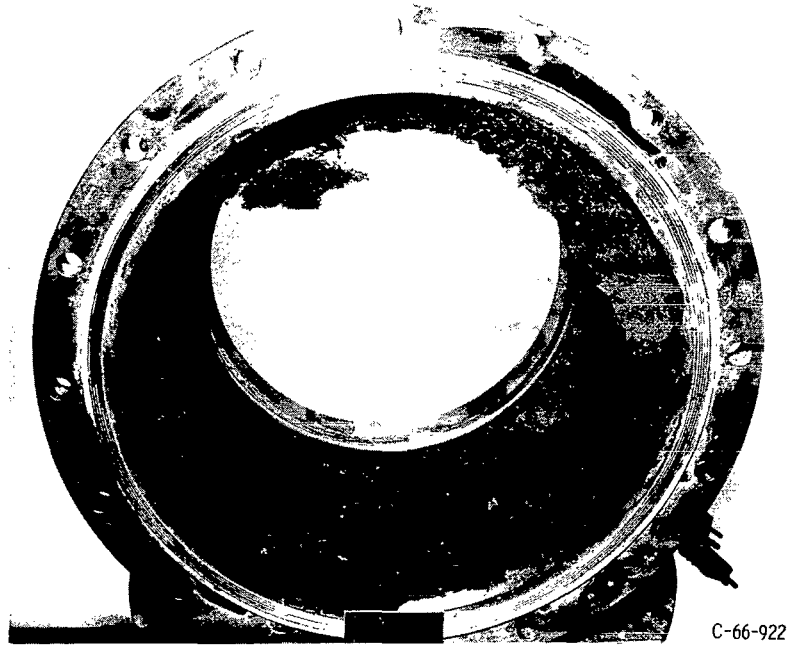

Figure 53. - Postfire condition of steel-wool packing in liner cavity.

Liner application in storable-propellant rocket engines. - This portion of the liner investigation (ref. 12) also utilized a 10.78-inch- (27.381-cm-) diameter thrust chamber, but the chamber pressure was 100 psia (689.47 kN/m^2 abs). As in the study of injector parameters with earth-storable propellants, stability rating of the various liner configurations was accomplished by subjecting the 42-inch- (106.68-cm-) -characteristic-length L^* combustor to tangential pressure pulses generated by RDX explosive charges of several grain sizes. In addition, the various liner configurations were tested in a longer (56-inch or 142.24-cm L^*) chamber with the same injector as was used in the 42-inch (106.68-cm) L^* tests. The longer combustor was spontaneously unstable without the liner.

The test engine consisted of a 487-triplet-element (with film-cooling showerheads) injector, an acoustic liner assembly, a bomb ring, and a convergent-divergent nozzle with a contraction ratio of 1.9 and an expansion ratio of 1.3 (fig. 54). The heat-sink

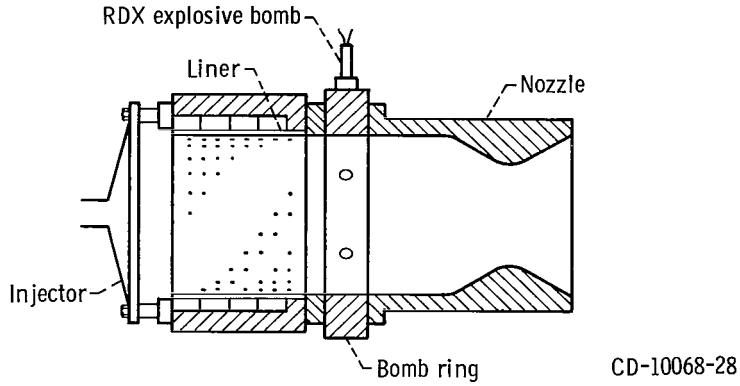

Figure 54. - Cross-sectional view of thrust chamber showing arrangement of components.

bomb ring, a four-port tangential-firing type, was mounted immediately downstream of the liner. The length of the combustor from the injector to the throat was 23.8 inches (60.45 cm), or L^* = 42 inches (106.68 cm). When the 56-inch (142.24-cm) L^* combustor was used, the bomb ring was replaced with a 10-inch (25.4-cm) spoolpiece that made the total length 30.5 inches (77.47 cm).

The liner assembly consisted of a heat-sink pressure jacket and a removable acoustic liner. The backing distance and thickness were held constant at 0.971 and 0.1875 inch (2.47 and 0.476 cm), respectively. Open-area-ratio aperture size and shape, and liner length were varied. At the beginning of the program, either one or two circumferential partitions were attached to the jacket to minimize axial gas flow behind the liner. It was necessary, however, to use three partitions attached to the outside of the liner to improve structural support and to facilitate removal from the jacket. The

TABLE II. - TEST CONFIGURATIONS

Aperture geometry	Aperture size		Open area ratio	Liner length	
	in.	cm		in.	cm
Circular	1/8	0.317	2.5	8	20.32
	1/8	.317	5		
	1/8	.317	10		
	1/4	.635	5		
	1/4	.635	10		
	1/4	.635	20		
	1/8	.317	10	4	10.16
	1/8	.317	10	2	5.08
	1/4	.635	10	4	10.16
Axial slots	1/16	0.159	5	8	20.32
	1/8	.317	10	8	20.32
	3/16	.476	15	8	20.32
Crosses	1/32	0.071	10	8	20.32
	1/16	.159	10	8	20.32
	1/8	.317	10	8	20.32
Grid slots	1/16	0.159	10	8	20.32

test configurations are listed in table II. Photographs of three types of liner configurations (the same as those used in the hydrogen-oxygen study) are presented in figure 48.

Grains of explosive rather than bomb pressure spike amplitude were selected as a rating criterion because of large data scatter in the amplitude results (fig. 55). The scatter exhibited here with storable propellants was similar to the results obtained with other unlined storable-propellant combustors (shown in fig. 30). Bomb-rating results of the 42-inch (106.68-cm) L^* engine without a liner, presented in figure 56, show that a bomb size of about 6 to 8 grains (388.7 to 518.4 mg) of RDX drove the combustor unstable. The predominant screech mode was first radial (5000 Hz) at an oxidant-fuel ratio of 2 but was second radial (9100 Hz) at an oxidant-fuel ratio of 1.6. Data obtained at various open areas with several liners having circular apertures of either a 1/8- or 1/4-inch (0.317- or 0.635-cm) diameter are shown in figure 57. Configurations with open areas of 5 percent or greater of either aperture diameter successfully damped a pressure disturbance of a 41-grain (2656.7-mg) bomb (limiting size). The high open-area-ratio liners were also effective in suppressing tangential modes in the spontaneously unstable combustor (L^* of 56 in. or 142.24 cm). Longitudinal modes, which were present during tests

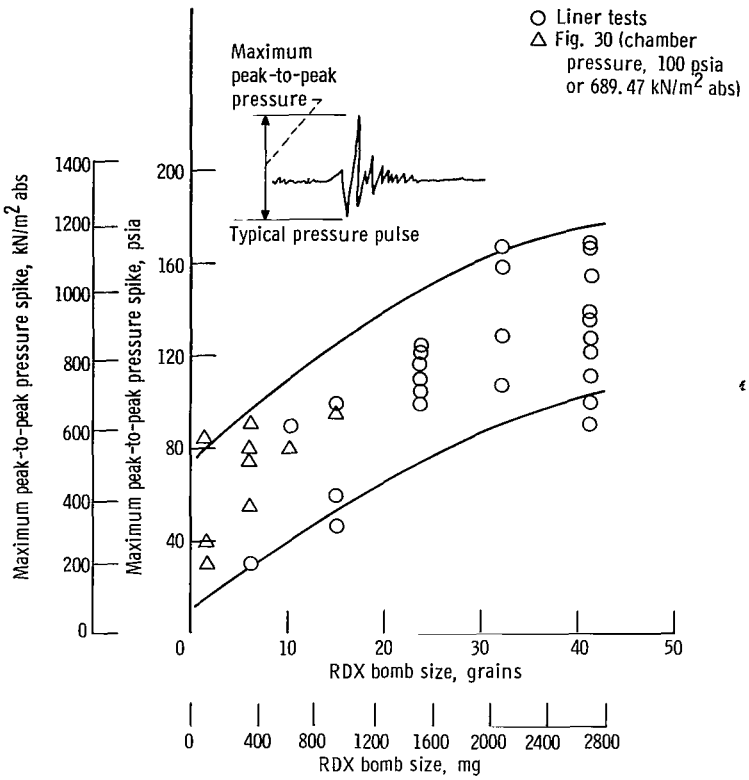

Figure 55. - Pressure spike produced by detonating various sized RDX bombs.

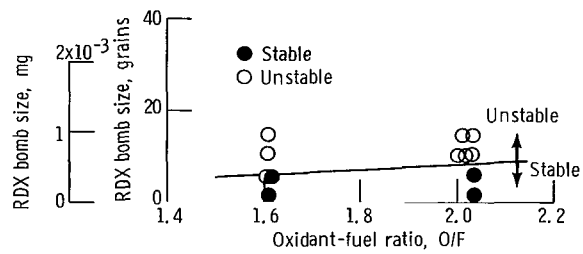

Figure 56. - Stability characteristics of basic engine without liner. Characteristic length, 42 inches (106.68 cm); 487-element triplet injector.

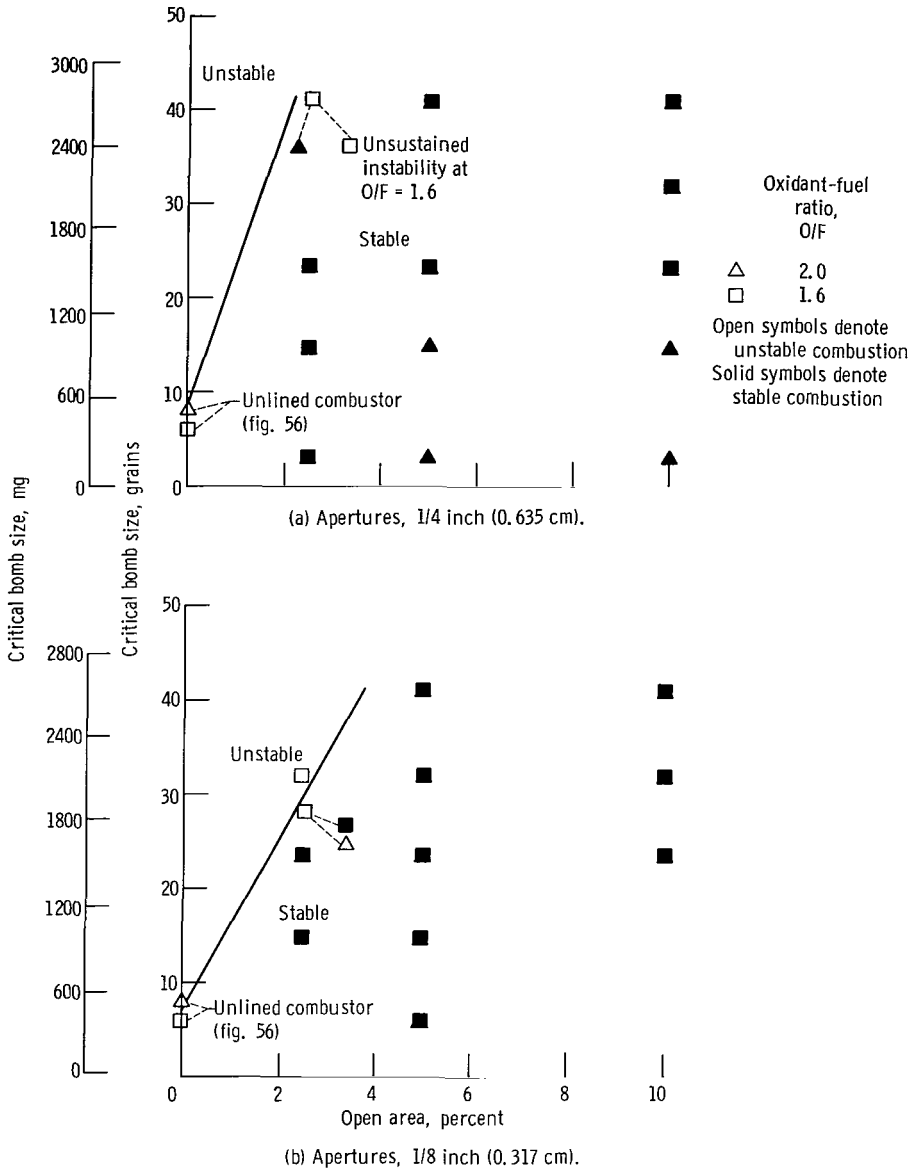

Figure 57. - Typical stability data obtained for several liner configurations.

of the 56-inch (142.24-cm) L^* chambers, were not damped by the liner configurations.

A plot of bomb size against theoretical absorption coefficient is shown in figure 58. The theoretical absorption coefficients were obtained by use of the computer program described in reference 11. Liner-cavity gas properties were determined from temperature measurements and theoretical thermodynamic calculations. The calculations were made for both a zero velocity (fig. 58(a)) and a velocity corresponding to a Mach number of 0.24 (based on the findings of the hydrogen-oxygen study), which was near the free-

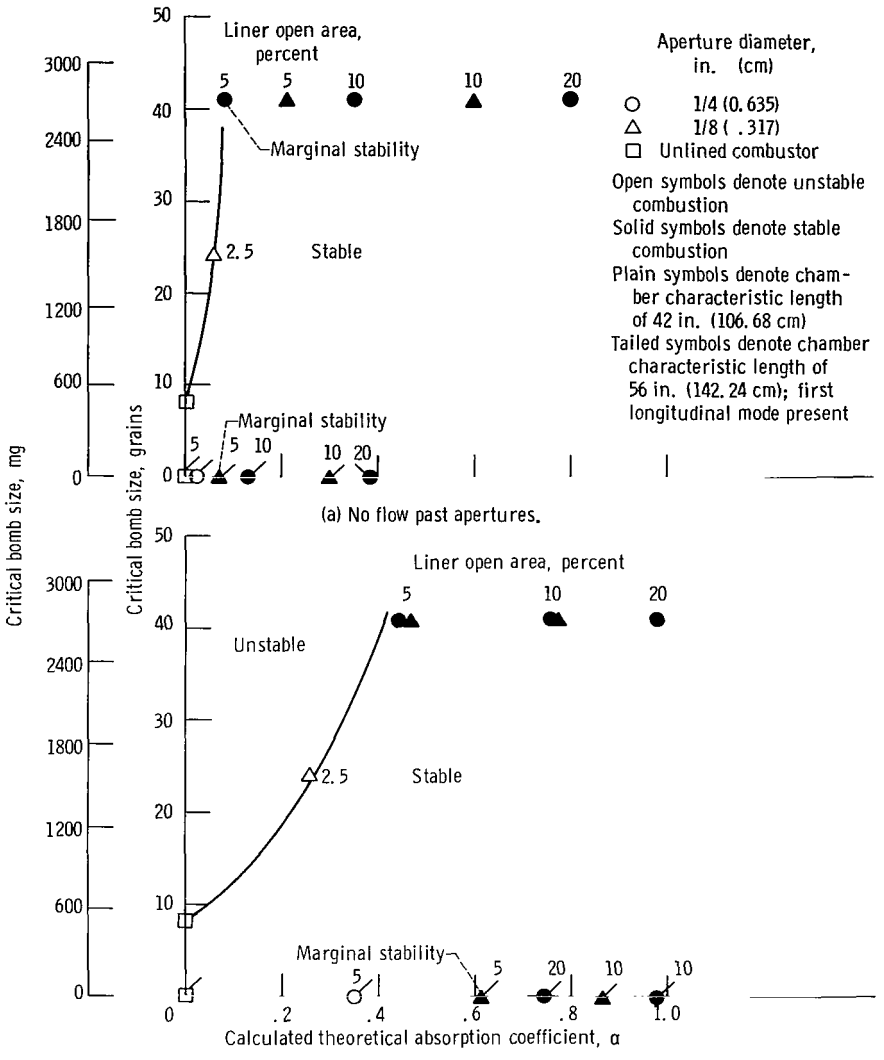

Figure 58. - Calculated absorption coefficients of full-length liners tested. Oxidant-fuel ratio, 2.0.

stream Mach number past the apertures (fig. 58(b)). As shown, a similar relation between bomb size and theoretical absorption coefficient was obtained for both velocity assumptions. Thus, with the available data, it was not possible to verify the effects of flow-past velocity as with the hydrogen-oxygen results. This ambiguity may have been the result of the coarse increments of the bomb charges. If flow past the apertures is assumed to be the same as that of the hydrogen-oxygen results (Mach 0.24), it is seen from figure 58(b) that an absorption coefficient of about 0.5 would be required for complete stabilization. In any event, liners that were successful in damping instabilities

were shown to have resonant frequencies near the screech frequency; that is, these liners were tuned.

Other results of the study (ref. 12) that deserve mention include the variation in cavity gas temperature with open area ratio and the performance of noncircular-aperture liner configurations. A comparison of measured cavity gas temperatures (prescreech) during tests of the same liners, 3/16-inch (0.476-cm) wall, 1/4-inch (0.635-cm) aperture with storable and hydrogen-oxygen propellants is shown in figure 59. With storable propellants, the average temperature varied between about 1800° and 2800° R (1000.0 and 1555.6 K), depending on the open area ratio, as compared with the average for the hydrogen-oxygen propellants of about 600° to 1000° R (333.3 to 555.6 K). Thus, another unknown, the effect of propellant combination (and injector type), must be added to the already difficult problem of predicting the appropriate temperature for use in the design calculations.

Both the slotted- and cross-shaped liners (fig. 48) were tested to determine the effect of aperture shape on absorption, and the results were similar to those for the circular-aperture liners of the same percent open area. The damping was controlled by tuning rather than by aperture shape, which had only a secondary effect. Although cross-shaped apertures probably could not be adapted to a rocket, the slots could be designed into a tube-type regeneratively cooled engine.

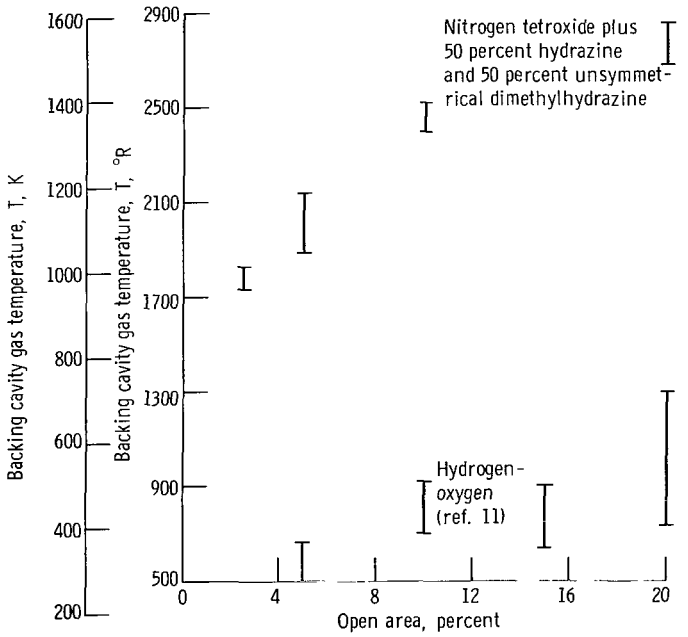

Figure 59. - Effect of propellant combination on liner-cavity gas temperature.

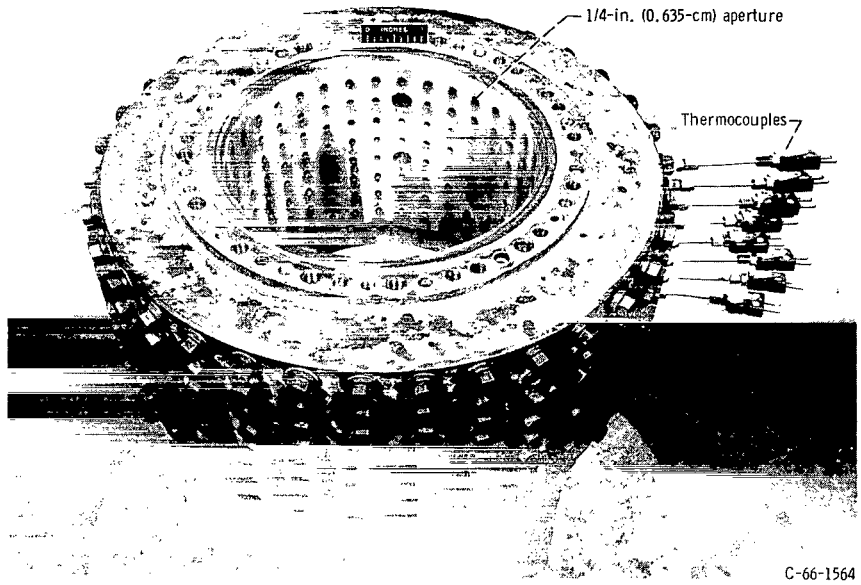

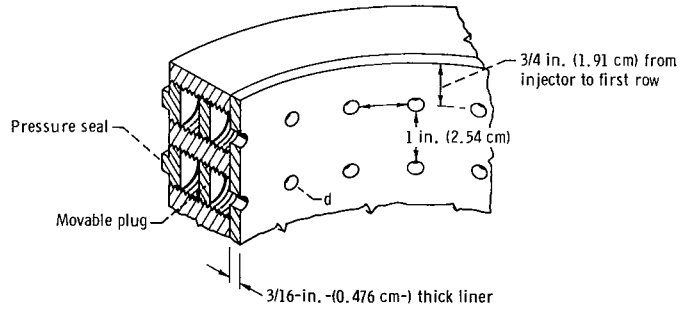

Figure 60. - Tunable acoustic liner.

Variable-resonator-volume acoustic liner studies. - As noted in the previous section, more information is required on gas properties in the resonator cavities and on the effects of flow velocity past the resonator orifices before rigorous design is possible. Additional information on these design factors was acquired from an investigation of an adjustable liner, conceived and evaluated experimentally, using hydrogen-oxygen propellants. The configuration (fig. 60) consisted of 272 individual resonators (8 rows of 34), each of which had a variable cavity depth (volume). Provisions were made to measure cavity (gas) temperatures in each of the eight rows and also to sample and analyze the gas composition in the third row from the injector. The experiments for this tunable liner involved the determination of (1) cavity gas composition and temperature and subsequent tuning of different rows of resonators, (2) resonator effectiveness as a function of axial position, and (3) effect of flow velocity past the apertures. Optimum tuning was determined by the amount of reduction in the hydrogen transition temperature compared with that of the configuration when all the resonators were plugged. A detailed discussion and analysis of all the results are given in reference 13; only the highlights are presented herein.

The experimentally determined mole fraction of water vapor in the cavity gas samples is compared in figure 61 with that of a simple theoretical prediction made in reference 37. Both experiment and theory showed that the mole fraction of water vapor increased rapidly as the cavity gas temperature increased from about 600° R (333.3 K) and asymptotically approached a limiting value at a higher temperature. The experimental curve, however, showed only about one-fifth as much water vapor as the simple theoretical prediction; hence, there is a correspondingly higher hydrogen concentration.

The 800° R (444.4 K) variation in cavity gas temperature shown in figure 61 occurred largely as a result of the decreasing hydrogen-injection temperature during the temperature ramps, which were employed for screech rating the configuration. Although convection cooling of the cavity gases to the heat-sink walls may have had some effect, the magnitude of this change as well as the chemical sample analysis data indicate the probable existence of a hydrogen-rich boundary layer near the walls of the thrust chamber, even though no film-cooling holes were used in the injector.

From these findings, it follows that tuning of the cavity is important and that the cavity gas properties just prior to screech inception are necessary in the liner design calculations to achieve tuning. Transition cavity gas temperatures are accordingly given in figure 62 for each of the eight rows of resonators. The variation for each row was due largely to variations in cavity depth. For the injector used, the average cavity temperature increased from about 550° R (305.6 K) near the injector to about 800° R (444.4 K) 4 inches (10.16 cm) downstream and remained constant at larger distances. Combining these cavity temperatures with the gas composition (in fig. 61) yields the sonic velocity

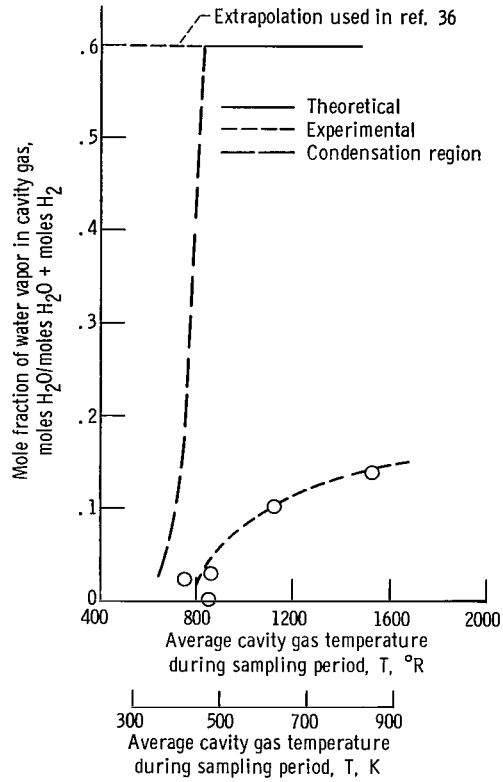

Figure 61. - Cavity gas composition as function of cavity gas temperature for row three. Oxidant-fuel ratio, 5; cavity depth, 7/16 to 3.2 inches (1.11 to 8.12 cm).

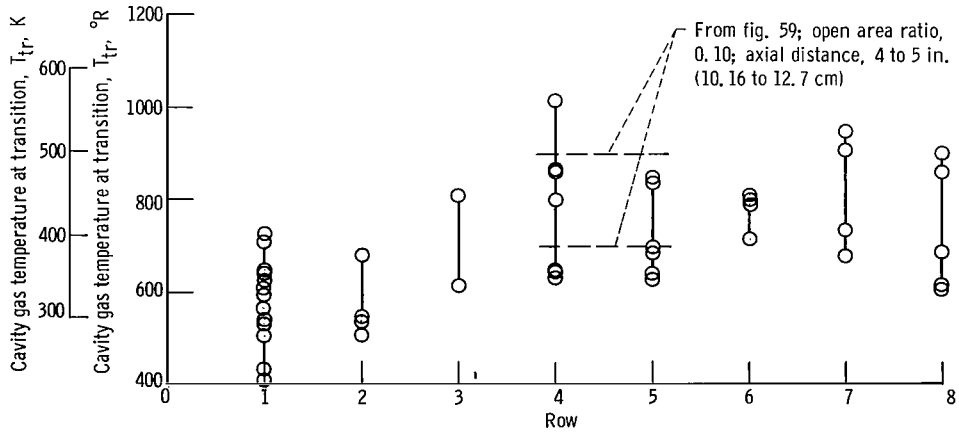

Figure 62. - Axial variation of cavity gas temperature at transition. Oxidant-fuel ratio, 5. (Data spread is result of variation in cavity gas temperature for all cavity depths.)

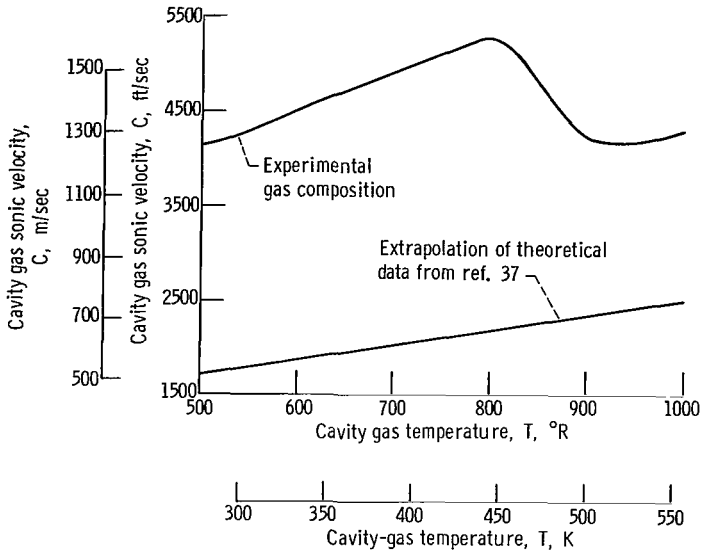

Figure 63. - Theoretical cavity gas sonic velocity as function of cavity gas temperature.

in the cavity shown in figure 63. This experimental curve is significantly different from the theoretically predicted curve used earlier for design calculations.

When the cavity depth of all the resonators was varied simultaneously, the effectiveness of the liner was changed as shown in figure 64, where an increase in hydrogen temperature margin indicates an increase in liner absorptivity. Maximum effectiveness occurred at a depth of about 1.75 inches (4.45 cm) and reduced the transition tempera-

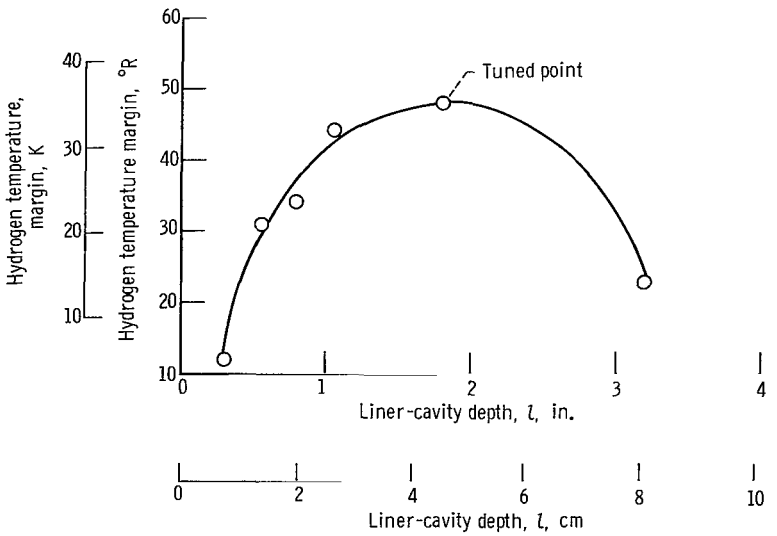

Figure 64. - Hydrogen temperature margin as function of liner-cavity depth. Oxidant-fuel ratio, 5; number of rows, 8.

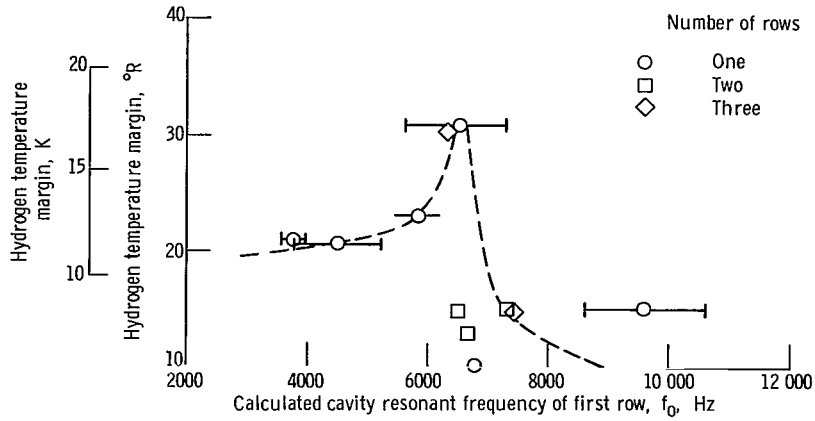

Figure 65. - Effect of liner length on stability. Oxidant-fuel ratio, 5.

ture from 112° R (62.2 K) to about 65° R (36.1 K), a reduction of 47° R (26.1 K). Although this was within 5° R (2.78 K) of the minimum hydrogen temperature possible with the facility, complete suppression was not achieved. The curve of figure 64 might be thought of initially as a tuning curve, which defines an optimum for the particular liner geometry; however, it is obvious from the data of figures 61 to 63 that each row, from 1 to 4 at least, will optimize individually at a different depth even if the effect of local flow velocity past the resonators is ignored.

Because of the large number of cavity depth combinations possible by using either a single row or various groups of rows, complete optimization of cavity depth was not attempted for the full assembly. Some indication regarding the importance of liner length may, however, be obtained by examination of figures 65 and 66. A plot of the hydrogen temperature margin against the calculated resonant frequency (no flow) for several partial-length liners is presented in figure 65. All configurations tested appear to fall near a single curve which indicates that, to within the accuracy of the temperature data, the second and third rows had no significant effect on liner absorption. In addition to these results, a few tests were conducted with a partial-length liner having only the first row of holes. Examination of the results of figure 66 shows that the optimum cavity depth of the first row was 9/16 inches (1.43 cm). The results again indicate that the first row was responsible for most of the reduction in transition temperature. Clearly, for those configurations reported herein, the predominant fraction of the improvement in the screech limit was accomplished by the resonators located 1 inch (2.54 cm) from the injector face.

The third objective associated with the use of the tunable liner was to define the effective gas velocity past each of the rows of the resonator assembly. Unfortunately, it has not been possible to determine this velocity accurately. The velocity term used in the liner design equations is based on an empirical relation (ref. 33) between mean-

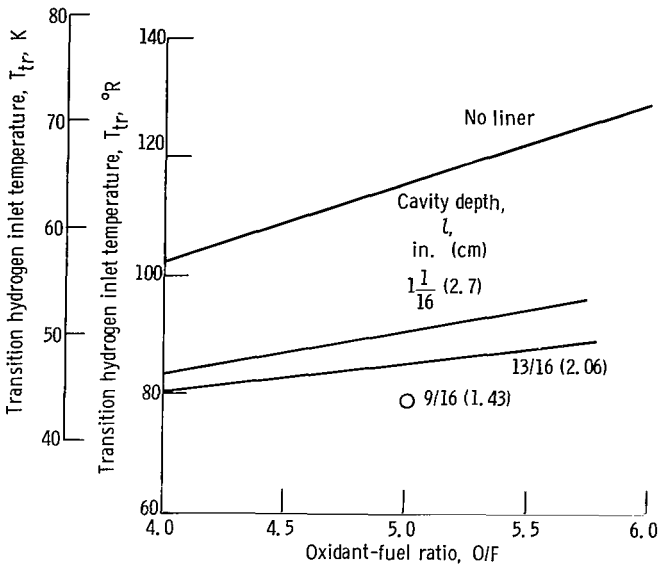

Figure 66. - Stability of partial-length liners (first row only).

stream velocity and the frequency shift of resonators away from the resonant frequency with no flow. By use of the data evolved with this adjustable liner, such a velocity could be found. However, the value of this mean-stream velocity is questionable since it seems more likely that resonator frequency should respond to local flow conditions in the boundary layer near the aperture rather than to the free-stream or bulk velocity. Nevertheless, the use of this mean-velocity factor from reference 34 did correct the calculated cavity resonance frequency to correspond to the experimental optimum tuning against the impressed prescreech frequency (frequency in the region of linear instability). Thus, the velocity correction based on the mean velocity and the continuity equation appears to work when used in the design calculation.

When all the information presented herein on screech liners is considered, this suppression technique is very effective for both propellant combinations, and although progress regarding knowledge of design variables is evident, some additional information is yet needed to allow rigorous design.

Effect of injector-face baffles in hydrogen-oxygen engines. - The usefulness of injector-face baffles for screech suppression in rocket engines is now well recognized but not well understood. These devices have been used in many engines, such as the F-1, M-1, J-2, Transtage, and Apollo service module, and have undoubtedly contributed greatly to the stability achieved. In most cases, the final baffle configuration was attained by a cut-and-try process inasmuch as design information did not exist.

It is obvious that engine designers would like to minimize both the axial length and the number of injector baffles to reduce cost and complexity, but not to the extent that

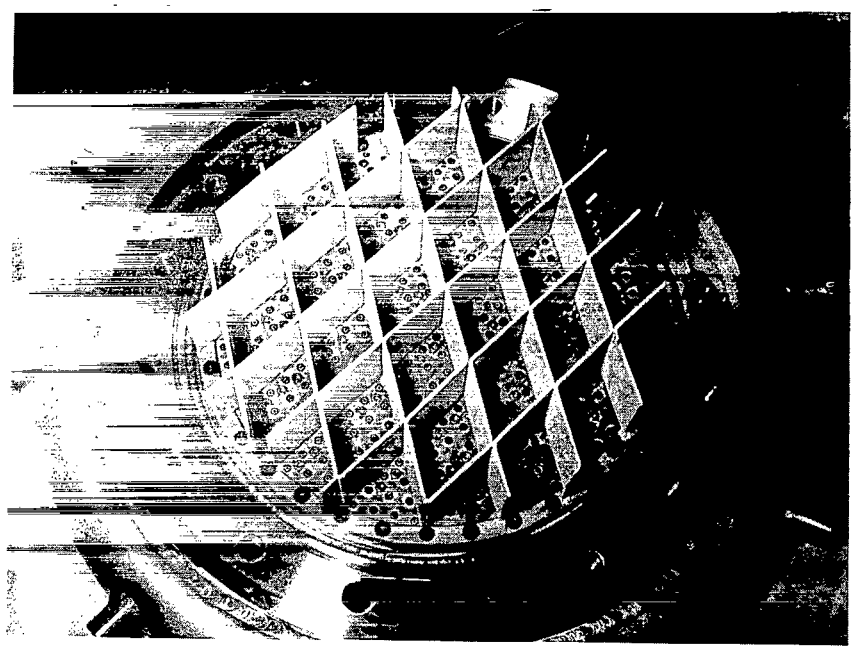

(a) Two-inch-(5.08-cm-) long, 25-compartment egg-crate baffle with injector.

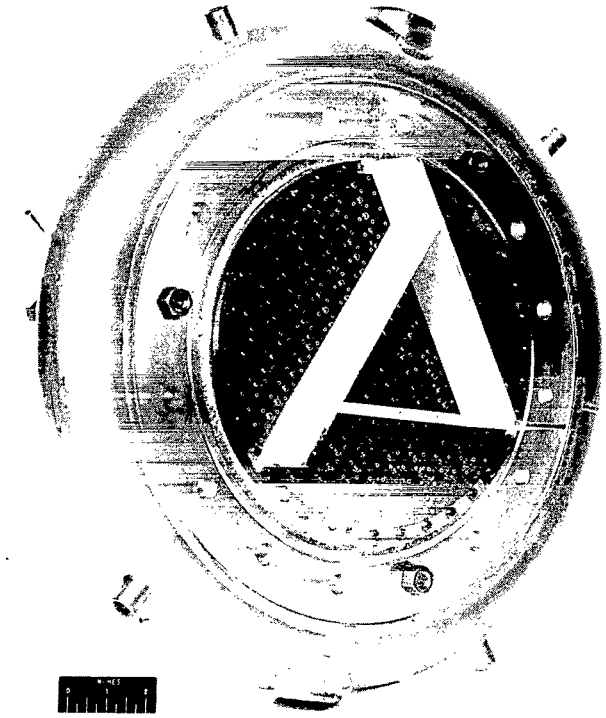

(b) Two-inch-(5.08-cm-) long, extended-triangle baffle with injector.

Type
7-Blade
4-Blade
3-Blade
Extended triangle
100-Compartment egg crate
25-Compartment egg crate
7-Compartment egg crate

(c) Baffle patterns.

Figure 67. - Typical uncooled baffle configurations.

the retention of adequate dynamic stability would not be ensured. Experience has indicated that long baffles are much more difficult to cool because of the marked increase in heat flux with distance from the injector face (ref. 38). A logical inquiry, then, is whether or not there is a trade-off whereby stability lost by reducing the baffle length might be regained by employing more baffles. The results summarized herein (from ref. 14) are intended to provide the designer with some preliminary information regarding the effects of the number and length of baffles.

Nominal 10.78-inch- (27.381-cm-) diameter hardware was used at a chamber pressure of 300 psia (2068.41 kN/m^2 abs). Run time was kept very short (3 sec) to allow the use of uncooled baffles made of mild steel with a 0.030-inch (0.0762-cm) coating of aluminum oxide. Typical configurations are illustrated in figure 67. Particular care was taken to ensure that no gap existed between the baffle and the injector faceplate, in view of the finding in reference 39 that even relatively small gaps may disrupt the stabilizing

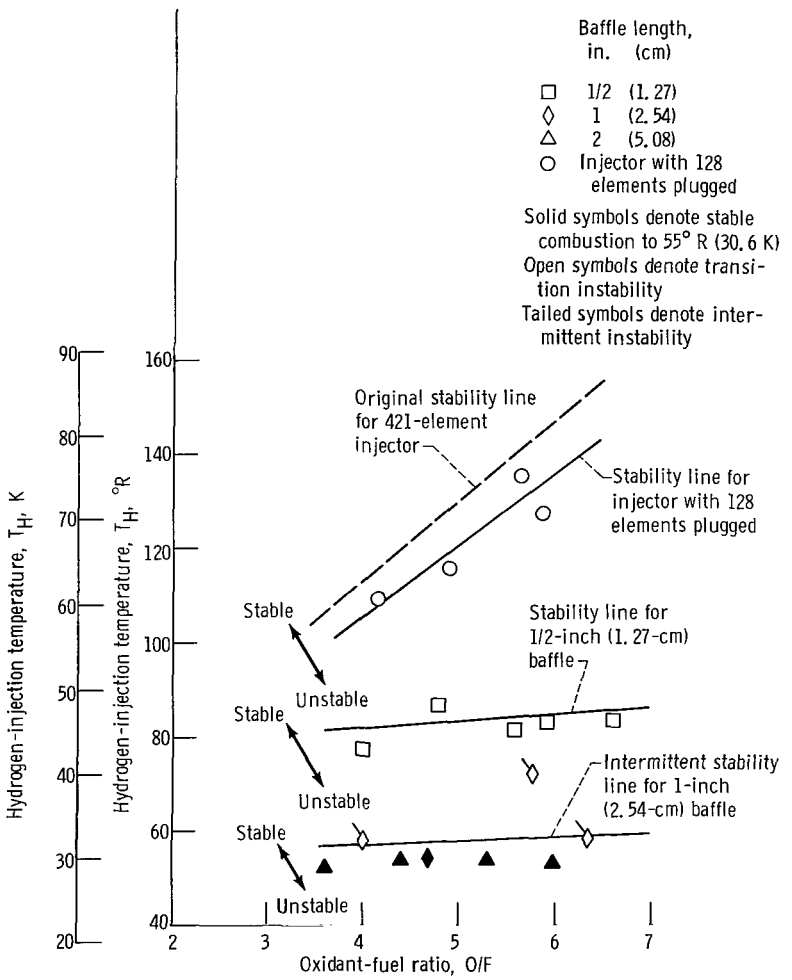

Figure 68. - Effect of baffle length on combustion stability limit with seven-blade baffle.

effect. Stability was rated in terms of the hydrogen temperature at screech inception.

Typical results are shown in figure 68 where hydrogen-temperature-transition data are shown as a function of the oxidant-fuel ratio for three seven-blade baffle configurations of different lengths. Note that 128 elements of the basic 421-element injector were plugged to accommodate the baffle. As seen, this modification had no significant effect on stability. Stability improved as baffles were added, and complete stabilization was achieved with a 2-inch- (5.08-cm-) long baffle to the minimum hydrogen temperature attainable in the facility (55° R or 30.6 K).

Baffle data such as these were cross plotted at an oxidant-fuel ratio of 5.0 to establish the summary plot given in figure 69 where the degree of stability is denoted by the symbols on a map of baffle length against maximum baffle compartment dimension. Screech was suppressed to the minimum hydrogen temperature (55° R or 30.6 K) by all the baffle patterns when a 2-inch (5.08-cm) length was used. One-inch- (2.54-cm-) long baffles provided stability to 55° R (30.6 K) for baffle compartment sizes of less than about 4.5 inches (11.43 cm); however, for larger cavity dimensions, longer lengths were required. Baffle lengths below 1 inch (2.54 cm) did not appear to be fully effective for any compartment size, a result which was not unexpected since the baffles must intrude into the axial zone of maximum heat release to be effective.

The selection of the maximum compartment dimension as a correlating factor in figure 69 was not made on any rigorous basis; the number of cavities could have been

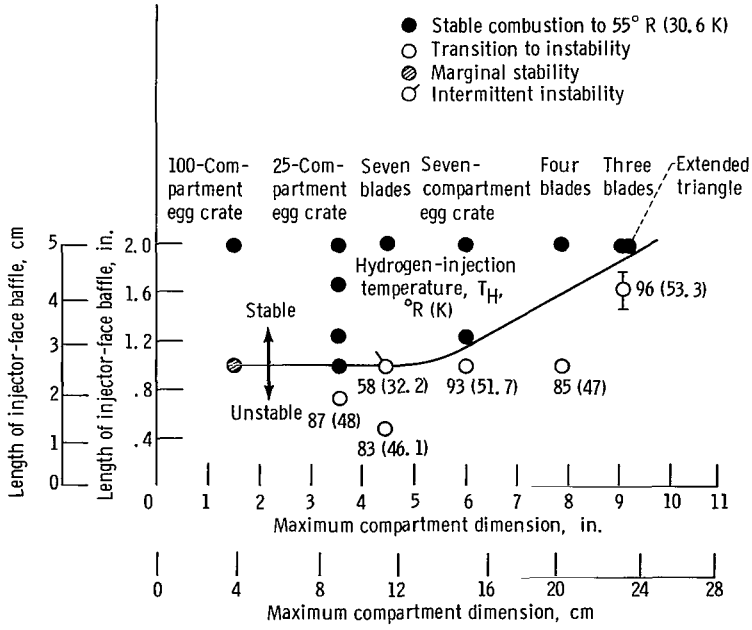

Figure 69. - Correlation of baffle length and maximum compartment dimension. Oxidant-fuel ratio, 5.0.

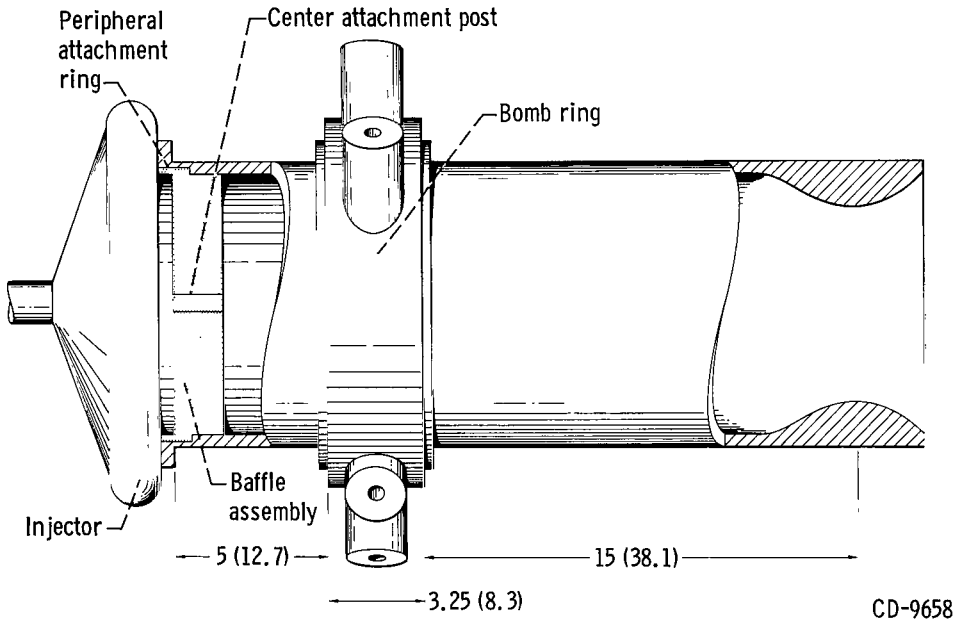

(a) Component arrangement. (All dimensions are in inches (cm).)

	Baffle length, in. (cm)			
	4.5 (11.43)	1.5 (3.81)	1.0 (2.54)	0.75 (1.91)
20 Compartments			x	x
10 Blades	x	x	x	
5 Blades	x	x	x	x
4 Blades	x	x	x	
3 Blades		x		

(b) Baffle configurations (x's indicate configurations tested).

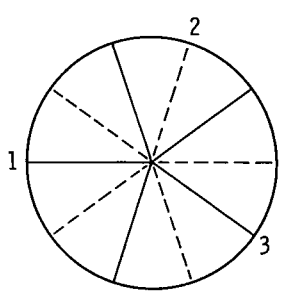

3, 5, and 10 Blades

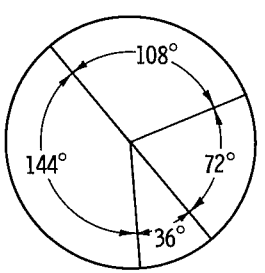

4 Blades

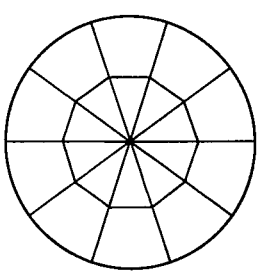

20 Compartments

(c) Baffle patterns.

Figure 70. - Combustor and baffle configurations.

used just as well. When more information is accumulated, the cavity dimension in a preferential direction (depending on the nonbaffled screech mode) may become most significant. As yet, the data available are not sufficient to confirm this supposition.

Effect of injector-face baffles in storable-propellant engines. - Similar to the work just discussed for hydrogen-oxygen propellants, the effects of several baffle variables on the stability characteristics of earth-storable propellants have also been investigated (ref. 15). Details of another extensive earth-storable propellant investigation are reported in reference 40. However, the purpose of the limited amount of work reported herein was to determine any gross differences existing between the results of the hydrogen-oxygen work and those of the storable-propellant work. The thrust chamber hardware chosen was the same size as that used in the hydrogen-oxygen program. The combustor and baffle configurations are presented in figure 70. Presented in figure 71 is a photograph of the 10-blade radial-baffle configuration assembled on the face of the 100-element (triplet) injector employed in the investigation. At a constant length of 1-inch (2.54 cm), each configuration was bombed with various charge sizes to determine the minimum bomb size that could cause sustained instability. Each baffle configuration was run over a range of lengths to establish a critical length at which it could be driven unstable by the maximum bomb size of 41 grains (2656.7 mb) of RDX. These data are presented as a function of the maximum compartment dimension (in in. and cm) which was used as a correlating parameter in the hydrogen-oxygen work.

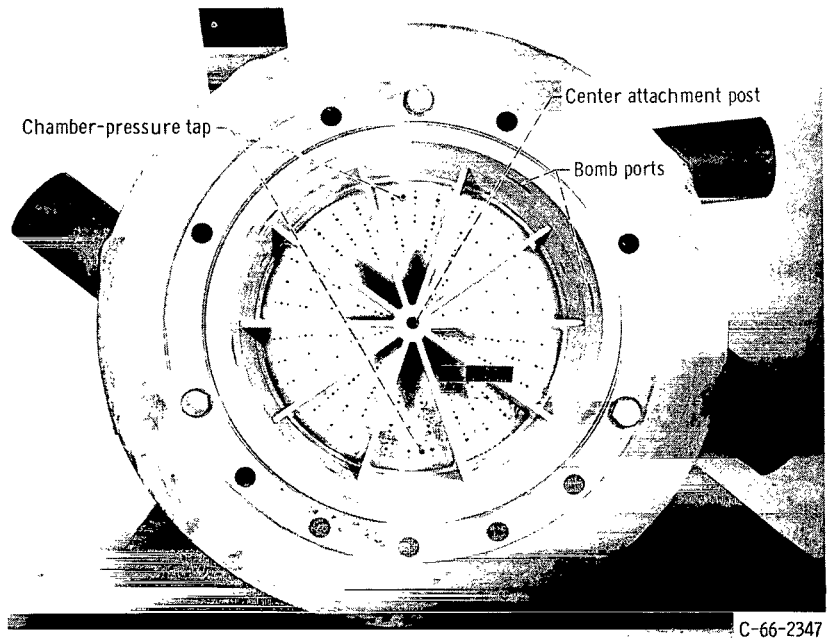

Figure 71. - Ten-blade radial baffle assembled with bomb ring.

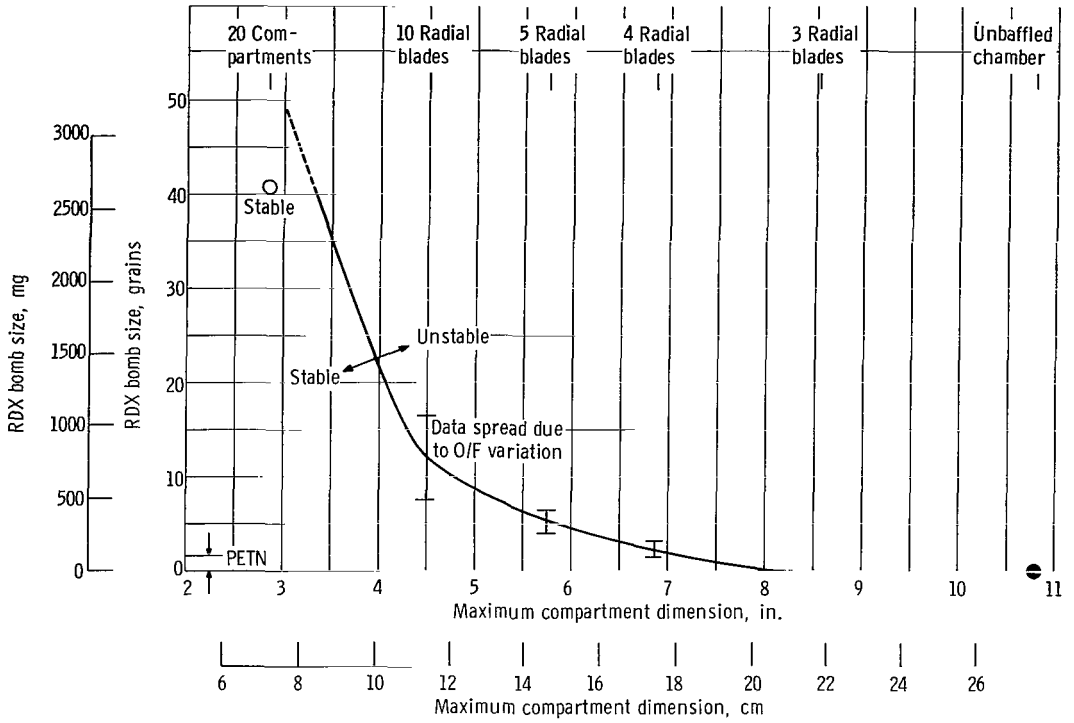

Figure 72. - Correlation of results for constant blade axial length of 1.0 inch (2.54 cm). Oxidant-fuel ratio, 1.6 to 1.8 (using faired curves).

Presented in figure 72 is the 1-inch- (2.54-cm-) length data plotted as a function of the compartment size parameter. This discussion is concerned with data obtained between oxidant-fuel ratios of 1.6 to 1.8. The 20-compartment baffle, which had a very small maximum compartment dimension of 2.85 inches (7.24 cm), was stable to the maximum charge size of 41 grains (2656.7 mg) of RDX. The configurations became progressively less stable as the compartment size increased, with a data point (open symbol) representing the bare chamber spontaneously unstable at the chamber diameter of 10.78 inches (27.381 cm). The curve drawn through the data points tends to show a change in slope at a maximum compartment dimension of about 4.5 inches (11.43 cm), which is the same as the critical cavity dimension found for the hydrogen-oxygen data.

All the data obtained for the various configurations at an oxidant-fuel ratio of 1.8 are presented in figure 73. For a baffle length of 1.5 inches (3.81 cm), a maximum compartment size of less than 6 inches (15.24 cm) is required for stability when the configuration is subjected to a 41-grain (2656.7-mg) charge size. For a 1-inch (2.54-cm) baffle length, the maximum compartment size must be less than 3.5 inches (8.89 cm) for stability when the configuration is subjected to the 41-grain (2656.7-mg) charge size. The hydrogen-oxygen baffle data are similar to that for earth storables, as can be seen by a comparison of figures 69 and 73.

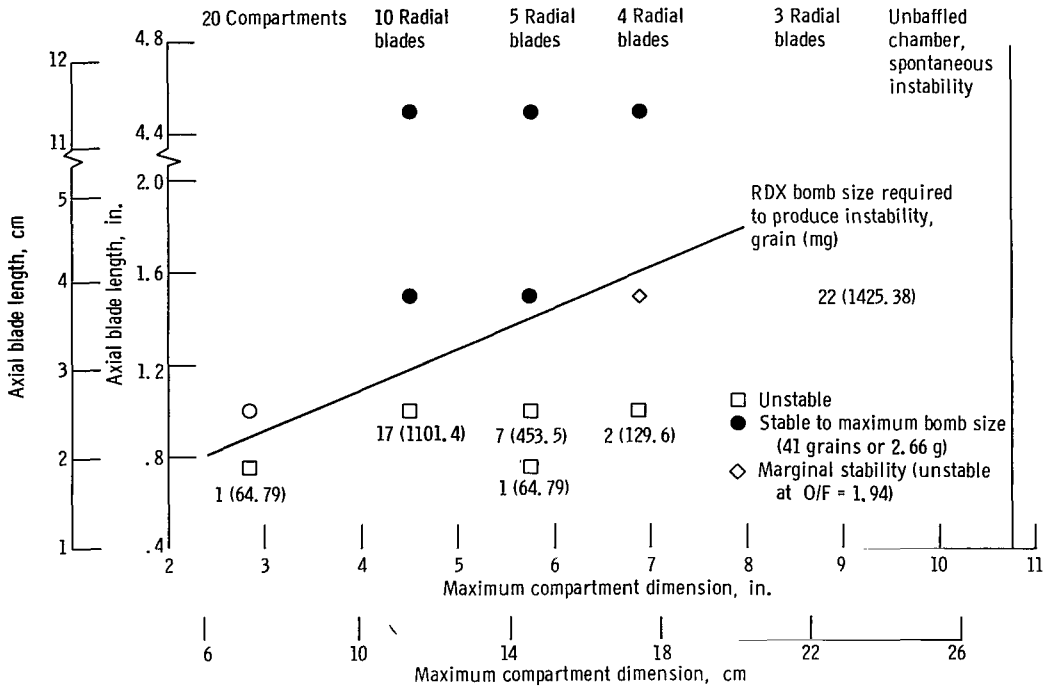

Figure 73. - Correlation of baffle results at oxidant-fuel ratio of 1.8.

The authors postulate that these results may be explained qualitatively by chemical augmentation which increases the strength of the shock wave produced by the bombs (or a naturally occurring pop). It is suggested that shock waves "feed upon" the vaporized propellants and grow until an obstacle (baffle) is encountered. The baffle then reflects the shock back into a region where the chemical energy was just consumed, causing the reflected shock to be dissipated by friction or turbulence. The authors also speculate that during and immediately after the passage of the initial shock, the high local chamber pressure reduces or stops propellant injection into the area, thus depriving the reflected shock of an energy source. The effects of baffle cavity size and length would then affect the mean-free path for amplification, and, hence, the shock strength and its chances to reach a level required to be sustained. The shorter baffles would tend to allow the wave to amplify in the zone of prepared, but not fully burned, propellant just downstream of the baffle tips.

In retrospect, the investigation showed that the use of baffles could provide complete screech suppression for both propellant combinations under the conditions tested, and thus this technique is regarded as an important one for achieving engine stability. Although a significant increase in knowledge regarding the trade-off between the length and number of baffles was obtained, the explanation of the mechanism involved is still uncertain.

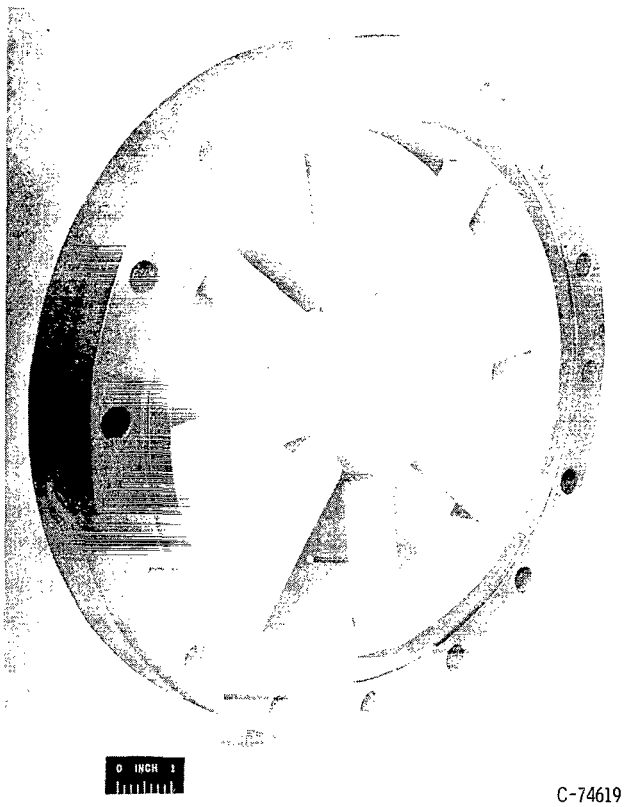

Figure 74. - "Wagon wheel nozzle" used to simulate plug-type nozzle.

Effect of nozzle-area radial distribution in hydrogen-oxygen engines. - For the tangential mode of screech, the pressure distribution reaches a maximum at the walls of the combustor. Then it seems reasonable that, if nozzle losses are affected by amplitude (as indicated in ref. 41), locating the nozzle throat area at the chamber wall should have a marked effect on stability. This hypothesis was explored by using a form of a plug nozzle (annular flow) shown in figure 74.

The stability limits of the combustor using a conventional convergent-divergent nozzle and then the plug nozzle are compared in figure 75. The hydrogen-temperature stable operating limits were improved by about 20° R (11.1 K) with the plug nozzle in comparison with those of the conventional nozzle configuration. The occurrence of the potential longitudinal mode of instability was expected with the short subsonic-length plug nozzle; however, longitudinal instability was not experienced.

Effect of porous injector faceplates in hydrogen-oxygen engines. - One of the several phases of the screech investigation reported in reference 7 included determining the effect of porous injector faceplates on stability limits. It was postulated that the porous material through which is flowing a compressible fluid could act as an acoustic absorber and thereby reduce the strength of reflected waves. Therefore, two series of runs were

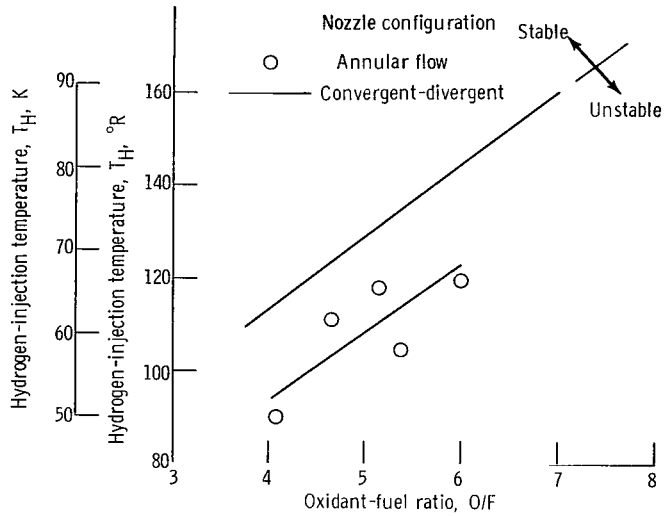

Figure 75. - Stability characteristics of combustor with convergent-divergent nozzle and with annular-flow nozzle (wagon wheel).

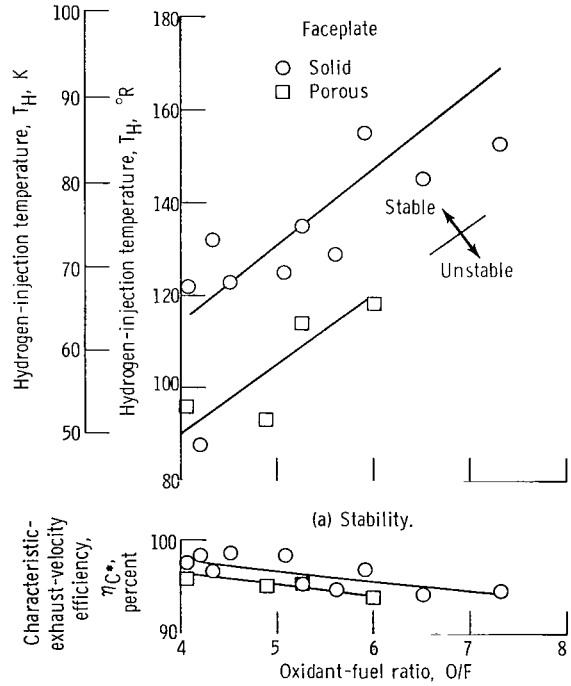

Figure 76. - Effect of porous injector faceplate on stability and performance characteristics of 421-element injector.

made wherein the injector and thrust chambers were identical except for the faceplate type. The results are given in figure 76(a) where the screech limit (transition temperature) is plotted against the oxidant-fuel ratio for both solid and porous faceplates. The porous material was a sintered screen assembly rated at 300 standard cubic feet (8.49 standard cu m^3) at a pressure drop of 2 psia (13.79 kN/m^2 abs). The figure shows that, for the configuration tested, the porous faceplate improved stability by a significant amount, with the screech transition temperature being reduced about 25° R (13.9 K) at an oxidant-fuel ratio of 5.0.

Shown in figure 76(b) is the effect of a porous injector faceplate on engine performance. The weight flow of hydrogen through the porous material was calculated to be approximately 5 percent of the total hydrogen weight flow to the engine. Examination of figure 76(b) shows that the effect of diverting about 5 percent of the hydrogen for faceplate cooling was to reduce the characteristic-exhaust-velocity efficiency by about $1\frac{1}{2}$ percent.

SUMMARY OF RESULTS

Acoustic-mode-stability data for both hydrogen-oxygen and earth-storable (nitrogen tetroxide and 50 percent unsymmetrical dimethylhydrazine and 50 percent hydrazine) propellant combinations were collected and correlated as far as possible. The data were obtained in the rocket engine test facilities of the NASA Lewis Research Center by using engines of about 20 000 pounds (88.964 kN) thrust. The investigations yielded the following results:

1. The hydrogen temperature margin is a good measure of the dynamic stability of an engine.

2. The hydrogen temperature at which screech occurred could be reduced to less than 60° R (33.3 K) (minimum available) by selection of a hydrogen-oxygen-injection area ratio of less than 0.5.

3. Variations in contraction ratio and the resulting changes in chamber pressure or total propellant flow had a strong effect on stability. Decreasing the contraction ratio improved the stable operating limits.

4. The hydrogen-temperature stable operating limit was represented by a constant value of the parameter

$$\left(\frac{2g\ \Delta P_H}{\rho_H}\right)^{1/2} \rho_O (D_O)^{1.25} \left(\frac{1}{O/F}\right)^{1/2}$$

where

g	gravitational constant
ΔP_H	hydrogen-injector pressure drop
ρ_H	hydrogen-injection density
ρ_O	oxygen-injection density
D_O	oxygen-injection orifice diameter
O/F	oxidant-fuel ratio

At values of the parameter above 4.4, combustion was stable and below 4.4 was unstable for an injector with an 85-percent-element radial face coverage.

5. Increasing the weight flow per element beyond 0.6 pound per second (0.272 kg/sec) by reducing the number of injection elements provided stable operation to the lower hydrogen temperature limit of the facility (60° R or 33.3 K). The improvement in stability was accompanied by a loss in performance.

6. Recessing the oxidizer tubes of a concentric-tube injector below the surface of the faceplate improved both the stability and performance of a 20 000-pound (88.964-kN) hydrogen-oxygen engine. A 0.1-inch (0.254-cm) recess provided an increase of 50° R (27.8 K) in the screech temperature margin and improved the characteristic-exhaust-velocity C^* efficiency by 3 percent.

7. Extending the oxidizer tubes completely stabilized a 100-element injector that had been unstable at a hydrogen temperature of 78° R (43.3 K) and an oxidant-fuel ratio of 5.0. The extension, however, reduced the C^* efficiency by about 4 percent over the entire range of oxidant-fuel ratios at comparable hydrogen temperatures.

8. Increasing the oxygen-injection temperature had a detrimental effect on the hydrogen-temperature stable operating limits. Screech temperature increased about 50° R (27.8 K) as the oxygen temperature was raised from 140° to 240° R (77.8 to 133.3 K).

9. Adding fluorine 30 percent by weight to oxygen produced no significant effect on the stability characteristics of a 421-element injector. Engine performance increased 1 to 3 percent with fluorine-oxygen mixtures.

10. The stability characteristics were not markedly affected by diverting 10 to 20 percent of the available hydrogen for film cooling, although at high oxidant-fuel ratios, some of the data for the 10-percent film cooling appear to show a destabilizing effect. Performance decreased 2 to 3 percent for each 10 percent of the total hydrogen flow diverted for film cooling.

11. With earth-storable propellants (nitrogen tetroxide and a mixture of 50 percent hydrazine plus 50 percent unsymmetrical dimethylhydrazine), a narrow band of maximum stability occurred between velocity ratios (oxidant to fuel) of 1.0 and 1.4 at a chamber

pressure of 300 psia (2068.41 kN/m^2 abs). At 100 psia (689.47 kN/m^2 abs), stability appeared to increase with velocity ratio for the range investigated (0.55 to 1.65). Peak performance for both chamber pressures occurred between velocity ratios of 0.5 to 0.7, which is about 25 percent less than the ratio predicted by Jet Propulsion Laboratory's "uniform mixture ratio distribution" criteria.

12. Variations in impingement angle from 38^o to 120^o had no significant effect on the performance or stability of a 20 000-pound (88.964-kN) rocket using earth-storable propellants. The ratio of the oxidant velocity to the radial component of the fuel velocity (V_O/V_{Fr}) provided the best correlation of the earth-storable stability data.

13. Extending the fuel impingement distance from 1/2 to 1 inch (1.27 to 2.54 cm) from the injector face had only a minor destabilizing effect on a rocket using earth-storable propellants. Performance did not change significantly as the impingement distance was increased.

14. Both element size and/or the mass-flow-per-element variation at various velocity ratios indicated an interrelation between the fuel weight flow per element W_F/E and the ratio of the oxidant velocity to the radial component of the fuel velocity V_O/V_{Fr}, and a proper selection of both is necessary to obtain maximum stability and performance.

15. Alternating-grid-pattern injectors were generally less stable and had a 1 to 2 percent higher characteristic-exhaust-velocity efficiency than that of circular-pattern injectors having an equal thrust per element with earth-storable propellants.

16. Interchanging the propellant arrangement of a triplet injector (from fuel-oxidant-fuel to oxidant-fuel-oxidant) resulted in less stability and slightly higher performance with earth-storable propellants. The oxidizer-fuel-oxidizer triplet injectors were very erosive to chamber hardware compared with fuel-oxidizer-fuel triplets.

17. The absorption of a resonator is a strong function of how closely it is tuned to the wave frequency. Maximum absorption is obtained when the resonator frequency is equal to the wave frequency. A liner not tuned to the screech frequency tends to shift the screech frequency away from the liner resonant frequency because of a change in wall impedance.

18. There is no advantage to tilting the holes of an acoustic liner to increase absorption.

19. In the cold acoustic investigation, all axial positions in the chamber were equally favorable for damping devices. This was not true for a rocket combustor with a localized region of high heat release.

20. Longitudinal partitions in the back cavity aided in damping tangential waves.

21. Results indicated that a liner formed by superimposing two different hole diameters behaves as an average of two different liners, each with only one of the hold diameters. The absorption bandwidth, however, may be greatly expanded. Consequently,

by proper choice of a range of hole sizes, a perforated liner may be designed to operate effectively over a wide range of conditions.

22. When there is no frequency-hole-spacing-flow interaction, the theoretical expressions for the effect of flow apparently predict the experimental trends.

23. The expression for calculating the effective length of a resonator neck is valid to within experimental error.

24. High-frequency combustion instability in hydrogen-oxygen engines of the size investigated can be suppressed by using a properly designed array of Helmholtz resonators.

25. Liner-cavity gas temperature that varied with liner variables, such as aperture size, open area ratio, and axial position, has a strong effect on liner absorption characteristics. Thus, unless a means of predicting or controlling cavity temperature and gas composition is found, no exact design is possible.

26. Analytical predictions based on acoustic theory were in limited agreement with experimental results of liner tests with hydrogen-oxygen propellants, provided that the effects of flow past the apertures of 280 feet per second (85.34 m/sec) were included in the calculation of the absorption coefficient. Additional data evaluating the effect of flow past the apertures are required before liner absorption characteristics can be predicted.

27. Liners with absorption coefficients of 0.25 or higher, calculated with flow past the apertures included, were required to eliminate screech in the hydrogen-oxyen rocket tested at a hydrogen-injection temperature of 60° R (33.3 K) (minimum available).

28. Full-length combustor liners were not required to suppress acoustic-mode in stability for the particular hydrogen-oxygen combustor used in the investigation. A 17-percent partial-length liner positioned at the injector end of the thrust chamber provided stable combustion to a hydrogen-injection temperature of 60° R (33.3 K).

29. Aperture shape had no first-order effect on absorption.

30. Fitting the resonator volume with porous material had a beneficial effect on stability because it extended the frequency range of absorption and increased the absorption coefficient.

31. Individual-row tuning by varying the cavity depths provided better stabilization characteristics than by simply tuning the entire array of liner cavities to the same depth. Knowledge of the properties of the gas present in the liner cavities and the flow through and past the resonators is required before a tuned liner can be designed.

32. Complete suppression of screech in storable-propellant rockets required an absorption coefficient of about 0.5 (with an assumed flow-past velocity of Mach 0.24) for the marginally unstable combustor (characteristic length $L^* = 42$ in. or 106.68 cm), and a slightly higher value was required for the spontaneously unstable combustor ($L^* = 56$ in. or 142.24 cm). Similar to the hydrogen-oxygen results, aperture shape had no first-order effect on liner effectiveness.

33. Baffles 2 inches (5.08 cm) in length produced stable operation in a hydrogen-oxygen engine down to a hydrogen-injection temperature of 55° R (30.6 K) with as few as three baffle compartments. Injector-face baffles 1 inch (2.54 cm) long produced marginal stability down to a hydrogen temperature of 55° R (30.6 K) when the maximum baffle cavity dimension was less than 4.5 inches (11.43 cm).

34. In storable-propellant engines, the stability trends with baffle compartment size were similar to those of the hydrogen-oxygen results. For a 1-inch (2.54-cm) baffle length, the maximum compartment dimension must be less than 3.5 inches (8.89 cm) for stability when the configuration is subjected to a 41-grain (2656.7-mg) bomb size.

35. The simulated plug nozzle (annular flow) provided an improvement in hydrogen temperature margin of about 20° R (11.1 K) as compared with a conventional convergent-divergent nozzle.

36. The stability characteristics of a 20 000-pound (88.964 kN) hydrogen-oxygen rocket were significantly improved by provision of a porous injector faceplate. The stable temperature limit was lowered by 25° R (13.9 K) over the range of oxidant-fuel ratio investigated.

CONCLUDING REMARKS

In the light of the data presented, it is clear that with the hydrogen-oxygen-propellant combination, major design improvements or methods to prevent screech may be achieved by variations made in the injection technique. On the other hand, with the earth-storable-propellant combination (N_2O_4 plus 50 percent N_2H_4 - 50 percent UDMH) no major improvement seems likely through changes in the propellant-injection process. Usually, when some improvement in stability was achieved, performance was not optimum, and rational design guides were not obvious.

Conversely, those devices classified herein as energy absorbing, or changes which would tend to alter or break up wave fronts, were effective in suppressing or eliminating screech with both propellant combinations. In this regard, both baffles and acoustic liners were effective when properly designed, and some preliminary design guides are given, although all necessary design variables are not yet quantitatively evaluated.

Finally, the results of the investigation provided some insight into the combustion instability phenomenon, especially with hydrogen-oxygen rocket engines. Experiments showed that the contribution of the hydrogen on stability is through the injector pressure drop. Variations in weight flow per element, contraction ratio, and hydrogen-injection area all affect stability according to their effect on the hydrogen pressure drop. Also determined was that the stability of a hydrogen-oxygen rocket is not a function of the oxy-

gen velocity but rather of the oxygen-injector orifice diameter and the oxygen temperature or density.

It must be understood that, whereas the information herein is expected to be valuable in the design of new rocket engines and trends indicated are expected to hold, complete confidence in stable operation is not possible until the effects of scaling factors such as chamber size are determined.

Lewis Research Center,
National Aeronautics and Space Administration,
Cleveland, Ohio, July 23, 1968,
128-31-06-05-22.

REFERENCES

1. Crocco, Luigi; and Cheng, Sin-I: Theory of Combustion Instability in Liquid Propellant Rocket Motors. Butterworth Scientific Publ., 1956.

2. Priem, Richard J.; and Guentert, Donald C.: Combustion Instability Limits Determined by a Nonlinear Theory and a One-Dimensional Model. NASA TN D-1409, 1962.

3. Beltran, M. R.; et al.: Analysis of Liquid Rocket Engine Combustion Instability. Rep. SN-68-S2, Dynamic Science Corp. (AFRPL-TR-65-254, DDC No. AD-482021), Jan. 1966.

4. Clayton, R. M.; and Rogero, R. S.: Experimental Measurements on a Rotating Detonation-Like Wave Observed During Liquid Rocket Resonant Combustion. Tech. Rep. 32-788, Jet Propulsion Lab., California Inst. Tech. (NASA CR-67259), Aug. 15, 1965.

5. Wanhainen, John P.; Parish, Harold C.; and Conrad, E. William: Effect of Propellant Injection Velocity on Screech in 20,000-Pound Hydrogen-Oxygen Rocket Engine. NASA TN D-3373, 1966.

6. Wanhainen, John P.; Feiler, Charles E.; and Morgan, C. Joe: Influence of Chamber Pressure, Flow per Element, and Contraction Ratio on Acoustic-Mode Instability in Hydrogen-Oxygen Rockets. NASA TN D-4733, 1968.

7. Wanhainen, John P.; Hannum, Ned P.; and Russell, Louis M.: Evaluation of Screech Suppression Concepts in a 20,000-Pound Thrust-Hydrogen-Oxygen Rocket. NASA TM X-1435, 1967.

8. Salmi, R. J.; Hannum, N. P.; and Wanhainen, John P.: Effect of Thrust-per-Element on Combustion Stability Characteristics of Hydrogen-Oxygen Rocket Engines. NASA TN D-4851, 1968.

9. Tabata, William K.; Antl, Robert J.; and Vincent, David W.: Storable Propellant Combustion Instability Program at Lewis Research Center. Paper No. 66-602, AIAA, June 1966.

10. Phillips, Bert; and Morgan, C. Joe: Mechanical Absorption of Acoustic Oscillations in Simulated Rocket Combustion Chambers. NASA TN D-3792, 1967.

11. Wanhainen, John P.; Bloomer, Harry E.; Vincent, David W.; and Curley, Jerome K.: Experimental Investigation of Acoustic Liners to Suppress Screech in Hydrogen-Oxygen Rockets. NASA TN D-3822, 1967.

12. Vincent, David W.; Phillips, Bert; and Wanhainen, John P.: Experimental Investigation of Acoustic Liners to Suppress Screech in Storable Propellant Rocket Motors. NASA TN D-4442, 1968.

13. Phillips, Bert: Experimental Investigation of an Acoustic Liner with a Variable Cavity Depth. NASA TN D-4492, 1968.

14. Hannum, Ned P.; Bloomer, Harry E.; and Goelz, Ralph R.: Stabilizing Effects of Several Injector Face Baffle Configurations on Screech in a 20,000-Pound-Thrust Hydrogen-Oxygen Rocket. NASA TN D-4515, 1968.

15. Vincent, David W.; Sokolowski, Daniel E.; and Bloomer, Harry E.: Screech Suppression Techniques for Rocket Combustors using Earth-Storable Propellants. NASA TM X-1595, 1968.

16. Hannum, Ned P.; and Conrad, E. William: Performance and Screech Characteristics of a Series of 2500-Pound-Thrust-per-Element Injectors for a Liquid-Oxygen-Hydrogen Rocket Engine. NASA TM X-1253, 1966.

17. Feiler, Charles E.; and Heidmann, Marcus F.: Dynamic Response of Gaseous-Hydrogen Flow System and its Application to High-Frequency Combustion Instability. NASA TN D-4040, 1967.

18. Heidmann, Marcus F.; and Wieber, Paul R.: Analysis of Frequency Response Characteristics of Propellant Vaporization. NASA TN D-3749, 1966.

19. Dahlberg, D. E.: Investigation of Combustion Instability with Liquid Oxygen and Liquid or Cold Gaseous Hydrogen Propellant, Phase II. Rep. PWA-FR-1374, Pratt & Whitney Aircraft (NASA CR-63758), May 14, 1965.

20. Anon: An Experimental Investigation of Combustion Stability Characteristics at High Chamber Pressure. Rep. 11741/SA6-F, Vols. 1 and 2, Aerojet-General Corp. (NASA CR-78691 and CR-78715), Aug. 1966.

21. Bloomer, Harry E.; Wanhainen, John P.; and Vincent, David W.: Chamber Shape Effects on Combustion Instability. Fourth ICRPG Combustion Conference. Rep. CPIA Publ. No. 162, vol. 1, Applied Physics Lab., Johns Hopkins Univ., Dec. 1967, pp. 39-55.

22. Weiss, Richard R.: Investigation of Hybaline A_{14} as a Combustion Instability Suppressant in a LO_2/RP-1 Combustion System. AFRPL-TR-66-130, Air Force Systems Command, June 1966. (Available from DDC as AD-802488.)

23. Nicholls, J. A.; Dabora, E. K.; and Raglano, K. W.: A Study of Two-Phase Detonation as it Relates to Rocket Motor Combustion Instability. NASA CR-272, 1965.

24. Combs, L. P.; Hoehn, F. W.; and Webb, S. R.: Combustion Stability Rating Techniques. Rep. R-6355-4, Rocketdyne Div., North American Aviation, Inc. (AFRPL-TR-66-229, DDC No. AD-801897), Sept. 1966.

25. Priem, Richard J.; and Heidmann, Marcus F.: Propellant Vaporization as a Design Criterion for Rocket-Engine Combustion Chambers. NASA TR R-67, 1960.

26. Elverum, G. W., Jr.; and Morey, T. F.: Criteria for Optimum Mixture-Ratio Distribution Using Several Types of Impinging-Stream Injector Elements. Memo 30-5, Jet Propulsion Lab., California Inst. Tech., Feb. 25, 1959.

27. Somogyi, Dezso; and Feiler, Charles E.: Liquid-Phase Heat-Release Rates of the Systems Hydrazine-Nitric Acid and Unsymmetrical Dimethylhydrazine-Nitric Acid. NASA TN D-469, 1960.

28. Burrows, Marshall C.: Mixing and Reaction Studies of Hydrazine and Nitrogen Tetroxide Using Photographic and Spectral Techniques. NASA TN D-4467, 1968.

29. Osborn, J. R.; and Davis, L. R.: Effects of Injection Location in Combustion Instability in Premixed Gaseous Bipropellant Rocket Motors. Rep. I-61-1, Purdue Univ., Jan. 1961.

30. Reardon, F. H.; McBride, J. M.; and Smith, A. J., Jr.: Effect of Injection Distribution on Combustion Stability. AIAA J. vol. 4, no. 3, Mar. 1966, pp. 506-512.

31. Morse, Phillip M.: Vibration and Sound. Second ed., McGraw-Hill Book Co., Inc., 1948.

32. Ingaard, Uno: On the Theory and Design of Acoustic Resonators. Accoust. Soc. Am. J., vol. 25, no. 6, Nov. 1953, pp. 1037-1061.

33. Blackman, A. W.: Effect of Nonlinear Losses on the Design of Absorbers for Combustion Instabilities. ARS J., vol. 30, no. 11, Nov. 1960, pp. 1022-1028.

34. Mechel, F.; Mertens, P.; and Schilz, W.: Research on Sound Propagation in Sound-Absorbent Ducts with Superimposed Air Streams. Final Rep., Physikalisches Inst., Univ. Göttengen, West Germany (AMRL-TDR-62-140, vol. III), Dec. 1962.

35. Russell, P. L.; Bohn, N.; and Garrison, G. D.: Absorbing Liners for Storable Propellant Rocket Engines, Part I - Uncooled Liner Tests. Fourth ICRPG Combustion Conference. Rep. CPIA Publ. No. 162, vol. 1, Applied Physics Lab., Johns Hopkins Univ., Dec. 1967, pp. 125-134.

36. Zwikker, C.; and Kosten, C. W.: Sound Absorbing Materials. Elsevier Publ. Co., Inc., 1949.

37. Svehla, Roger A.: Thermodynamic and Transport Properties for the Hydrogen-Oxygen System. NASA SP-3011, 1964.

38. Conrad, E. William; Wanhainen, John P.; and Curley, Jerome K.: Cooled Baffle Development for M-1 Engine Using a Subscale Rocket Engine. NASA TM X-1267, 1966.

39. Senneff, John M.; and Morgante, Paul J.: Combustion Stability Investigation of the LEM Ascent Engine. Second Combustion Conference, Interagency Chemical Rocket Propulsion Group. Vol. 1. Thomas W. Christian, ed. Rep. CPIA Publ. -105, Applied Physics Lab., Johns Hopkins Univ., May 1966, pp. 23-46. (Available from DDC as AD-484561.)

40. Nord, W. J., ed.: Analytical Model. Vol. 3 of Gemini Stability Improvement Program (Gemsip). Rep. GEMSIP-FR-1, Aerojet General Corp. (AFSSD-TR-66-2, DDC No. AD-626766), Aug. 31, 1965.

41. Gordon, Colin; and Smith, P. W., Jr.: Acoustic Losses of a Resonator with Steady Gas Flow. Acoust. Soc. Am. J., vol. 37, no. 2, Feb. 1965, pp. 257-267.

NASA-Langley, 1968 — 28 E-4500

NATIONAL AERONAUTICS AND SPACE ADMINISTRATION
WASHINGTON, D.C. 20546

OFFICIAL BUSINESS

FIRST CLASS MAIL

POSTAGE AND FEES PAID
NATIONAL AERONAUTICS AN
SPACE ADMINISTRATION

POSTMASTER: If Undeliverable (Section 15
Postal Manual) Do Not Retu

"The aeronautical and space activities of the United States shall be conducted so as to contribute . . . to the expansion of human knowledge of phenomena in the atmosphere and space. The Administration shall provide for the widest practicable and appropriate dissemination of information concerning its activities and the results thereof."

—NATIONAL AERONAUTICS AND SPACE ACT OF 1958

NASA SCIENTIFIC AND TECHNICAL PUBLICATIONS

TECHNICAL REPORTS: Scientific and technical information considered important, complete, and a lasting contribution to existing knowledge.

TECHNICAL NOTES: Information less broad in scope but nevertheless of importance as a contribution to existing knowledge.

TECHNICAL MEMORANDUMS: Information receiving limited distribution because of preliminary data, security classification, or other reasons.

CONTRACTOR REPORTS: Scientific and technical information generated under a NASA contract or grant and considered an important contribution to existing knowledge.

TECHNICAL TRANSLATIONS: Information published in a foreign language considered to merit NASA distribution in English.

SPECIAL PUBLICATIONS: Information derived from or of value to NASA activities. Publications include conference proceedings, monographs, data compilations, handbooks, sourcebooks, and special bibliographies.

TECHNOLOGY UTILIZATION PUBLICATIONS: Information on technology used by NASA that may be of particular interest in commercial and other non-aerospace applications. Publications include Tech Briefs, Technology Utilization Reports and Notes, and Technology Surveys.

Details on the availability of these publications may be obtained from:

SCIENTIFIC AND TECHNICAL INFORMATION DIVISION

NATIONAL AERONAUTICS AND SPACE ADMINISTRATION

Washington, D.C. 20546